POLITECNICO DI TORINO
Repository ISTITUZIONALE

Investigation Into Advanced Architecture and Strategies For Turbocharged Compressed Natural Gas Heavy Duty SI-engine

Original
Investigation Into Advanced Architecture and Strategies For Turbocharged Compressed Natural Gas Heavy Duty SI-engine / Kheshtinejad, Hamed. - (2017).

Availability:
This version is available at: 11583/2689169 since: 2017-11-02T20:52:39Z

Publisher:
Politecnico di Torino

Published
DOI:10.6092/polito/porto/2689169

Terms of use:
openAccess

This article is made available under terms and conditions as specified in the corresponding bibliographic description in the repository

Publisher copyright

(Article begins on next page)

04 August 2020

Doctoral Dissertation

Doctoral Program in Energy Engineering (29^{th}cycle)

Investigation Into Advanced Architecture and Strategies For Turbocharged Compressed Natural Gas Heavy Duty SI-engine

By

Hamed Kheshtinejad

******

Supervisor(s):

Prof. Daniela Misul., Supervisor

Prof. Mirko Baratta, Co-Supervisor

Doctoral Examination Committee:

Prof. Carlo Beatrice, Referee, Istituto Motori - Consiglio Nazionale delle Ricerche CNR

Prof. Gianluca d'Errico, Referee, Politecnico Di Milano

Prof. Antonio Mittica, Politecnico Di Torino

Prof. Luis Parras Anguita, Università di Malaga

Prof. Roberto Gentili, Università di Pisa

Politecnico di Torino

2017

Declaration

I hereby declare that, the contents and organization of this dissertation constitute my own original work and does not compromise in any way the rights of third parties, including those relating to the security of personal data.

Hamed Kheshtinejad
2017

* This dissertation is presented in partial fulfillment of the requirements for **Ph.D. degree** in the Graduate School of Politecnico di Torino (ScuDo).

I would like to dedicate this thesis to my loving wife Parisa, whose love, company and understanding can never be forgotten.

Also I have dedication to my parents, Mahin and Abbas for their support and company from the first days of my school where my mom was watching me from the classroom window, wishing his son to be a good student. I did my best to make you proud.

And finally, I dedicate this humble effort to my future child/children whom I might have if I did not choose to pursue my PhD studies. Since you may read this later, remember that to achieve your goals in your life you will need a wise plan, hard work and big hope.

Acknowledgements

And I would like to acknowledge and thank my supervisors Prof. Daniela Misul and Prof. Mirko Baratta, you have been a tremendous mentor for me. Words cannot express how grateful I am to you for encouraging my research and for allowing me to grow as a researcher. Your advice on both research as well as on my career have been priceless.

I would especially like to thank all members our research group of "Internal Combustion Engine Advanced Laboratory (ICEAL)" and professors of Energy department of Politecnico di Torino. All of you have been there to support me when I was progressing my research for my Ph.D. thesis.

A special thanks to my colleages, Danilo Laurenzano and Andrea Bottega who helped me during my research specially for providing me perfect atmosphere in our office. I was lucky to meet Prof. Dongiovanni who inspired me to become whoever I want in my future.

I am grateful to my family for all of the sacrifices that they've made on my behalf. I would also like to thank all of my friends; Fariba, Vincenzo, Iman, Sahar, Hessam, Mahsa, Mohsen, Farshid, Behrouz, Nasim, Kasra and ... who supported me in my studies, and helped me to strive towards my goal.

Finally, I would like to express appreciation to my beloved wife Parisa who spent every days of PhD with me and was always my support in the moments when there was no one to answer my queries.

Abstract

CNG is at present retaining a growing interest as a factual alternative to traditional fuel for SI engine thanks to its high potentials in reducing the engine-out emissions. Increasing thrust into the exploitation of NG in the transport field is in fact produced by the even more stringent emission regulations which are being introduced into the worldwide scenario. Specific attention is also to be devoted to heavy duty engines given the high impact they retain due to the diesel oil exploitation and to the PM emissions, the latter issue assessing for the need to shift towards alternative fuels such as natural gas.

A thorough control of the air-to-fuel ratio appears to be mandatory in spark ignition CNG engines in order to meet the even more stringent thresholds set by the current regulations. The accuracy of the air/fuel mixture highly depends on the injection system dynamic behavior and to its coupling to the engine fluid-dynamic. The amount of injected fuel should in fact be properly targeted by the ECU basing on the estimation of the induced air and accounting for the embedded closed-loop strategies. Still, these latter are normally derived from engine-base routines and totally ignore the injection system dynamics. Thus, a sound investigation into the mixing process can only be achieved provided that a proper analysis of the injection rail and of the injectors is carried out.

The first part of the present work carries out a numerical investigation into the fluid dynamic behavior of a commercial CNG injection system by means of a 0D-1D code. The research has been focused on defining the set of parameters to be precisely reproduced in the 0D-1D simulation so as to match the injection system experimental behavior. Specific attention has been paid to the one component which significantly contributes to fully defining its dynamic response, i.e. the pressure reducing valve. The pressure reducer is made up of various elements that retain diverse weights on the valve behavior and should consequently be differently addressed to. A refined model of the pressure reducer has hence been proposed and the model has been calibrated, tested and run under various operating conditions so as to assess for the set-up validity. Comparisons have been carried out on steady state points as well as through out a vehicle driving cycle and the model

capability to properly reproduce the real system characteristic has been investigated into. The proposed valve model has proved to consistently replicate the injection system response for different speed and load conditions. A few methodological indications concerning modeling aspects of a pressure regulator can be drawn from the present study. The model has been run in a predictive mode so as to inquiry into the response of the system to fast transient operations, both in terms of speed and load. The model outputs have highlighted mismatches between the ECU target mass and the actually injected one and have hinted at the need for dedicated and refined control strategies capable of preventing anomalies in the mixture formation and hence in the engine functioning.

The second part of the presnt work aims at deeply investigating into the potentials of a heavy duty engine running on CNG and equipped with two different injection systems, an advanced SP one and a prototype MP one. The considered 7.8 liter engine was designed and produced to implement a Sigle-Point (SP) strategy and has hence been modified to run with a dedicated Multi-Point (MP) system so as to take advantage of its flexibility in terms of control strategies. More specifically, a thorough comparison between the experimental performances of the engine equipped with the two injection systems has been carried out at steady state as well as at transient operations. Better performances in terms of cycle-to-cycle variability were proved for the MP system despite poorer mixture homogeneity. Attention has also been paid to the different engine control strategies to be eventually adopted in compliance with the constraints set by the two different layouts. A 0D-1D model has also been built and validated on the experimental data set to be hence exploited for investigating into different strategies both for the SP and for the MP layout. An extensive simulation has been carried out on the effects of the injection phasing on the SP system performance referring to the engine power output and to the air-to-fuel ratio homogeneity amongst the cylinders. Finally, as far as the MP injection system is concerned, the innovative fire-skipping (DSF) or cylinder deactivation has been considered and deployed by means of the numerical model, assessing for an overall decrease in the fuel consumption of 12% at part load operations.

Contents

List of Figures **x**

List of Tables **xiv**

Nomenclature **xv**

1 CNG Injection Systems for Spark Ignition Engines – a review **1**

1.1 Introduction 1

1.1.1 Natural gas as fuel 1

1.1.2 CNG engines 3

1.1.3 Technical aspect of CNG engines 5

1.1.4 Environmental aspect of CNG engines 6

1.2 Combustion characteristics of spark ignition CNG engines 7

1.2.1 Lean burn natural gas engines 7

1.2.2 Stoichiometric natural gas engines 8

1.3 CNG fueling systems for SI engines 10

1.3.1 Cylinder direct injection (DI) 11

1.3.2 Mixer type single-point injection (SPI) 13

1.3.3 Intake port multi-point injection (MPI) 14

1.4 Fuel injection characteristics of MPI spark ignition CNG engines 16

1.4.1 CNG injection system components 17

1.4.2 CNG injection modeling and control 20

1.5 Research formulation 23

2 Fluid-dynamic Modeling of a CNG MPI System 25

2.1 Introduction 25

2.2 CNG MPI system layout 27

2.3 Experimental set-up 28

2.4 CNG MPI model 30

2.4.1 Introduction to AMESim 0D-1D modeling environment 30

2.4.2 Model description 33

2.5 Model calibration 35

2.5.1 Injector calibration 35

2.5.2 Numerical model calibration 36

2.6 Results and discussion 41

2.7 Sensitivity analysis 46

2.8 Summary 49

3 Development of a predictive model of pressure regulator for CNG MPI system 50

3.1 Introduction 50

3.2 Injection system and experimental set-up 51

3.3 Pressure regulator model description 52

3.3.1 First release 54

3.3.2 Second release 55

3.3.3 Third release 57

3.3.4 Regulator model tuning 58

3.4 Results and discussion 60

3.4.1 Single shot run 60

3.4.2 Steady state points 63

3.4.3 Driving cycle simulations (cut-off phases) 67

3.4.4 Transient simulations 69

3.5 Conclusions 73

4 Potentials of MP Injection System for a production NG SP Heavy-Duty Engine 75

4.1 Introduction 75

4.2 Experimental Set-up 76

4.2.1 Test engine 76

4.2.2 Test bench and data acquisition 77

4.2.3 Experimental data set 79

4.3 Experimental Results and discussion 79

4.3.1 Steady-state points 79

4.3.2 Cycle-to-cycle analysis 83

4.3.3 MPI sensitivity to injection phasing 87

4.4 Numerical model 89

4.4.1 Single-point and multi-point injection system models 90

4.4.2 Models validation 91

4.5 SPI system: injection phasing 94

4.6 MPI system optimization by fire skipping (Cylinder deactivation) 99

4.7 Conclusions 103

References 105

List of Figures

1.1 Global greenhouse gas emissions by source 2

1.2 The impact of energy resources on global warming 2

1.3 The growth in number of natural gas vehicles in Europe from 2004 to 2015 . 4

1.4 Engine emission change in CNG over gasoline in percentage at 50% and 80% throttle position at stoichiometric condition for a retrofitted engine 6

1.5 Limits in load and dilution for engine mapping 7

1.6 Specific NO_x emissions Vs. lambda (a) before 3-way catalyst and (b) after 3-way catalyst 9

1.7 (a) brake efficiency and (b) catalyst efficiency Vs. EGR level for CNG engine with EGR 9

1.8 Different types of CNG fueling systems 10

1.9 Spark ignition direct injection mixture preparation system 11

1.10 Turbocharged CNG engine map equipped with mixer type single point injection 13

1.11 Spark ignition port fuel injection mixture preparation system 14

1.12 Schematic diagram of MPI system with closed-loop lambda control 15

1.13 A block scheme of MP CNG injection system 17

1.14 Block scheme of pressure regulator for CNG MPI system 19

1.15 injection strategies: (a) Peak and hold, (b) pulse interruption 20

1.16 CNG engine as MIMO system 20

2.1 Experimental set up: pressure regulator and injector rail 28

2.2 Model map of the CNG injection system 33

2.3 Pressure regulator model 34

2.4 Injector needle lift profile 35

2.5 Experimental pressure at the regulator outlet port as compared to the numerical simulations (part 1) 37

2.6 Experimental pressure at the regulator outlet port as compared to the numerical simulations (part 2) 38

2.7 Experimental rail pressure as compared to the numerical model output (part 1) 39

2.8 Experimental rail pressure as compared to the numerical model output (part 2) 40

2.9 Comparison between the target mass as calculated by the ECU and the measured injected one 42

2.10 Comparison between the percentage errors in the injected mass and the pressure during the injection event with respect to the rail average one . . . 43

2.11 Comparison between the target mass as calculated by the ECU and the measured injected one at constant ET (a) and at constant speed (b) 45

2.12 Simulated rail pressure as a function of the rail diameter (a) and of the fuel hose (b) 47

2.13 Percentage error in the injected mass as a function of the rail diameter (a) and of the fuel hose (b) 48

3.1 Pressure regulator model: first release. 54

3.2 Exemplification of the pressure drop phenomenon 55

3.3 Pressure regulator model: second release. 56

3.4 Comparison between the first and the second release of the pressure regulator model: pressure drop. 57

3.5 Pressure regulator model: third release. 58

3.6 Experimental pressure (blue line) as compared to the output produced by the three releases downstream from the pressure regulator (a) and in the rail (b) for 1st single shot run, ET=4000 ms. 61

3.7 Experimental pressure (blue line) as compared to the output produced by the three releases downstream from the pressure regulator (a) and in the rail (b) for 2nd single shot run, ET=14000 ms. 62

3.8 Experimental rail pressure (blue line) as compared to the output produced by the three releases. 64

3.9 Experimental rail pressure (blue line) as compared to the output produced by the second and the third release. 66

3.10 Driving cycle simulation for the first (a), the second (b) and the third (c) release adopted for the pressure regulator description. 68

3.11 Highlight on the driving cycle simulation for the third release adopted for the pressure regulator description. 69

3.12 Speed transient simulations (ET=4000 ms). 70

3.13 Load transient simulations (N=3000 rpm). 72

4.1 YUCHAI YC6G Engine with SPI system. 77

4.2 Engine measuring set-up YUCHAI YC6G. 78

4.3 Engine steady state operating points. 79

4.4 Comparison of SPI and MPI engines performance. 80

4.5 Cylinder to cylinder lambda variations for SPI and MPI. 81

4.6 Transient operations: (a) Load transient; (b) Speed transient. 82

4.7 SPI vs. MPI COV for IMEP at WOT 83

4.8 SPI vs. MPI COV for IMEP at 50% load. 84

4.9 SPI vs. MPI cyclic variation for IMEP vs. PFP at WOT 85

4.10 SPI vs. MPI cyclic variation for IMEP vs. PFP att 50% load. 86

4.11 MPI sensitivity to phase variation COV for IMEP at WOT 88

4.12 MPI sensitivity to phase variation COV for IMEP at 50% load 88

4.13 SP Injection system, GT-POWER model map 90

4.14 MP Injection system, GT-POWER model map 91

4.15 SPI model results under steady-state operating conditions, as function of engine speed 92

4.16 MPI model results under steady-state operating conditions, as function of engine speed 93

4.17 SPI model versus experimental in-cylinder pressure (Cylinder No.2) at WOT and 50% load 93

4.18 MPI model versus experimental in-cylinder pressure (Cylinder No.2) at WOT and 50% load 94

4.19 CNG mass flow rate for 1 , 2 , 4 and 6 injection events per cycle 95

4.20 Engine performance for the different injection patterns at WOT. 96

4.21 Cylinder-to-cylinder lambda variation for the different injection strategies at WOT for the indicated speeds. 97

4.22 Cylinder-to-cylinder lambda variation in the SPI system for the different injection strategies (800 rpm – WOT). 98

4.23 Fuel economy gain in the fire skipping compared to throttled operations. . . 100

4.24 Engine performance at part loads with and without the fire skipping strategy.101

4.25 In-Cylinder pressure traces (Cyl 2) at part loads with and without fire skipping 102

List of Tables

1.1 Physiochemical properties of CNG vs. gasoline and diesel 3
1.2 Modelling properties of engine processes and feasible applications 22

2.1 Test engine and related injection system characteristics 28
2.2 Experimental runs on steady state points data set. 29
2.3 Case definition at constant ET 44
2.4 Case definition at constant speed 44

3.1 Summary of the regulator parameters for the three releases. 59

4.1 Characteristics of the studied engine 76
4.2 Experimental cases: injection duration and EOI phasing 87
4.3 Fire skipping strategy benefit at part load operations 99

Nomenclature

Acronyms / Abbreviations

AFR	Air to Fuel Ratio
BDC	Bottom Dead Center
BMEP	Brake Mean Effective Pressure
BSFC	Brake Specific Fuel Consumption
CFD	computational Fluid Dynamics
CI	Compression Ignition
CNG	Compressed Natural Gas
CoV	Coefficient of Variance
DI	Direct Injection
DOE	Design of Experiment
DSF	Dynamic Skip Fire
ECI	E-controls Injection
ECU	Engine Control Unit
EFI	Electronic Fuel Injection
EGR	Exhaust Gas Recirculation
EMS	Engine Management System
EOI	End of Injection

ET Energizing Time

GHG Green House Gas

HC Hydrocarbons

HCNG Hydrogen enriched Compressed Natural Gas

IMEP Indicated Mean Effective Pressure

L.H.V Lower Heating Value

MAP Manifold Absolute Pressure

MBT Maximum Brake Torque

MIMO multi-input/multi-output

MPI Multi Point Injection

NEDC New European Driving Cycle

NOx Oxides of Nitrogen

PFP Peak Firing Pressure

PI Proportional Integral

SA Spark Advance

SI Spark Ignition

SPI Single Point Injection

TDC Top Dead Center

VVA Variable Valve Actuation

WOT Wide Open Throttle

Chapter 1

CNG Injection Systems for Spark Ignition Engines – a review

1.1 Introduction

1.1.1 Natural gas as fuel

Human activities since 1750 were the drivers of climate change by altering the energy balance of climate system and changes in the atmospheric concentrations of greenhouse gases (GHGs): carbon dioxide (CO_2), nitrous oxide (N_2O) and methane (CH_4). Among different resources of the global GHGs emissions the transport sector plays a major role and accounts for 13% of the global GHGs emissions (Fig. 1.1)[1]. The current transport sector is more than 98% dependent on oil which can be refined to gasoline, diesel and aviation fuel. Natural gas as a fuel has become an interesting subject and represents a promising alternative fuel due to its high hydrogen-to-carbon ratio and high research octane number. Changing fuels from diesel or gasoline (with H/C approximately 1.8 - 2.2) to natural gas (with H/C equal to 4) results in considering natural gas as an environment friendly fuel [2]. Compared with oil, to produce the same amount of energy, the impact of natural gas on global warming is half and therefore, recently gained more attention so as to meet the engine strict emission regulations (Fig. 1.2) [3].

In the world today about 23% of the world primary energy consumption is provided by natural gas and discovery success of new conventional gas fields and technological innovation insures the availability of global gas resources up to about 240 years of current consumption. Furthermore, the price of natural gas is 45% less than oil in Europe and

the natural gas vehicle technology is relatively mature [4]. Obviously natural gas plays an important role in development of future global energy by reducing the impact on global warming and providing the sustainable energy supplies.

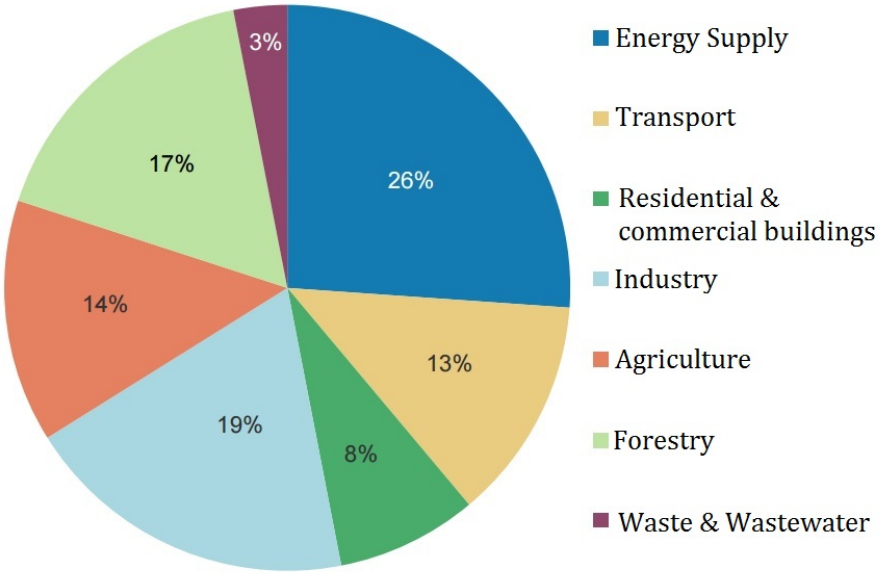

Fig. 1.1 Global greenhouse gas emissions by source [1]

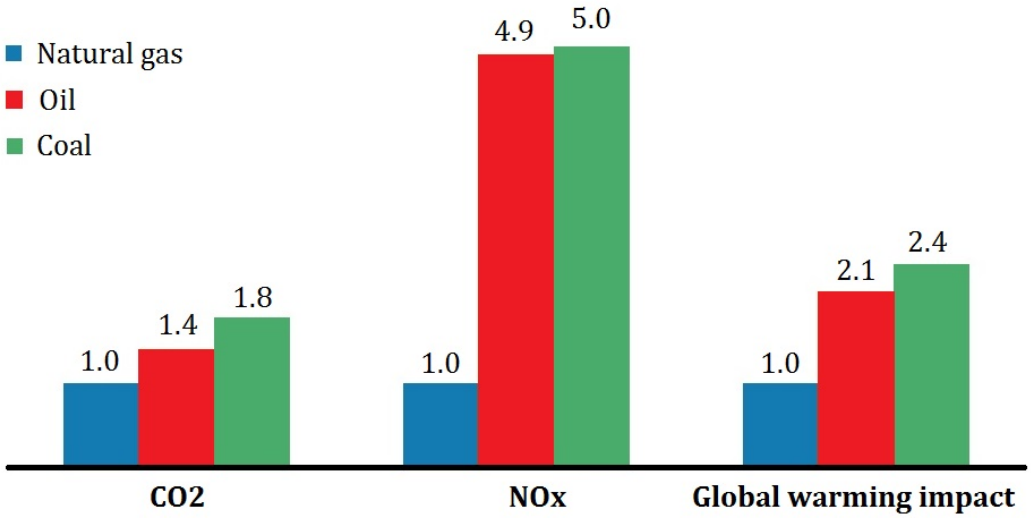

Fig. 1.2 The impact of energy resources on global warming [3]

Natural gas can be reformed to the compressed natural gas (CNG) by being compressed to less than 1% of its volume at the atmospheric pressure. CNG is stored at a pressure ranging around 200-250 bar in purposely designed rigid container usually in cylindrical shapes. Table 1.1 describes the main properties of CNG compared to that of diesel and gasoline. CNG physical properties such as its narrow range of flammability (4.3% to 15.2% by volume of air), high auto-ignition temperature (540°C) and very low density, makes it a safer fuel with respect to gasoline and diesel. Moreover, CNG cylinders with high design safety factors (> 2) are safer than conventional liquid fuel tanks [5].

Table 1.1 Physiochemical properties of CNG vs. gasoline and diesel

Properties	**CNG**	**Gasoline**	**Diesel**
Octane/cetane number	120-130	85-95	45-55
Molar mass (kg/mol)	17.3	109	204
Stoichiometric (A/F)s mass	17.2	14.7	14.6
Stoichiometric mixture density (kg/m3)	1.25	1.42	1.46
L.H.V (MJ/kg)	47.5	43.5	42.7
L.H.V of stoichiometric mixture (MJ/kg)	2.62	2.85	2.75
Combustion Energy (MJ/m3)	24.6	42.7	36
Flammability limit in air (vol% in air)	4.3-15.2	1.4-7.6	1-6
Flame propagation speed (m/s)	0.41	0.5	-
Adiabatic flame temp. (°C)	1890	2150	2054
Auto-ignition temp. (°C)	540	258	316
Wobe index (MJ/m3)	51-58	-	-

1.1.2 CNG engines

The use of natural gas as fuel for vehicle was introduced first in Italy in the 1930s. After the energy crisis in 1970s, CNG vehicles became more attractive as a promising alternative to gasoline vehicles [6]. Until the improvised rise in oil price in 2000s, it was challenging for CNG to attract the market due to the additional costs for CNG systems with respect to pure gasoline engines. In order to lower the price of CNG vehicles, a reduction about 30% in CNG fueling system is necessary to come down at least to the level of diesel-fueled vehicles [7]. Fig. 1.3 shows the growth in number of natural gas vehicles from 2004 to 2015 in Europe [8]. The increasing demand for natural gas vehicles points out

the urgency of specific research and development activity to enhance a better vehicle performance-to-cost ratio.

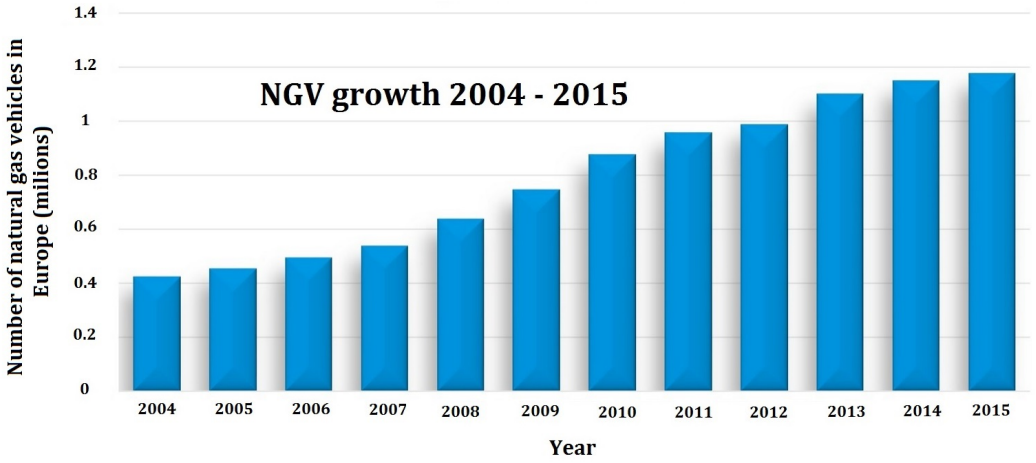

Fig. 1.3 The growth in number of natural gas vehicles in Europe from 2004 to 2015 [8]

The fuel induction mechanism required for CNG differs from the conventional gasoline and diesel engines due to the gas form of CNG at normal temperatures and pressures. The performance of engines fuelled by CNG depends on type of engine fuel supply i.e. mono fuel, bi fuel and dual fuel. Natural gas engines in terms of fuel supply type can be categorized in three groups:

- **Dedicated (mono-fuel) CNG engines;** the spark ignition engines designed with higher compression ratio considering the higher octane number with respect to gasoline.
- **Bi-fuel gasoline engines;** which work by either CNG or gasoline selected by driver by a switch on the dashboard. Most of the CNG cars are retrofitted gasoline engines which are optimized to work with CNG.
- **Dual-fuel diesel engines;** which are based on compression ignition engines and can run either on diesel or the mixture of CNG and diesel. In these engines the mixture of CNG and air is ignited by a diesel pilot injection.

Although the research has some successes to optimize bi-fuel retrofitted gasoline and dual-fuel diesel engines, these types of engines are not able to use the maximum potential of CNG as an alternative fuel. As a consequence, development of dedicated CNG engine is getting more attention [9].

1.1.3 Technical aspect of CNG engines

Natural gas has the octane number ranging from 120 to 130 which makes it more resistant to knock with respect to gasoline. As a result the dedicated CNG engine can use higher compression ratio up to 16:1 without knocking and thus boosts the engine thermal efficiency up to 35% which is about 10% above that of gasoline engine. Moreover, unlike gasoline, CNG as a gaseous fuel doesn't need atomization and evaporation time. It makes CNG favourable for having improved air-fuel mixture and enhancing good combustion [10, 11]. On the other hand, compared to the gasoline engines, the naturally aspirated CNG engines with stoichiometric air-to-fuel ratio have 18-22% lower brake specific fuel consumption (BSFC) and 15-20% lower brake power [12–14]. These draw backs are due to the limited flame speed, absence of fuel evaporation and lower volumetric efficiency of CNG engines.

As far as the flame propagation speed is concerned, CNG represents lower flame speed compared to gasoline [15]. The lower flame propagation speed results in prolonged combustion duration in CNG engines which proceeds till the end of expansion stroke. Longer combustion duration along with higher compression ratio conduce to higher exhaust gas temperature of CNG engines than that of gasoline engines throughout the load range [11]. One effective method to overcome the problem of low flame speed of CNG and the corresponding shortcomings is to use hydrogen as an additive to boost the flame speed. As a matter of fact hydrogen flame speed is about 7 times higher than that of CNG. Hydrogen enriched CNG (HCNG) improves the engine thermal efficiency due to the shorter combustion duration and higher degree of constant volume combustion [16, 17].

Absence of heat of fuel evaporation for CNG results in higher charge-air temperature and in consequence higher peak cylinder temperature which increases the amount of nitrogen oxides emissions in the exhaust. Moreover, CNG, due to its gaseous nature, has lower mass density and occupies larger volume of intake system with respect to liquid fuels such as gasoline and diesel. Thus, CNG displaces the available air for combustion which causes the reduction of about 10% in volumetric efficiency for CNG engines. The other major problem of CNG engines is the low quality of homogenization of fuel-air mixture due to low fuel penetration [18–20]. These drawbacks associated with CNG results in the necessity of specific research and development activity to achieve a better mixture formation and to enhance the combustion and emissions through optimizing the fuel injection systems and engine control strategies.

1.1.4 Environmental aspect of CNG engines

The primary component of CNG is methane which is composed of one carbon atom and four hydrogen atoms. Methane is the simplest alkane without any carbon-to-carbon bound which makes it a so called "green" fuel. Since CO_2 and H_2O are the ideal products of combustion, then the ratio of hydrogen-to-carbon is the main indication of CO_2 production. Higher H/C ratio corresponds to lower amount of CO_2 emissions [21].

Level of unburned hydrocarbons (HC) for CNG engines is lower than gasoline engines because of the absence of wall wetting effect in cylinder liner and intake manifold for CNG. Carbon monoxide (CO) is another important engine emission which is generated due to incomplete combustion and poor mixing of air and fuel. In addition, nitrogen oxides (NO_x) are by-products of combustion of carbon based fuels which are formed in combustion process at high temperature (above 1300°C) and availability of excess air. Concentration of HC, CO and NO_x highly depends on the air-fuel-ratio and combustion quality. The level of NO_x concentrations increases at stoichiometric combustion process with high temperatures [22]. On the other hand, for lean burn engines with too much excess air, the combustion occurs with lower flame propagation speed which causes low in-cylinder temperature and hence higher HC and CO emissions [23–25].

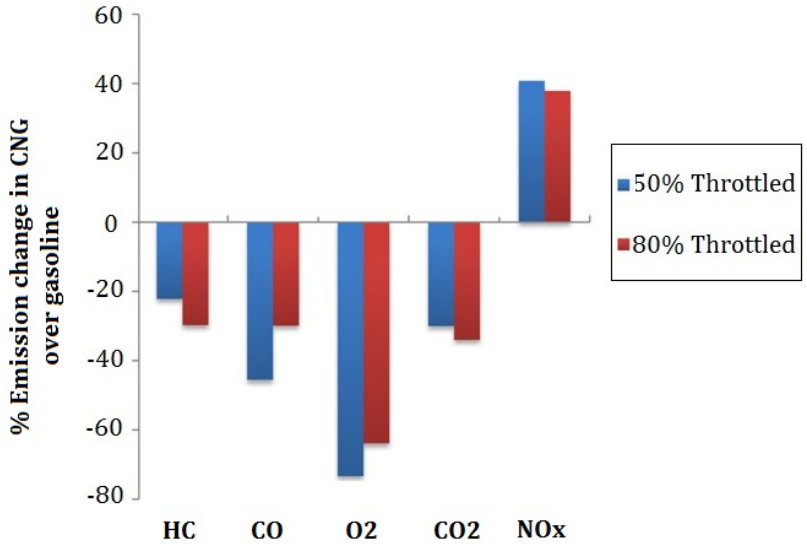

Fig. 1.4 Engine emission change in CNG over gasoline in percentage at 50% and 80% throttle position at stoichiometric condition for a retrofitted engine [23]

Fig. 1.4 shows the change in percentage of emissions produced by CNG with respect to gasoline in a retrofitted engine at 50% and 80% throttled condition of a stoichiometric

combustion [23]. Optimizing the spark advance is an efficient approach to reduce NO_x in CNG engines. In overall, in term of HC and CO emissions, CNG is a much cleaner energy than gasoline. Lean burn CNG engines or stoichiometric CNG engines with EGR and 3-way catalyst are the solutions to control NO_x emissions.

1.2 Combustion characteristics of spark ignition CNG engines

1.2.1 Lean burn natural gas engines

Lean burn strategy is a viable technique for reducing SI engine fuel consumption and emissions. Well-optimized lean burn spark ignition engine, can meet the emission regulations, as well as good fuel economy, for both heavy-duty and light-duty engines [26]. Air-to-fuel ratio is one of the most important parameters of CNG engines, which influences engine efficiency and emissions. The limits for air-to-fuel ratio in CNG engines are defined based on lean misfire and high fuel consumption for lean mixture, and high level of NO_x, knock and fuel consumption for too low air-to-fuel ratio. Fig. 1.5 shows the limits of mixture dilution for different load conditions.

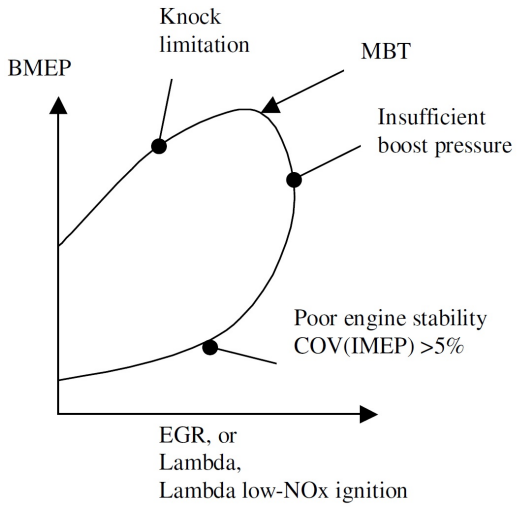

Fig. 1.5 Limits in load and dilution for engine mapping [27].

Too lean mixture (lower than lean limits) results in slower flame propagation and higher combustion duration, which leads to occurrence of incomplete combustion and misfire cycles. As a result, engine thermal efficiency decreases due to higher heat transfer to the cylinder walls. Moreover, slow heat release caused by lower flame speed and flame quenching generates combustion instability and cycle-to-cycle variations for multi-

cylinder engines. Lower combustion temperatures of lean burn CNG engines increase the level unburned hydrocarbons and CO emissions [28].

These drawbacks can be overcome by optimizing the factors such as: combustion chamber configuration, ignition system and turbulence at the end of compression stroke. At the same time, lean-burn engines can use oxidizing catalyst to control HC and CO emissions [27]. Higher turbulence levels can be achieved by properly designed intake ports and intake valves to produce swirl which ,in turn, increases the combustion speed and cyclic stability. Furthermore, the use of pre-chambers for CNG engines results in improved flame propagation speed and stable ignition. Higher ignition energy, achieved by high energy systems, extents the lean misfire limit for CNG engines. Still, these high power systems shorten the life of spark plug [29].

1.2.2 Stoichiometric natural gas engines

Typical heavy-duty CNG engines use lean burn strategy without after treatment systems (or with oxidation catalyst), to achieve high efficiency and low HC and CO emissions. But this technology cannot be used with 3-way catalyst to minimize NO_x emissions. 3-way catalytic converters, besides oxidizing CO and HC emissions, have the advantage of reducing the nitrogen oxides (NO_x). Stringent NO_x emission regulation can be met by stoichiometric combustion using 3-way catalyst after treatment system. The optimum functionality of 3-way catalyst is very sensitive to air-to-fuel ratio. A slight change of air-to-fuel ratio toward lean mixture decreases sharply NO_x conversion efficiency of the catalyst. Therefore, air-to-fuel ratio must be kept as close as possible to stoichiometric value for all the engine operation points by means of closed loop fuel control with a wide range exhaust gas oxygen sensor.

Furthermore, stoichiometric CNG engine have higher exhaust temperature resulting in reduction of unburned HC at cold start engine operation [30–32]. Fig. 1.6 shows the specific NO_x emissions with respect to lambda value for various loads measured before and after the catalyst. The high sensitivity of 3-way catalyst to air-to-fuel ratio is evident [31].

The main drawback of stoichiometric CNG engines is associated with lower efficiency, which can be overcome by means of exhaust gas recirculation (EGR). EGR reduces the combustion chamber temperature and thus the knock tendency. Then, the brake power and efficiency of stoichiometric CNG engine equipped with EGR system are higher than the pure stoichiometric engine. Adding EGR to the mixture has the same effects as diluting

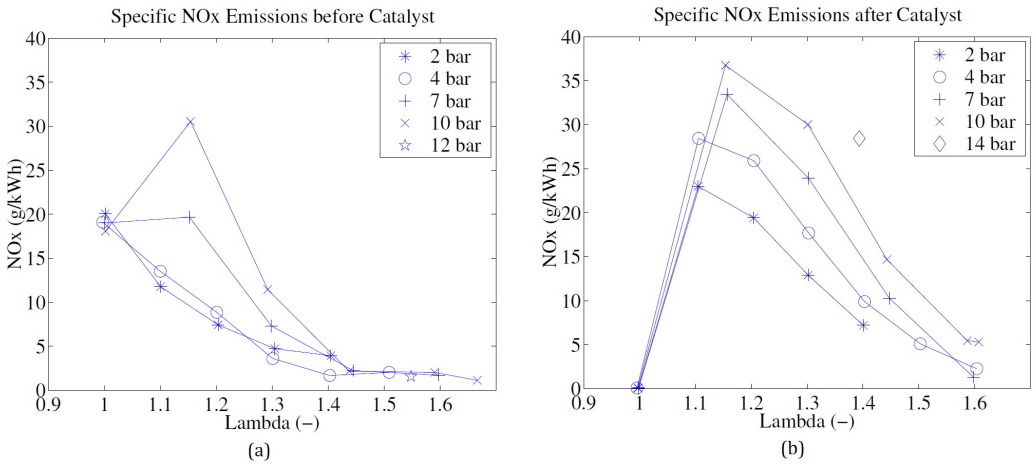

Fig. 1.6 Specific NO_x emissions Vs. lambda (a) before 3-way catalyst and (b) after 3-way catalyst [31]

the mixture by excess air, but unlike the lean burn CNG engines, stoichiometric engine with EGR can activate 3-way catalyst to reduce NO_x emissions [33–35]. EGR is used at partial loads for light-duty dedicated CNG engines to avoid power dispersion due to displacement of air at full load. Since heavy duty engines are typically equipped with turbocharger. So the power can be restored at full loads even with EGR.

Fig. 1.7a shows the brake efficiency improvement of dedicated CNG engine with EGR. The effect of EGR level on catalyst efficiency is depicted in Fig. 1.7b.

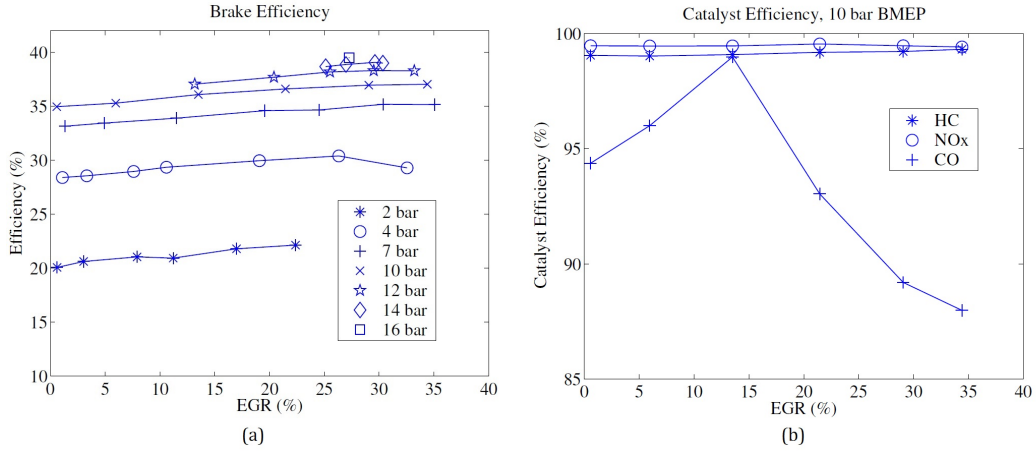

Fig. 1.7 (a) brake efficiency and (b) catalyst efficiency Vs. EGR level for CNG engine with EGR [31]

1.3 CNG fueling systems for SI engines

During last two decades, different car manufacturers have proposed and developed dedicated CNG engines to replace diesel and gasoline fuels. Fig. 1.8 shows different types of CNG fueling systems. Each fueling system has a unique strategy in terms of mixture preparation and combustion control. Still, the common goal of all systems is to achieve better fuel economy and lower engine emissions [36, 37].

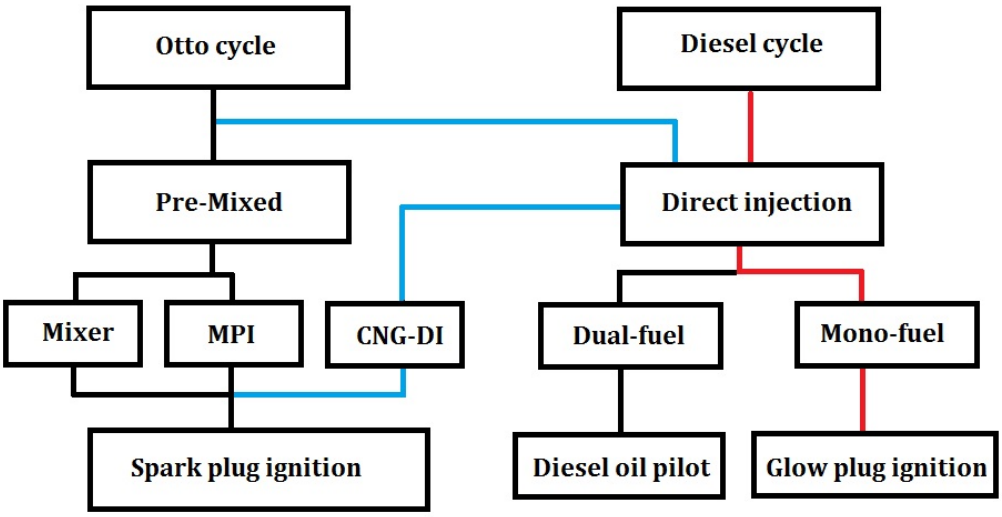

Fig. 1.8 Different types of CNG fueling systems [36]

Diesel-fuel engines, due to higher combustion rate, produce about 30% more power with respect to the same-size spark ignition engines. Moreover, lower compression ratio and high intake air pumping losses at partial loads results in 15-25% lower thermal efficiency for SI engines compared to diesel engines. However, the recent strict emission regulations demanded more advanced engine control technology and after treatment systems which made diesel engines more expensive. As a matter of fact, most of CNG engines run with Otto cycle either with pre-mixing air/fuel charge system or with direct injection system in which the combustion is initiated by spark plug. Since the current SI engine technology can use only part of CNG potential as an alternative fuel, improving the performance of spark ignition CNG engines is a must [38]. The main characteristics of direct injection and pre-mixed fueling systems for CNG spark ignition engines will be presented in following sections.

1.3.1 Cylinder direct injection (DI)

Direct injection spark ignition (SIDI) engines have been designed to combine the high specific power of gasoline engine with high efficiency of the diesel engine at partial loads. This type of engine can bring out the good fuel economy of CI engine along with the operating characteristics and specific power of SI engine. In DISI engines, like diesel engines, fuel is injected directly to the combustion chamber and the power output of the engine can be controlled by the amount of injected fuel. While, like SI engine, the mixture is ignited by means of spark plug direct ignition. Therefore, SIDI technology avoids the limitations regarding the throttling power loss in SI engine and auto-ignition limits in CI engine [39]. Fig. 1.9 illustrates the schematic of mixture preparation of SIDI engine.

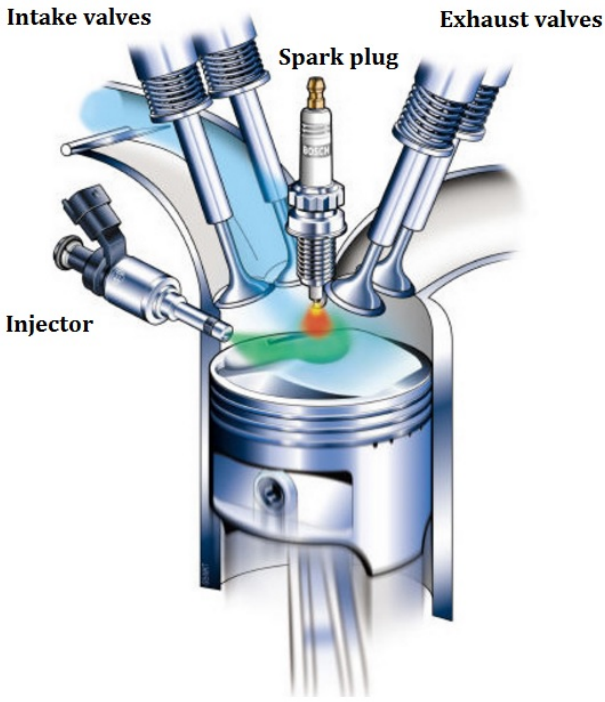

Fig. 1.9 Spark ignition direct injection mixture preparation system [40]

In recent years, the concept of SIDI fueled by CNG has been studied and developed to achieve better performance and fuel efficiency. Injection of CNG directly into the engine cylinder after the closure of intake valves, avoids the loss in volumetric efficiency and power which is associated with pre-mixing fueling systems. Since in DI technology the fuel is entering directly into the combustion chamber, the amount of trapped air is independent to the type of fuel. Therefore, the gaseous nature of CNG with molar fraction

approximately 4.2 times higher than gasoline has no influence on volumetric efficiency in DI CNG engines with respect to DI gasoline engines [41, 42].

Moreover, in contrast with external mixture formation which provides a homogeneous mixture of fuel and air throughout the whole combustion chamber, mixture preparation by DI technology is flexible. As a matter of fact, there are two types of mixture formation in combustion chamber when direct injection is involved: homogeneous mixture or stratified mixture. Homogeneous charge formation in DI CNG engines is achieved by advancing the fuel injection for medium and high engine loads. In this condition all the fresh air inside the combustion chamber take part in combustion process. Early injection timing at the end of intake stroke provides the adequate time for air-fuel mixture formation before the ignition and avoids the loss in volumetric efficiency. However, the ignitability of the mixture depends on the global lambda and to avoid misfire, the lean operation limit for homogeneous mixture cannot exceed leaner than $\lambda = 1.25$ [43].

On the other hand, DI technology is able to form stratified mixture which allows extremely lean combustion and high compression ratio with low cycle-to-cycle variations at idling and partial loads. Stratified mixture is formed by retarding fuel injection close to compression stroke, in which there is more fuel near the spark plug than the remaining parts of the combustion chamber. Rich local mixture near the ignition position results in high ignitability and leaner mixture near cylinder wall in stratified mixture reduces the level of knock limitations and allows for higher compression ratio to improve engine thermal efficiency. In addition, this technology permits the reduction in pumping loss by removing the need for throttle valve at partial loads which results in higher engine performance. Therefore, in absence of throttle valve, stratified direct injection engine can control the engine power by varying the amount of injected fuel [44–46].

Mixture formation by direct injection strategy reduces the BSFC about 20% to 40% less at partial loads and gives a better control of the pollutant emission with respect to pre-mixed systems. But it demands higher requirements of the whole system than pre-mixed fueling systems, such as CNG supply and injector systems. Many design parameters including compression ratio, combustion chamber geometry, rail pressure and turbulence intensity can affect the air-fuel mixture preparation for DI system. Still, application of DI technology to CNG engines is difficult and costly due to the cooling and lubricating problems of CNG DI injectors and optimization strategies must be investigated to maximize the CNG DI engine performance. Moreover, experiments proved that optimizing the charge stratification for DI gas engines has been hard to achieve [47–49].

1.3.2 Mixer type single-point injection (SPI)

The first type of pre-mixed fueling system is single point. The first generation of SP system was made of mechanical gaseous fuel mixer (carburetor). By introducing electronically controlled injector as a precise fuel metering component, the second generation of SP systems could achieve better mixture quality by injecting fuel at throttle body and before the throttle valve. The more complete type of SP fueling system was designed by coupling the throttle body injection with mixer. Homogeneous mixture of CNG and air before the air flow-splits of the intake manifold can be achieved by mixer type single point injection system. This electronically controlled CNG fuel metering system includes one or more injectors or fuel metering valves and a mechanical fuel mixer. The main advantage of this system is precise control of amount of injected gas with minimum number of injectors [50]. Fig. 1.10 shows the engine map equipped with SPI system.

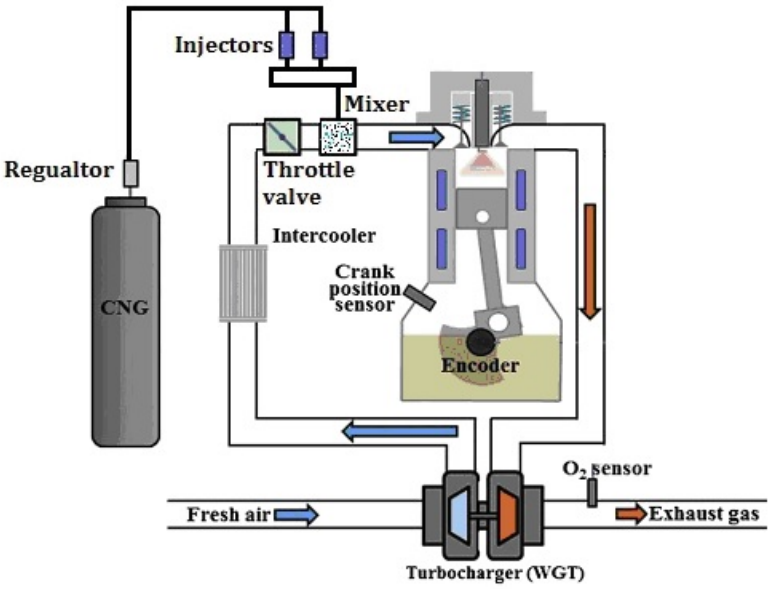

Fig. 1.10 Turbocharged CNG engine map equipped with mixer type single point injection

Mixer type SPI system is considered to prepare identical uniform air-fuel mixture composition for each cylinder. However, for multi-cylinder engines, individual intake manifold runner and port geometries can affect the flow pattern which results in cylinder-to-cylinder variations. Especially for turbocharged engines with high pressure intake air passing through the mixer, it becomes difficult to achieve an appropriate homogenous mixture of air and CNG. The amount of mixture received by each cylinder can be different depending on the geometry of intake system. For example for in-line cylinder

configuration, the outermost cylinders have lower efficiency than the other cylinders [51]. Moreover, small valve overlap angles are designed in SPI natural gas engines to avoid the escape of mixture during valve overlap and abnormal combustion in exhaust port. Therefore, exhaust gas temperatures increase with small valve overlap and result in higher heating loads on engine components [52].

1.3.3 Intake port multi-point injection (MPI)

Since early 1990s, almost all the SI engines for passenger cars have been equipped with Electronic Fuel Injection (EFI) systems. The carbureted fueling system was replaced with EFI system to comply better with stringent emission regulations. Sequential port fuel injection (or multi-point injection) technology was employed to retain the proper air-fuel mixture by maintaining the air-to-fuel ratio close to the target value defined by computer-controlled engine management system (EMS) [53].

In MPI fuel injection system, fuel is injected upstream of the intake port by one or more injectors for each individual cylinder. Fig. 1.11 shows the schematic of MPI system including the position of injector for SI engines. The EMS controls the air-to-fuel ratio path by implementing fast forward control in addition to feedback action for steady-state accuracy.

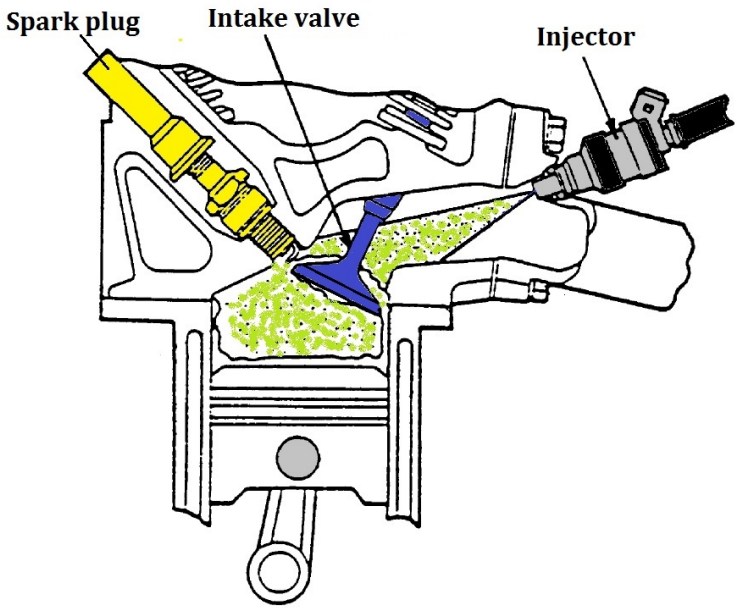

Fig. 1.11 Spark ignition port fuel injection mixture preparation system [38]

In MPI injection strategies, the injection pulse width is calculated by using proportional-integral (PI) feedback controller plus look-up tables based on engine speed and air-mass flow rate sensor mounted upstream the throttle valve or manifold absolute pressure (MAP) sensor mounted in intake manifold. To generate these look-up tables, empirical static dynamometer tests have to be performed for large number of load/speed regimes. The controller compares the oxygen concentration in the exhaust gas, detected by the signal from oxygen sensor and representing the air-fuel ratio of the mixture, with the reference value and regulates the amount of fuel to be injected [54]. Fig. 1.12 shows the schematic diagram of MPI system with closed loop lambda control.

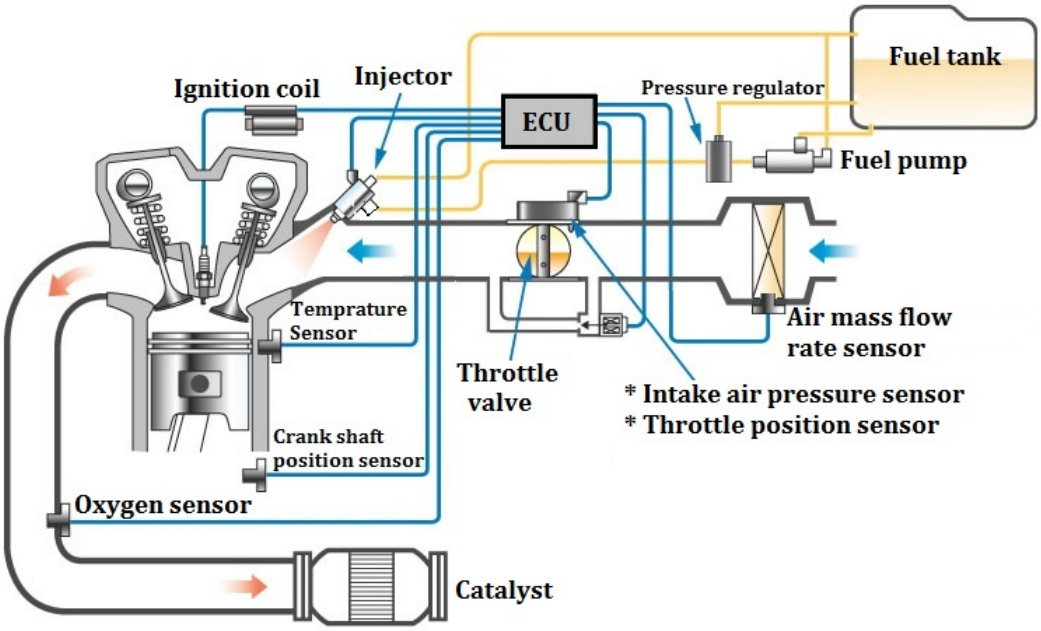

Fig. 1.12 Schematic diagram of MPI system with closed-loop lambda control [53]

MPI system gives better control of mixture formation and response to load/speed transient operations and hence better performance with respect to carburettor-type engine [52, 55]. In addition, low pressure fuel system hardware makes the MPI system simpler than the DI system which requires sophisticated fuel injection hardware and more complex engine control system. Besides, DISI engines contribute to higher levels of unburned hydrocarbons and particulate emissions compared to MPI SI engines [56, 57].

Using CNG as fuel avoids the fuel metering error of MPI system associated with fuel wall wetting in the intake port for gasoline engines. During last twenty years, MPI system has been proposed and developed by many car manufacturers for light duty CNG engines. Still, most of heavy duty CNG engines use mixer type SPI systems which have nearly

reached the limit of the potential of the system. Since MPI is relatively easier to implement and it can provide the opportunity to overcome the problems related to mixer type SPI system, it is feasible to employ MPI for heavy-duty CNG engines. Moreover, with MPI system it is possible to use more advanced injection strategies such as fire skipping (or cylinder deactivation) and accurate injection timing after valve overlap, to inject CNG only in intake stroke just after valve overlap and prevent the escape of mixture during the overlap, at low loads. Injecting fuel toward the end of intake stroke facilitates the temperature reduction in potential hot spots responsible for back-firing in intake port [52, 58, 59].

To improve the performance of a MPI heavy duty CNG engine, there is the need to use advanced injection strategies and optimize different engine parameters. For example, to better maintained cylinder equality for MPI engines an optimised intake manifold is required. High turbulence combustion chamber designs, dedicated to MPI CNG engines, are useful to achieve high quality air-fuel mixture and improve the engine performance [60]. Charge stratification in MPI engine can be realized by tuning the intake ports using swirl port combined with straight port and optimizing the injector position [61]. In addition, optimized design of injector nuzzle holes geometry improves the air-fuel mixture preparation. Fuel injectors with multi-hole geometry provide optimum air-fuel mixtures and increase the volumetric efficiency of MPI CNG engines. So MPI system eliminates the undesired back-fire phenomena [62].

1.4 Fuel injection characteristics of MPI spark ignition CNG engines

Precisely controlled air-to-fuel ratio can be achieved by developing MPI CNG engines. To this end, design and development of dedicated rail, pressure regulator and CNG injectors are required. Fuel metering system of MPI CNG engines consists of high-pressure gas cylinder to supply CNG. Passing through the pressure regulator, the pressure of gas reduces to 7-10 bars. Then gas is supplied to each injector by means of gas rail. The engine electronic control unit (ECU) controls the amount of fuel injection by each injector (Fig. 1.13). ECU collects the signals from different sensors for the various engine operation conditions and calculates the amount of gas to be injected at different load/speed condition [63, 64].

For the stoichiometric CNG engines with 3-way catalyst, it is critical to minimize the variation of instantaneous air-fuel-ratio and keep it within a narrow band centered on

stoichiometric condition. Carefully optimized ECU control maps along with precisely designed and configured fuel injection system components make it possible to employ MPI system for dedicated CNG engines [65].

Due to the strong influence of fuel injection system on engine combustion and performance, realistic investigations on hydraulic components (i.e. injectors, rail and pressure regulator) and control equipment must be realized. Therefore, modeling and simulation of the injection system in early phase of design process, provides a reliable view of the physical system and improves the integration of the mechanical subsystems and the controller. In addition, detailed models help to diagnose the system faults and investigate different system configurations [66]. In the following subsections the most important design challenges for MPI system are listed and briefly discussed.

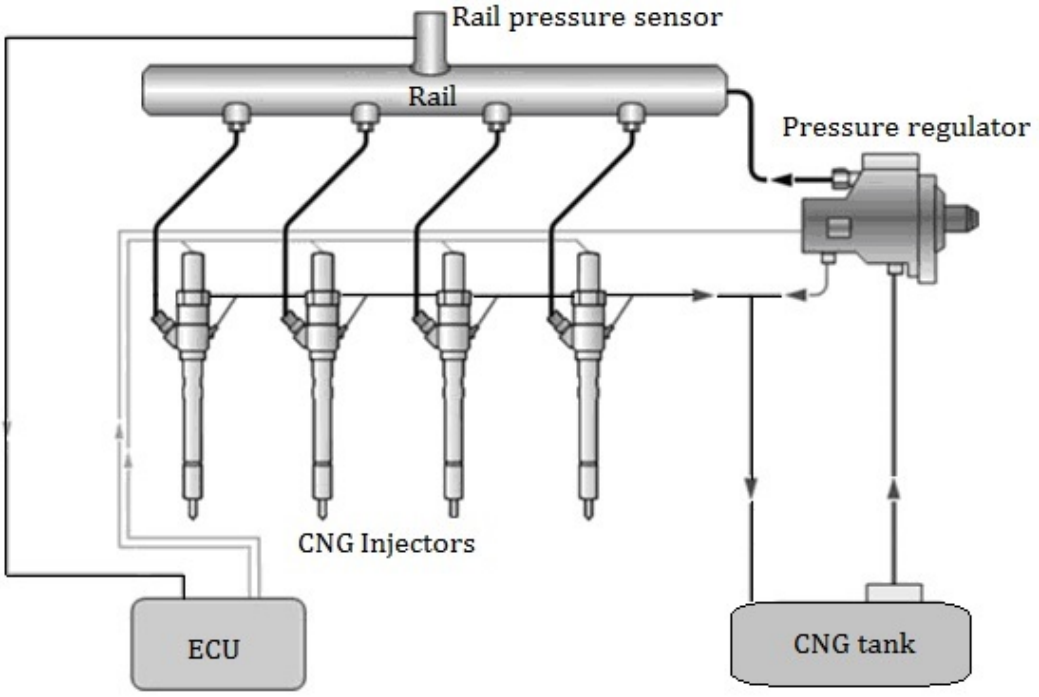

Fig. 1.13 A block scheme of MP CNG injection system

1.4.1 CNG injection system components

The main elements of CNG MPI system are: a high pressure fuel tank, a pressure regulator and the fuel metering system consisting of rail and CNG injectors. Unlike diesel and gasoline engines, in which the fuel is stored at atmospheric pressure and pumped to

the rail, CNG MPI system doesn't require high pressure or low pressure compressor to transport the fuel to rail. As a matter of fact, CNG is safely stored at high pressure (up to 200 bars) in fuel tank, and the pressure regulator reduces the gas pressure down to 7-12 bars and sends it to the rail. Engine coolant heats up the pressure regulator to prevent the fuel system from freezing due to sudden temperature reduction caused by gas expansion [67].

Pressure reducing valve is an important element of CNG MPI system which guarantees a constant pressure of the rail by minimizing the pressure oscillations. The pressure regulator includes two chambers: the main chamber and the control chamber. The volume and inflow section of the main chamber depends on the axial displacement of piston, placed between the two chambers, integral with a spherical shutter. Equilibrium of the flow drag force, pre-loaded force of shutter spring and forces generated by the pressure of the gas stored in the main chamber, control chamber and fuel tank, determines the dynamics of piston and shutter. The pressure of the control chamber is regulated by the solenoid valve. By energizing the solenoid valve more gas enters in control chamber and as a result increases the pressure on upper surface of the piston. The direction of the resulting force is downward and pushes down the piston with the shutter to open the shutter of the main chamber. So, it permits the gas to flow through the main chamber toward the rail. On the contrary, when the solenoid valve is closed, the pressure on the upper surface of the piston decreases and the pre-load force of shutter spring raises the piston along with shutter and prevents the gas to flow into the main chamber by closing the shutter (Fig. 1.14) [68, 69].

Common rail injection system technology firstly was introduced for diesel engines [66]. The common rail, which is a steel manifold capable of keeping the fuel at high pressure, plays the main role in this technology. All the injectors are connected to the common rail and the large volume of rail is useful to damp the pressure oscillations generated by injection operations. More precise fuel metering can be achieved by optimized design of rail volume along with electronic control of rail pressure. The injection flow rate depends on the rail pressure and injection timings defined by ECU. With lower rail pressure the fuel mass flow rate decreases and as a result injection window must be increased for requested amount of fuel mass. Longer injection durations, due to lower rail pressure, result in enhancing better air-fuel mixing rate at high engine speeds. On the other hand, since the prolonged injection event mainly occurs during the intake stroke, the volumetric efficiency decreases for low engine speed. Then, the engine performance can be optimized by precise controlling the rail pressure [70, 71].

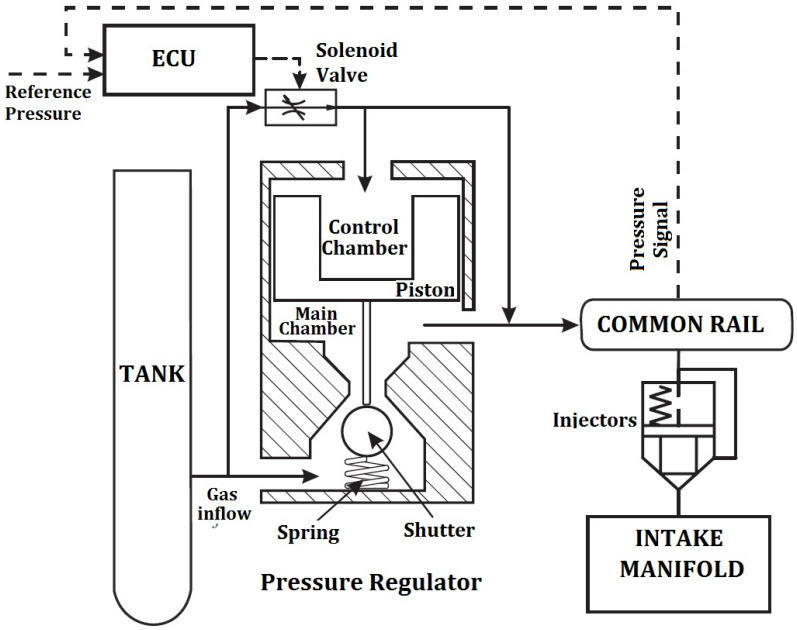

Fig. 1.14 Block scheme of pressure regulator for CNG MPI system [68]

Electrical solenoid injectors commonly used for CNG injection system are composed of mechanical part which is ball valve or needle operated by electrical part which is solenoid. Gaseous fuel injectors are developed considering different design aspects from gasoline injectors. Impact forces produced by moving parts of solenoid injectors cause wear and loss of calibration. Unlike the liquid fuels, gaseous fuels have lower impact damping and lubrication properties. Therefore, specific attention needs to be paid to design requirements of CNG injectors such as: impact damping, self-lubrication and enlarged injector nuzzle size [72].

To reduce the impact forces generated by bouncing of needle on its seat two types of injector driver strategies can be employed for CNG injectors: peak and hold driver and pulse interruption driver. Peak and hold injection strategy can prevent the needle bounces by using optimal peak voltage to keep the needle in closed position and the hold voltage to control its movement toward the open position (Fig. 1.15 a). While, the pulse interruption strategy divides the pulse module in two pulses; first pulse is needed to move the needle toward the open position without bouncing and the second pulse maintains the needle in the open position (Fig. 1.15 b) [73].

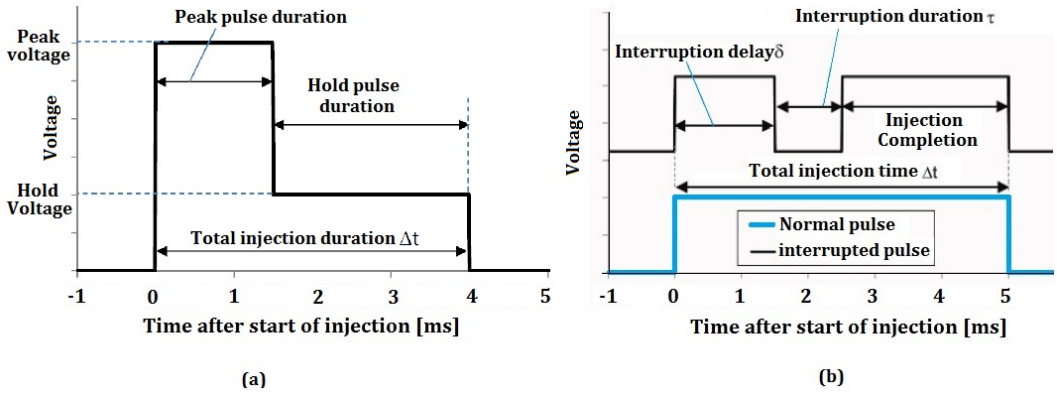

Fig. 1.15 injection strategies: (a) Peak and hold, (b) pulse interruption [73]

1.4.2 CNG injection modeling and control

The CNG engine control issues associated with MP injection system are similar to those of gasoline engines and both of the systems can be described as multi-input/multi-output (MIMO) structure (Fig. 1.16). A key factor to be controlled in CNG engine is the accurate amount of gas to be injected toward the appropriate air/fuel mixture. The conventional control strategies to control air-to-fuel ratio are designed based on static maps with proportional-integral (PI) controllers. These strategies are costly and time consuming due to the required calibration experiments [74, 75] Moreover, calibration processes for the new generation of internal combustion engines became more complicated because of their high degree of freedom which has been increased constantly during last decade. For instance, 20,000 calibration labels for a typical SI engine ECU are considered in 2012, which are four times more than the number of calibration labels for 2005 SI engine technology [76].

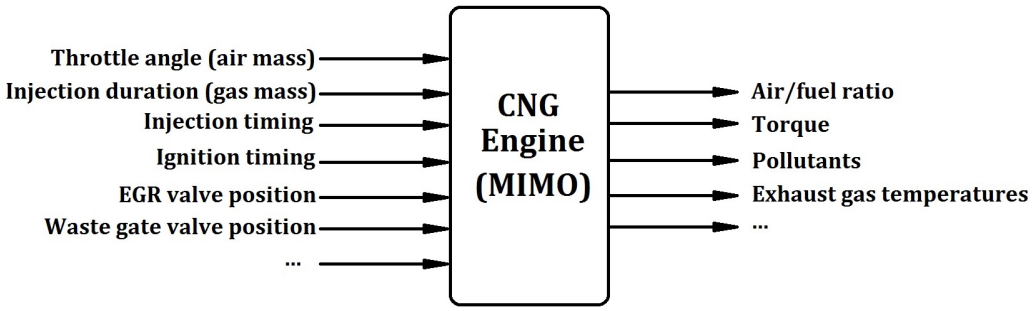

Fig. 1.16 CNG engine as MIMO system [74]

One solution for this problem is to employ “Virtual calibration”. Virtual calibration of functions in ECU can be accomplished by “modelling and simulation” to validate noble control strategies and to parametrize the data maps for optimal engine operations. To this end, accurate models of injection control systems can be developed by trading off between accuracy and simplicity of control system. For instance, to improve the control performance of CNG engines with less calibration efforts, intelligent control strategies such as fuzzy control and neural networks have been investigated. The Neuro-Fuzzy control approach can provide reliable results in identifying and controlling non-linear dynamic systems composed of several linear controllers retained by fuzzy clustering engine operating region [77, 78].

For engine simulations, physically based models including medium to high detailed engine models are preferred. In physically based model the important engine behaviours are presented by physical equations and the model is capable of reproducing or predicting the engine‘s behaviour.

Table 1.2 presents the different modelling types distinguished by their degree of spatial resolution. Non-dimensional models review the integral states without physical knowledge and consider neither absolute coordinates nor time scales of process. Simple mathematical algorithm of non-dimensional models makes them capable of fast calculations of the ECU. Zero-dimensional (0-D) models are mostly used for the thermodynamic and heat transfer analysis. State variables such as thermodynamic volume which describe the system status are assumed to be homogeneous and time dependent in the system boundaries in 0-D models. One-dimensional (1-D) models are suitable for wave propagation related and acoustic problems. These models are able to solve the continuity, momentum and energy equations for wave related engine phenomena such as engine intake and exhaust flow processes. Finally, three-dimensional (3-D) models by employing computational fluid dynamics (CFD) methods are able to calculate thermodynamics and turbulence at every component of the engine. 3-D models can evaluate complex fluid mechanics interactions and their reaction kinetics, but they need extensive expert knowledge and long computational time. Therefore, low-dimensional models are more practical to simulate a complete range of engine variability [79].

It is viable to select appropriate physical variables to develop an efficient predictive model. Although the control issues of MPI system for CNG and gasoline engines are much the same, there are minor differences between two systems which have to be considered when designing the engine control system. Two main features of MPI CNG engines which are not relevant in MPI gasoline engines are:

Table 1.2 Modelling properties of engine processes and feasible applications

Model	Detail level	Factor to Real Time	Application
Non-dimensional	Low	1 (real-time)	Real Time Neural network modelling
0-D	Medium	50-100	Combustion modelling/ analysis
1-D	Medium-high	100-1000	Gas exchange modelling/ analysis
3-D CFD	Very high	+10,000	Flow/ combustion modelling

1. Torque and pollutant production is dependent on injection timing due to charge stratification phenomena by injecting gas while the intake valve is open.
2. Occurrence of mixture backflow which causes the transport of charge back into the manifold.

By means of mean-value models and application of feedforward controllers, it is possible to damp the torque variation oscillation during transients. These models are able to identify the effect of mixture backflow and realize fast air/fuel ratio changes [80].

As far as the CNG engine is concerned, ECU has to drive the injectors based on the required load/speed and regulate the rail pressure by driving electro-mechanical pressure regulator. Accurate control of gas injection is possible by controlling both the rail pressure and the injection duration. In order to model the CNG injection system, the whole system can be represented by interaction of control volumes in which gas flows and the pressure distribution is uniform and time varying. The state variables of the system can be defined as: the pressures in main and control chamber of pressure regulator, the pressure in rail and pipes, the position and velocity of moving parts of the system. By applying the fundamental laws of ideal gas, the continuity and momentum equations, the Newton's second law, etc, a state-space model can be derived.

In literature it has been shown that the model-based control strategies are efficient and reliable to regulate pressure in common rail injection systems [81, 82] Therefore, in order to achieve an appropriate design of CNG injection control module, additional efforts is necessary to develop more precise and detailed models and investigate new injection control algorithms. 1-dimensional simulation of CNG injection system can help to gain a deeper insight into the behaviour and optimization of the system [83–85].

1.5 Research formulation

The previous sections summarized the characteristics of SI CNG engines along with the challenges regarding the application of multi-point injection system to SI CNG engines in the current state of technology. This research work studies in depth two fundamental issues related to application of MPI system in heavy-duty CNG engines:

1. Detailed fluid dynamic characterization of the MPI system to further enhance the understanding of the system which leads to achieve an appropriate design of injection system components and related control modules,
2. The conversion of traditional heavy-duty CNG engines equipped with SPI system to MPI system due to the difference between the SPI and the MPI injection systems on mixture formation, cycle-to-cycle variation and cylinder-to-cylinder variation.

The research project and therewith this thesis, investigates the two mentioned issues in three main chapters:

Chapter two of this work is focused on the development, calibration and application of a MPI CNG injection system model, by using AMESim simulation tool. Simulations and experiments on a two-cylinder CNG engine have shown interesting consistency of the 1-D injection system model with real one. The model calibration phase highlighted the intimate bond between the excitation driven by the injection events and that produced by the pressure regulator functioning. The two excitations determined the instantaneous pressure time history in the injection rail and assessed for the wave amplitude and frequency.

Chapter three aims at developing a thorough model of the pressure reducing valve which significantly contributes to fully defining dynamic response of the MPI injection system. The pressure reducer is made up of various elements that retain diverse weights on the valve behavior and should consequently be differently addressed to. The research has been focused on defining the set of parameters to be precisely reproduced in the 0D-1D simulation so as to match the injection system experimental behavior. A refined model of the pressure reducer has hence been proposed and the model has been calibrated, tested and run under various operating conditions so as to assess for the set-up validity.

Chapter four deals with the development of a dedicated 7.8 liter, heavy duty CNG engine equipped with two different injection systems: Multi-Point (MP) and Single-Point (SP). The research has been carried out by modelling the engine within the 0D-1D, GT-Power, environment in order to match precisely the experimental behaviour of the engine

and to carry out a thorough comparison of the two injection systems under steady and transient conditions. The difference between the Single-Point (SP) and the Multi-Point (MP) injection systems on mixture formation, cycle-to-cycle variation (CoV) and cylinder-to-cylinder variation was studied. The numerical and experimental results assessed for a relevant influence of the dynamic behaviour of the system in terms of pressure waves on the mixture formation and hence on the engine performance.

Chapter 2

Fluid-dynamic Modeling of a CNG MPI System

* *Part of the work described in this chapter has been previously published in: Misul, D., Baratta, M., and Kheshtinejad, H., Fluid-Dynamic Modeling and Advanced Control Strategies for a Gaseous-Fuel Injection System, SAE Technical Paper 2014-01-1096, 2014."*

2.1 Introduction

The conversion of a traditional gasoline SI engine to CNG operations requires major modifications on the fuelling system [86]. The first generation CNG fueling systems exploited a simple mixer system. Still, they resulted in excessively low engine volumetric efficiencies and relatively poor engine performance. Port injection and direct injection systems were hence considered in order to boost the CNG advantages. Port injection systems proved to reduce the CNG engine output by 10 to 14% with respect to production gasoline engines [87], as compared to the 10 to 30% power reduction induced by the mixer systems. Still, in order to improve the performance, emission and durability of a dedicated CNG engine, different engine parameters need to be properly optimized and advanced injection solutions have to be adopted [64, 72, 88]. Moreover, the injector has to be properly designed to guarantee the required amount of fuel, given the CNG lower density with respect to gasoline. CNG requires higher injection durations with respect to gasoline and injection generally takes place while the intake valves are open [80].

The common rail (CR) injection system technology exploited for CNG injection was originally introduced for diesel engines in order to meet the international regulation

by properly reducing the engine pollutant emissions as well as to satisfy the customer requirements for improved performance. The key device of this system is the common rail, i.e. a steel manifold where the fuel is kept at high pressure. The electronically controlled high pressure fuel injection system holds an important role for the emission control strategy as well as for the enhancement of the engine performance [66, 89, 90]. High pressure injection allows for finely atomizing the fuel spray, thus promoting the fuel-air mixing and resulting into significant combustion improvements [91, 92]. The control of the injection pressure hence plays a fundamental role for both SI and CI engines [80, 93]. Considerable R&D activity was carried out to further investigate into the effects of the pressure variations on the CNG injection system performance [94, 86, 88, 95, 96]. For a given amount of fuel mass, a lower rail pressure results in an increased injection window. Thus, injection mainly occurs during the engine intake stroke and the volumetric efficiency is reduced. This in turn leads to degraded power outputs at speeds for which the volumetric efficiency appears to be the key factor in determining the engine performance [87]. Conversely, high speed performances are controlled by the air-fuel mixing rate, this latter being enhanced by the longer injection duration induced by the lower rail pressure.

The injector rail acts as a dampening volume for the pressure oscillation induced by both the injection events and fuel supply from the tank line. The rail pressure transients can affect the injection behaviour and flow rate conditions for different engine cycles [97, 98]. It is worth observing that the ratio of the pressure upstream to the pressure downstream from the injector turns out to be lower with respect to the critical expansion ratio for CNG. Thus, the injected mass flow rate keeps constant for a given rail pressure whereas the injected fuel mass can be metered simply acting on the injection energizing time (ET). The pressure pulsation in the rail hence needs to be considered when defining the proper strategy to control the injected fuel. Electro-hydraulic valves [66] and pressure regulators [99, 100] are currently adopted to regulate the rail pressure and to compensate for the pressure oscillations. Precise and reliable fuel injection system appears to be mandatory to improve the fuel economy and to enhance the engine behaviour [86].

To that end, a thorough fluid-dynamic characterization of the natural gas injection system is strongly recommended if an appropriate design of the related control module and devices is to be achieved. In order to gain a deeper insight into the topic of 1-D simulation of the natural gas injection system, the present chapter is focused on the development, calibration and application of a CNG MPI system model. Simulations and experiments on a two-cylinder CNG injection system have shown an interesting consistency of the 1-D model to the real system.

2.2 CNG MPI system layout

The experimental set-up was designed so as to closely reproduce the outline of the on-board injection system. Compressed natural gas is stored at a pressure ranging around 200 bar in purposely designed tanks located either in the car boot or sited undercarriage of the vehicle. The gas cylinders are designed according to the ISO safety standard (ISO 11439:2013) which set the need for high-strength materials designed to withstand impact. The cylinders also display pressure relief devices so as to provide a controlled venting of the gas in case of fire. The increase of temperature induced by the flame would in fact produce a dangerous pressure build up that would otherwise lead to the cylinder explosion. Given the high stresses it undergoes, the cylinder demands a robust design and hence significantly contributes to the vehicle weight. The introduction of new high performance materials such as glass fiber composites allowed for a reduction of the cylinder weight down to a 60% thus making it suitable for automotive applications.

The compressed natural gas is delivered to the engine by means of a pressure regulator which reduces the gas pressure down to 9 bar. The valve is equipped with a filter to purge the impurity in the gas stream and plays a key role in the injection system functioning. The regulator should in fact guarantee a constant pressure to the rail independently of the supplied flow rate by reducing the pressure oscillations to a minimum. Due to the high pressure drop that the fluid experiences as it flows through the regulator, the temperature sensibly downfalls, thus introducing the need for a secondary heating circuit directly derived from the engine heating system.

The low pressure gas is hence delivered to the rail and to the injectors by means of a steel pipe and a hose. The injector phasing and timing is controlled by the engine ECU in order to provide the engine cylinders with the right amount of fuel so as to make the pollutant emission treatment possible. To that end, the fuel delivery pipe normally features a temperature sensor and a pressure transducer that supplies the inputs required by the ECU control strategies. The injection timings mapped in the ECU are consequently adjusted according to the average rail pressure and temperature in order to compensate for the injected fuel mass [6]. The use of averaged quantities in order to account for the system dynamic behavior inevitably introduces a mismatch between the ECU estimations and the actual amounts of fuel injected. The present chapter aims at investigating into the dynamic behavior of the system with specific reference to the pressure waves that arise in the rail during normal engine operation and that lead to a feeble control of the injected mass.

2.3 Experimental set-up

The experimental campaign has been carried out at the CRF (Centro Ricerche Fiat) laboratories. The bench layout has been designed so as to reproduce the on-board storage and supply for a 2-cylinder engine. The system is made up of a high pressure cylinder connected to the injection system by means of a pressure regulator (Fig. 2.1). The main specifications for the tested injection system and the engine it equips are reported in Table 2.1.

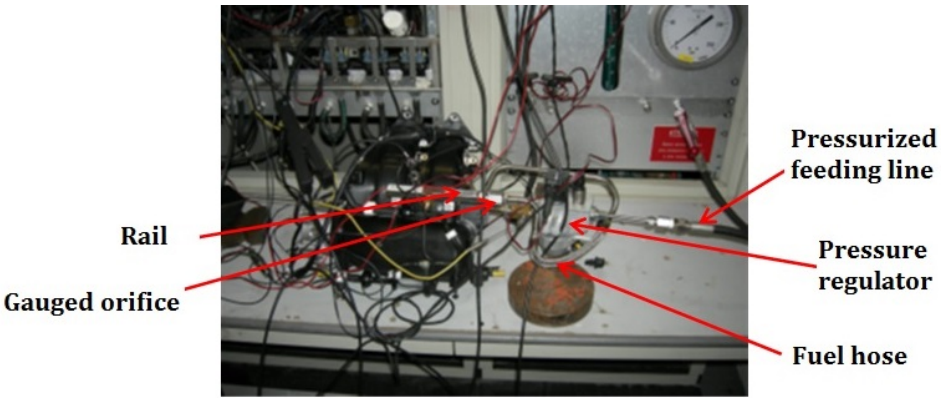

Fig. 2.1 Experimental set up: pressure regulator and injector rail.

Table 2.1 Test engine and related injection system characteristics

Specifications	**Value**
Bore	80.5 mm
Stroke	86 mm
Compression ratio	10
Cylinder number	2
Displacement	875 cm^3
Injection system type	MPI
Maximum injection pressure	12 bar
Injector manufacturer	METATRONIX
Regulator manufacturer	BOSCH

The test rig is equipped with: a mass flow meter, a high-frequency pressure transducer and a thermocouple sited downstream from the regulator; a high-frequency pressure sensor located in the fuel rail and a current probe to precisely determine the injectors

opening and closing commands. The ECU control parameters have been in time adjusted so as to reproduce and meet the equivalent engine operating conditions. Different tests have been carried out so as to thoroughly characterize the injection system:

- **Static run:** the injector is kept wide open for the full test duration and gets fed with a constant rail pressure. The experimental test was meant to verify the nozzle cross section and discharge coefficient as well as to provide the model with the data to properly describe the injector nozzle.
- **Single injection:** the injector is opened once at the beginning of the test and attention is paid to the system free response. The case was used to check on the injection system characteristic frequencies and damping factor.
- **Multiple injection or dynamic run:** the injectors were driven by the ECU so as to reproduce the actual injection phasing and timing that would correspond to a given engine speed and load.

Table 2.2 Experimental runs on steady state points data set.

Case number	**Speed** [RPM]	**ET** [μS]	**bmep**[bar]
1	1100	4000	1
3	1100	5000	3
5	1100	8000	6
8	2300	4000	2
10	2300	6000	4
14	2300	14000	12
16	3000	4000	1
18	3000	5300	3
21	3000	10000	7.5
24	3000	14000	12

For all of the cases, the pressure signals have been acquired at a frequency of 3200 Hz. The tests have been carried out using air instead of CNG and the injectors discharged the pressurized fluid in the open air at a pressure of 1 bar. The experimental data set for the dynamic run here consists of 10 points at different loads and speeds, as depicted in Table 2.2. The engine outputs as well as the model results have been normalized to those pertaining case 10 due to a confidentiality agreement.

2.4 CNG MPI model

2.4.1 Introduction to AMESim 0D-1D modeling environment

AMESim is modeling and simulation software, runs on UNIX platform and developed by LMS International for analyzing 1-dimentional systems. AMESim permits to model and analyze multidisciplinary systems using the components available in the AMESim libraries. AMESim as an engine simulation package solves 1-D compressible Navier-Stokes equation consisting of equations for laws of conservation of momentum, mass and energy in direction mean flow in order to fully describe the fluid flow. 1-D simulation software give the possibility to study and analyze the mass and energy flows through individual engine components and work and heat transfer within each component.

Conservation of mass is calculated as the rate of change in mass within a subsystem which is equal to the difference between the sum of inlet mass flow rate and outlet mass flow rate from the system $\frac{d_m}{d_t}$:

$$\dot{m}_{sub} = \sum_i \dot{m}_i - \sum_e \dot{m}_e \tag{2.1}$$

In 1-D flow the mass flow rate is defined by:

$$\dot{m} = \rho AU \tag{2.2}$$

Where ρ is the density, A is the cross-sectional flow area and U is the fluid velocity. Conservation of energy is defined as the rate of change of energy in a subsystem which is equal to the sum of the system energy transfer which can be written in the following from:

$$\frac{DE}{Dt} = \frac{DW}{Dt} + \frac{DQ}{Dt} \tag{2.3}$$

Where E is the Energy, W is the work and Q is the heat. The above formula results in:

$$\frac{d(me)}{dt} = P\frac{dV}{dt} + \sum_i \dot{m}_i H - \sum_e \dot{m}_e H - h_g A(T_{gas} - T_{wall}) \tag{2.4}$$

Where e is the internal energy, H is the total enthalpy, h_g is the heat transfer coefficient, T_{gas} and T_{wall} is the temperature of the gas and wall respectively. To calculate the heat transfer from the internal fluids to the pipe and flow split walls, it is necessary to have the heat transfer coefficient, the predicted fluid temperature and the internal wall temperature. The heat transfer coefficient is function of fluid velocity, thermo-physical

properties and the wall surface roughness and is calculated every time step. The user defines the internal wall temperature.

$$h_g = \frac{1}{2} C_f U_{eff} C_p Pr^{-\frac{2}{3}} \tag{2.5}$$

In this equation C_f is the friction coefficient, U_{eff} is the effective speed outside boundary layer, C_p is the specific heat and Pr is the Prandtl number. The friction coefficient is related to the Reynolds number as follows:

$$Re = \frac{\rho U_c L_c}{\eta} \tag{2.6}$$

Where ρ is the density, U_c is the characteristic speed, L_c is the characteristic length and η the dynamic viscosity. The friction coefficient for smooth walls is given by:

$$C_f = \frac{16}{Re_D} \tag{2.7}$$

$$C_f = \frac{0.08}{Re_D^{0.25}} \tag{2.8}$$

In the region with $Re_D < 2000$, the equation 2.7 is used whereas equation 2.8 is used in the region where $Re_D > 4000$ with a linear transitional region in between. The Prandtl number is:

$$Pr = \frac{\eta C_p}{\lambda} = \frac{\nu}{a} \tag{2.9}$$

Where η is the dynamic viscosity, C_p is the specific heat, λ is the heat conduction coefficient, ν is the kinematic viscosity and a is the thermal diffusivity. In case of rough wall surface in which the flow is not laminar, the value of the friction coefficient above is given by Nikuradse's formula:

$$C_{f(rough)} = \frac{0.25}{(2\log_{10}\frac{D}{2h} + 1.74)^2} \tag{2.10}$$

Where D is the pipe diameter and h is the roughness height. If necessary, the friction attribute in pipes and flow splits can be used to scale the calculated friction.

For conservation of momentum, the net pressure forces and shear forces of wall acting on a sub system are equal to the rate of change of momentum in the system:

$$\frac{\dot{m}}{dt} = \frac{dpA + \sum_i \dot{m}_i u + \sum_e \dot{m}_e u - 4C_f \frac{\rho u^2}{2} \frac{dxA}{D} - C_p(\frac{1}{2}\rho u^2)A}{dx} \tag{2.11}$$

Where u is Fluid velocity, C_f is the friction loss coefficient, D is the equivalent diameter, C_P is the pressure loss coefficient and dx is the element length. Empirical correlations are used by 1-D simulation software to obtain the correct pressure and friction loss coefficients by considering the pipe curvature and surface roughness. The pressure loss coefficient is calculated as follow:

$$C_{presuure} = \frac{P_1 - P_2}{\frac{1}{2}\rho V^2} \tag{2.12}$$

Where P_1 is the inlet pressure, P_2 is the outlet pressure, ρ is the density and V_1 is the inlet velocity. When the model is constructed, the equations to be solved are generated representing physics of the components modeled in the system. The flow through the system is solved using the above mentioned 1D Navier-Stokes equation.

In the 1D simulation software the whole system is divided to the smaller pieces of volumes. Scalar physical properties of each volume like pressure, temperature, density etc. are considered to behave uniformly. The volumes are connected to others by boundaries. The equation for continuity, momentum and energy are solved one dimensionally. So the values across an area of the flow direction are averaged values. The scalar quantities are calculated at the center of subsystem. While, the vector quantities (mass flux and mass flux fractions) are calculated at the subsystem boundaries. An explicit method is used for time integration to govern the equations. Considering the $Y(t)$ and $Y(t+\delta t)$ the current state of the system and its state at the later time respectively, the explicit method is:

$$Y(t+\delta t) = F(Y(t)) \tag{2.13}$$

Using small time steps, the flow is reached by explicit time integration of the equations for energy, momentum and continuity. Courant condition limits the time step during this integration, which restricts the time step to be less than 0.8 of the time required for the pressure and flow to propagate across any discredited volume:

$$\frac{\delta t}{\delta x}(u+c) \leq 0.8 \tag{2.14}$$

Where δx is the discretized length, δt is the time step,, u is the fluid velocity and c is the speed of sound. According to the relation of time step and discretization length, smaller discretization length results in slow execution of the software.

AMESim has high level post processing capability. Batch run capability of AMESim is useful to study the influence of certain parameters in the system. The number of

simulation runs depends on the number of batch parameter and the step size of the batch parameters. When an engine needs to be modeled with a great level of detail, the 1-D CFD library can be used by user. And when the system does not need great detailing, IFP-engine library can be used. The user can choose the level of detailing in the simulation model by defining the discretization length, which is limited by the size of time step [101].

2.4.2 Model description

The injection system has been modeled at ICEAL (Internal Combustion Engines Advanced Laboratories) of Politecnico di Torino using the AMESim code. An outline of the model is reported in in Fig. 2.2. The model has been built according to the geometry marked by the technical drawings from the injection system supplier. Each system component has been properly characterized in terms of its specific geometric features such as length, diameter, bend radius, etc. Moreover, joints and connections have been carefully designed so as to account for the concentrated losses induced by the sudden changes in the flow section. The distributed losses have in turn been estimated by suitably setting the pipes surface roughness. As depicted in Fig. 2.2, the system downstream from the pressure regulator is made up of:

- a steel bending pipe;
- a steel fuel hose;
- the injectors rail;
- the CNG injectors.

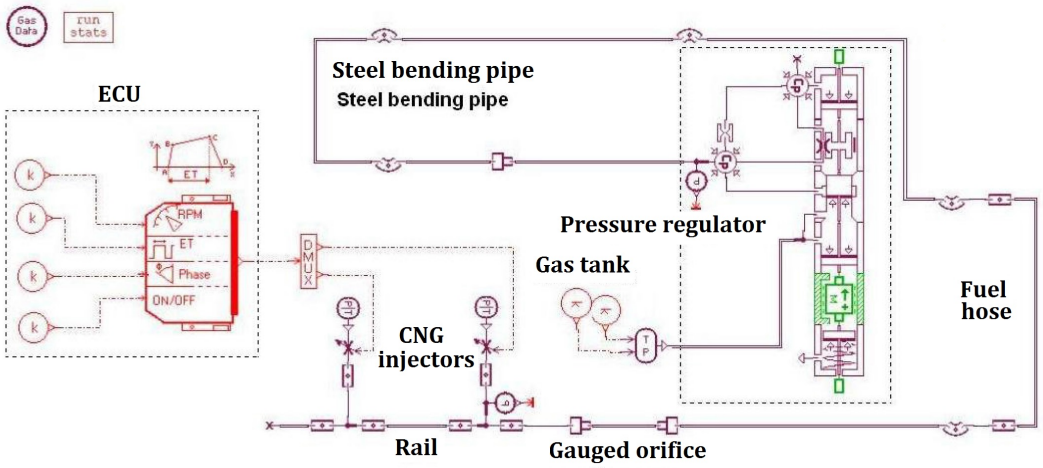

Fig. 2.2 Model map of the CNG injection system.

The pressure regulator was modeled by using the 'Pressure Regulator' component from the standard code library. The CNG is supplied to the valve through port P whereas the regulated pressure outcomes from port A. The pressure at port A is also derived to a pilot line to control the spool position (Fig. 2.3). The model embeds the representation for the springs as well as for the fluid passages and an equivalent mass is used to account for the inertial effects. Y represents the drain to the reservoir.

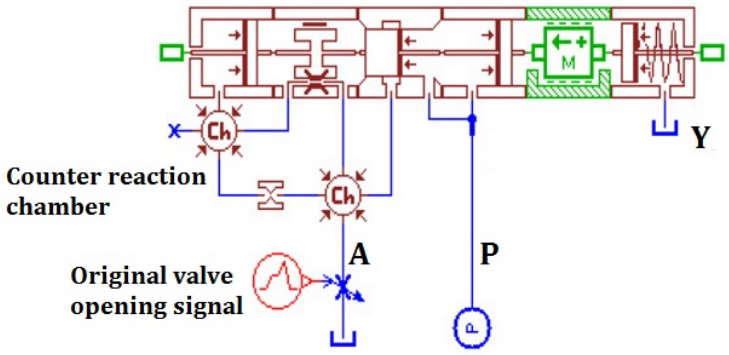

Fig. 2.3 Pressure regulator model.

Since a thorough and detailed fluid-dynamic simulation of the injection system was required and given the impact of the injector fluid-dynamics on the system behavior, the injector has been represented by means of a pipe coupled with a gauged orifice. The former is meant to simulate the fuel path inside the injector body whereas the latter represents the injector outflow cross section. The orifice diameter has been determined by running the model under steady state conditions so that the calculated injector mass flow rate matched the experimental one for the given rail pressure [23]. It is also worth highlighting that the engine was not represented in the model. Therefore, a driver has been adopted in order to convert the time simulation domain into a crank angle based domain, thus allowing for properly phasing the injection events with respect to the considered engine speed. Previous studies were carried out by the authors to achieve a thorough and detailed fluid-dynamic simulation of a CNG injection system [23]. The simulations represented a primary step to evaluate the impact of the injector fluid-dynamics on the system behavior. A sensitivity analysis was also carried out with respect to the some of the main geometrical parameters of the injection system in terms of the rail pressure waves frequency and amplitude. The present work aims at further enhancing the understanding of such phenomena and at investigating their effect on the injected fuel masses. To that end, a thorough validation of the model has been carried out by means of experimentally acquired data.

2.5 Model calibration

2.5.1 Injector calibration

The injector dynamics during the opening as well as during the closing phase has to be properly accounted for in the definition of the lift profile. The action of the coil generated field on the injector needle is counteracted by the injector inertia as well as by the frictions, thus leading to an opening delay. More specifically, the lift profile can be divided into 3 parts (Fig. 2.4):

- **Opening ramp**: the needle is operated by the coil against the gas pressure and the spring force (t_j);
- **Maximum lift profile:** the needle reaches the maximum lift and allows for the maximum flow rate ($ET-t_j$);
- **Closing ramp:** the current extinguishes and the needle bounces back under the gases and the spring actions (t_c).

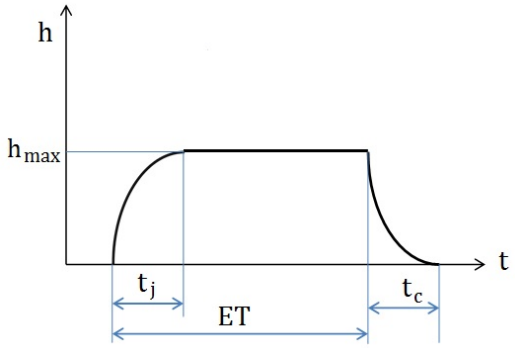

Fig. 2.4 Injector needle lift profile.

The energizing time only embeds the first and the second phase of the injection profile and the injector real behavior turns out to be markedly different with respect to the ideal one. In order to account for such discrepancy in times, the theoretical energizing time needs to be properly corrected so as to guarantee the target fuel mass.

The ECU calculates the ET required for the stoichiometric fuel mass at the given load and speed on the basis of the rail average pressure and by referring to a constant mass flow rate throughout the injection. In order to account for the opening delay and for the smooth closing ramp, the ET hence needs to be further modified. The correction factor, addressed to as the offset, was experimentally evaluated as a function of the nominal rail

pressure and recorded in the ECU maps so as to allow determining the proper injection duration according to the following equation:

$$m_{inj} = \dot{m}_{stat}\left(ET - offset\right) \tag{2.15}$$

Such timing has been numerically reproduced to match the model to the experiments. Finally, the orifice diameter has been set so as to achieve the static mass flow rate for the maximum lift at a constant pressure, as from the experimental readings More specifically, the orifice diameter has been determined by running the model under steady state conditions so that the calculated injector mass flow rate matched the experimental one for the given rail pressure.

2.5.2 Numerical model calibration

The model parameters had to be properly tuned in order to achieve a satisfying matching between the experimental readings and the simulation outputs. As far as the pressure regulator is concerned, the required parameters (spring stiffness, spring pre-load and equivalent inertial mass) have been derived from a commercial single-stage mechanical regulator and slight adjustments had to be made so achieve a fine model tuning. Attention has been paid to the pressure downstream from the regulator as well as to the rail pressure time history. Figs. 2.5, 2.6, 2.7 and 2.8 report the comparison between the experimental pressure and the simulated signal at the pressure regulator outlet port (Figs. 2.5 and 2.6) and in the fuel rail (Figs. 2.7 and 2.8) for some of the considered operation points.

The red and purple signals in Figs. 2.7 and 2.8represent the injection events for the 2-cylinder CNG system. A general satisfactory agreement can be observed both in terms of the pressure wave frequency and amplitude, thus assessing for the optimal model tuning. Despite the noise that arises on the experimental signal, a quasi-perfect matching can be inferred for the so called 'Regulated Pressure' for all of the cases as the pressure oscillations are accurately reproduced. As far as the rail pressure is concerned, the low frequency wave (carrier) displays a period corresponding to that of the injection events, which actually represent the main system excitation. The higher frequency wave that can be observed in cases 10 and 14 is to be ascribed to the combination of the injection phasing to the pressure regulator functioning, the latter representing the system secondary excitation. The pattern of the high frequency waves in Fig. 2.7a, b actually reproduces that of Fig. 2.5a, b.

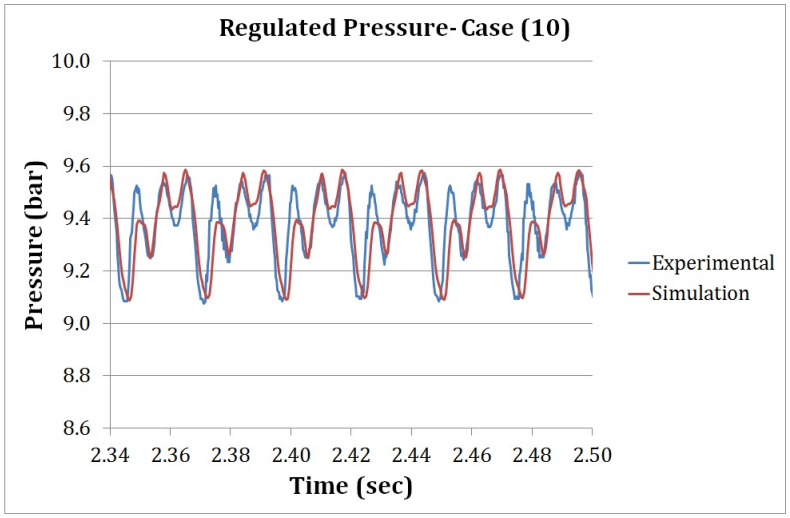

(a)

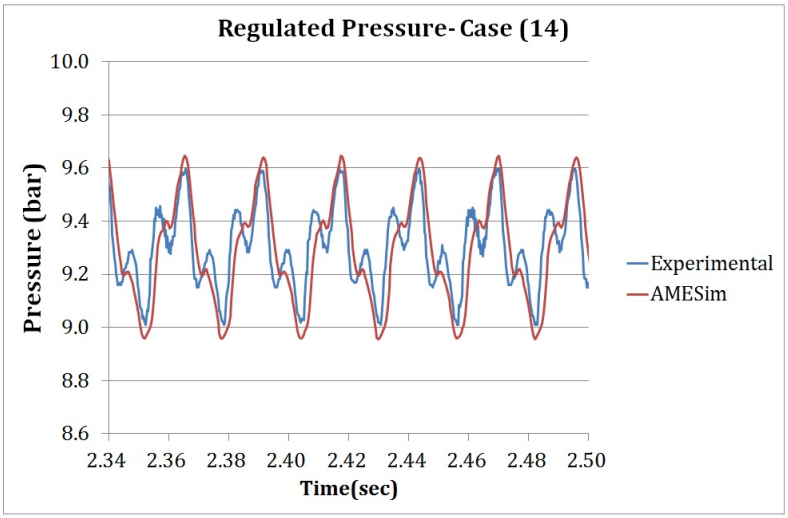

(b)

Fig. 2.5 Experimental pressure at the regulator outlet port as compared to the numerical simulations (part 1).

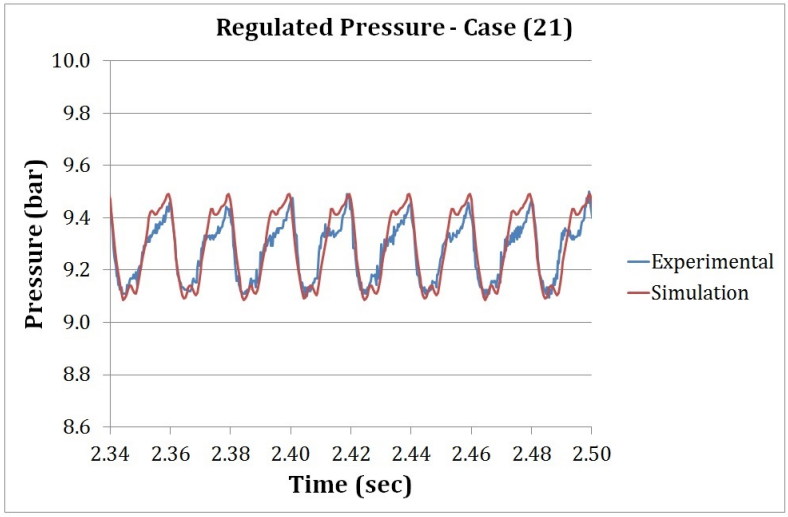

(a)

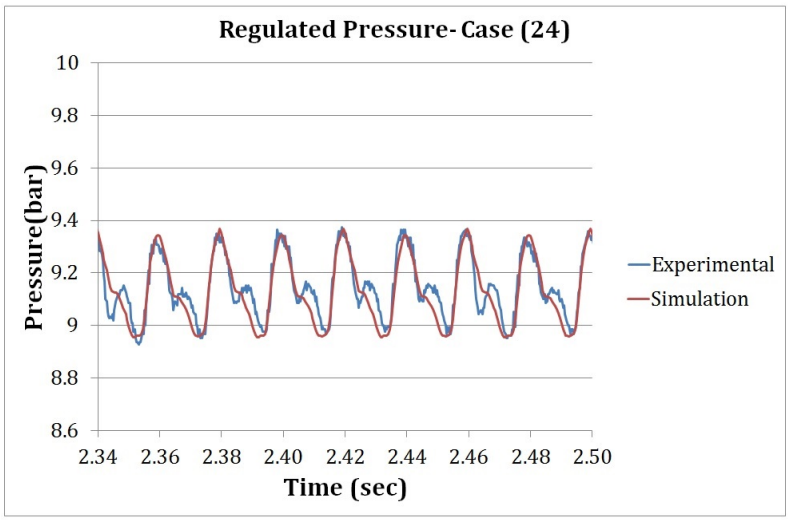

(b)

Fig. 2.6 Experimental pressure at the regulator outlet port as compared to the numerical simulations (part 2).

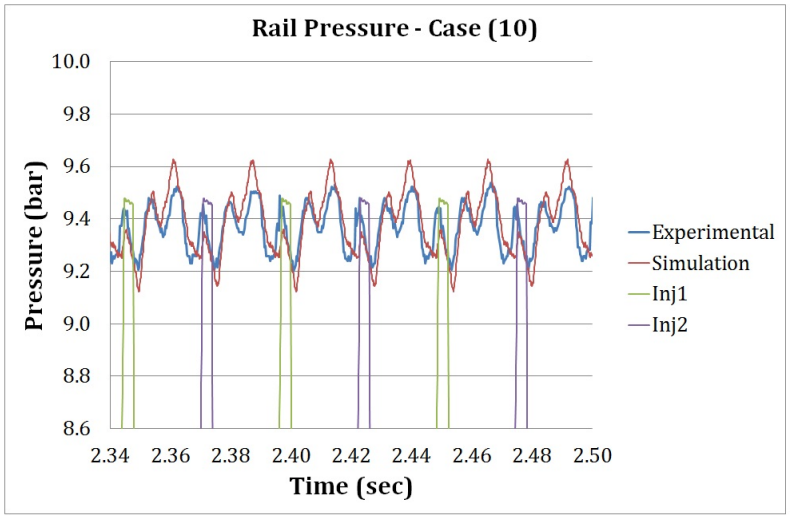

(a)

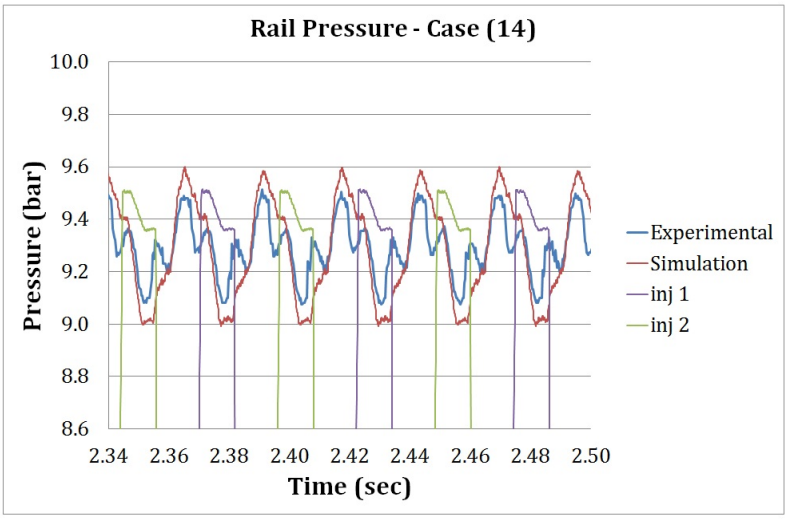

(b)

Fig. 2.7 Experimental rail pressure (blue line) as compared to the numerical model output (green line). The injection events are also depicted in the figure for the two injectors (red and purple lines)(part 1).

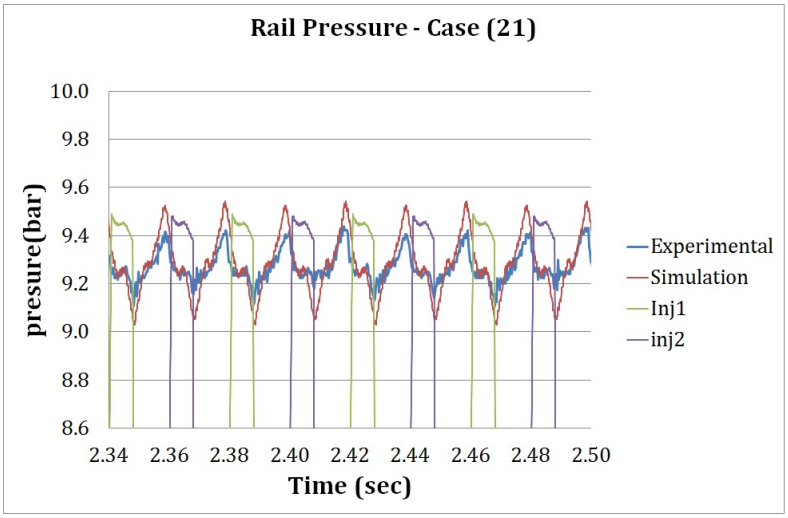

(a)

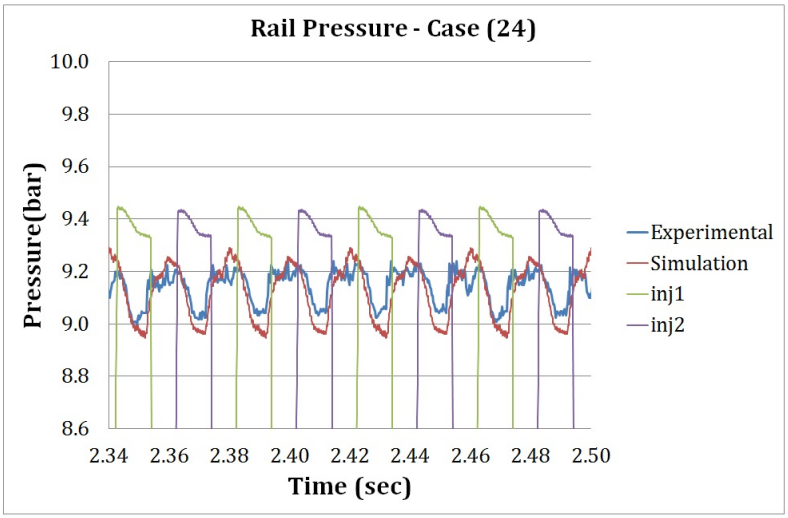

(b)

Fig. 2.8 Experimental rail pressure (blue line) as compared to the numerical model output (green line). The injection events are also depicted in the figure for the two injectors (red and purple lines)(part 2).

2.6 Results and discussion

The pressure during the injection window is variable and generally lower with respect to the rail average pressure. Such a difference is mostly likely to lead to a mismatch between the target fuel mass and the injected one. In the present section attention is hence paid to the comparison between the injected fuel mass and the theoretical one as determined according to the ECU embedded algorithm previously described.

Fig. 2.9 depicts the comparison between the injected fuel mass (blue bars) and the target mass set by the ECU (red bars) for the considered test cases for the two injectors (Figs. 2.9a and 2.9b respectively). It is worth recalling that the experimental data as well as the calculation results have been normalized with respect to the output for the theoretical fuel mass of case 10. Appreciable differences can be observed for all cases with a percentage mismatch ranging from a minimum value of 0.18% for cyl 1 in case 21 to a maximum figure of 2.55% for cyl 1 in case 5. The discrepancies in the injected fuel masses inevitably reflect on the air-to-fuel ratio, thus impairing the ECU air-to-fuel ratio closed-loop control.

The observed disparities in the injected fuel masses descend from the difference in the actual pressure during the injection window with respect to the average rail pressure. Fig. 2.10 compares the percentage errors between the injected masses (solid red squares) to the percentage errors between the rail average pressure and the average pressure for the considered injection event (solid blue diamonds). As previously stated, the target fuel mass is calculated by assuming a constant pressure equal to the average rail pressure and is hence corrected to account for the injector dynamics. The contribution of the opening and of the closing phases is anyhow modest with respect to that deriving from the maximum-lift injection window. The actual injected mass comes as a result of the real mass flow rates over the whole injection window. Such flow rates are intimately connected to the instantaneous pressure upstream from the injector, thus assessing for an overall dependence of the injected mass on the average pressure during the injection event. Still, given the higher influence of the constant lift phase, larger differences between the mass and the pressure errors arise for cases 14 and 24, i.e. for the cases where the ET grows bigger, thus amplifying the effect of the lower injection average pressure on the injected fuel mass.

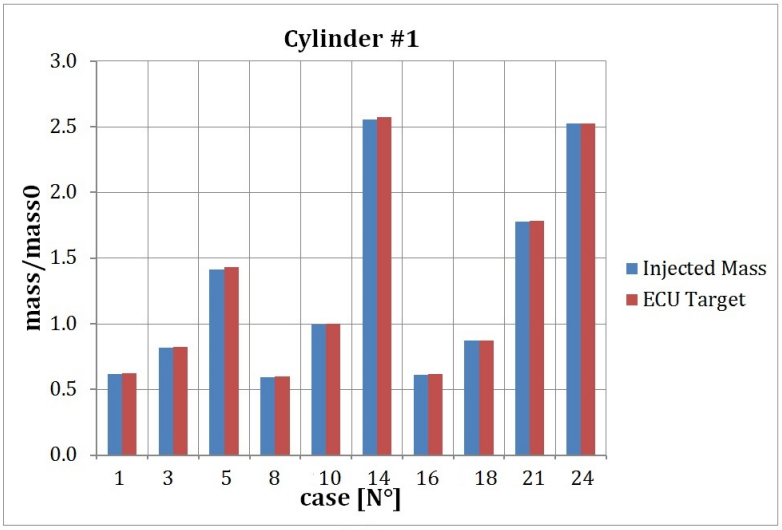

(a)

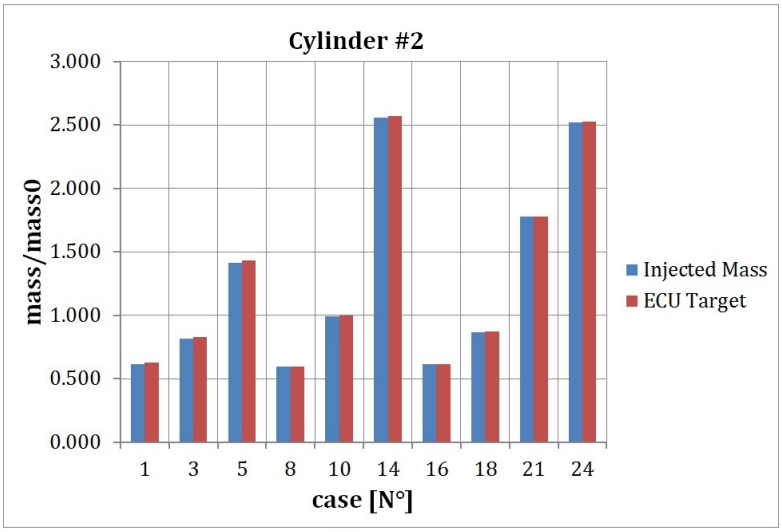

(b)

Fig. 2.9 Comparison between the target mass as calculated by the ECU and the measured injected one.

The model has also been used to predict the injection system behaviour for operating conditions different than those experimentally tested. The thorough validation campaign assesses for the consistency of such simulations. More specifically, the model has been run at different higher engine speeds in order to investigate into the influence of the latter on the pressure wave frequency as well as on the injected fuel masses mismatch. The ET has been kept constant and equal to that pertaining to cases 1, 8 and 16 so as to isolate the effect of the speed on the simulations results. Table 2.3 reports the complete test cases for the new simulations list. Similarly, an accurate comparison has been carried out on

the model outputs for a given speed at different engine loads, i.e. at various ETs. Table 2.4 summarizes the working conditions of the points sharing the speed of case 10.

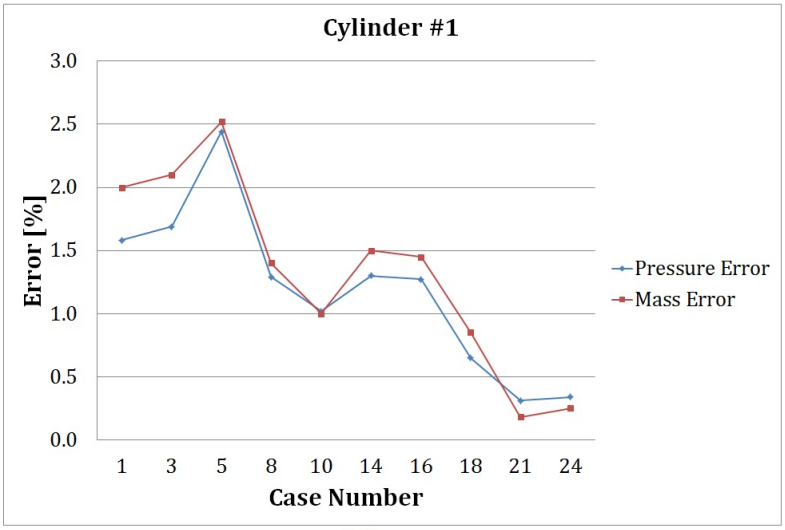

(a)

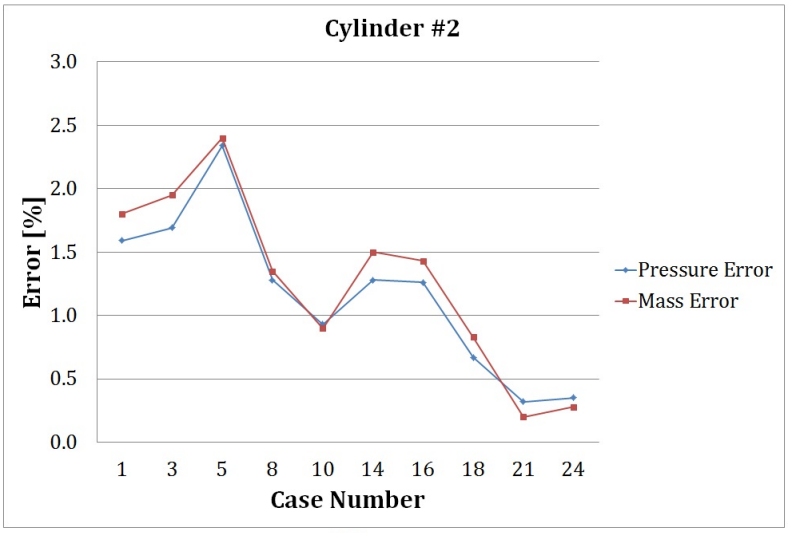

(b)

Fig. 2.10 Comparison between the percentage errors in the injected mass (see figure 2.9) and the pressure during the injection event with respect to the rail average one.

Fig. 2.11 displays the amounts of fuel injected according to the ECU calculations (red bars), and the actual masses (blue bars) for the operating conditions of Tables 3 and 4, respectively. Negligible dependence on the ET for a given speed can be observed (Fig. 2.11) whereas the effects of the speed at a given load stem from the results depicted in figure 2.11a. As previously stated, the pressure carrier wave frequency descends form

Table 2.3 Case definition at constant ET

Case number	Speed [RPM]
1	1100
8	2300
16	3000
35	4400
40	5000
45	5400

Table 2.4 Case definition at constant speed

Case number	ET [μs]
8	4000
10	6000
14	14000

the frequency of the main excitation, i.e. the injection events. The sequence of the injections is determined by the evenly phased ECU strategy and turns out to be constant at a given speed. Therefore, the difference between the average pressure during the injection window and the rail average pressure plays a comparable effect on all of the considered cases. The fuel masses difference was naturally small for case 10 (Fig. 2.9), thus assessing for the quasi-perfectly matching bars in Fig. 2.11b.

As far as the results in Fig. 2.11a are concerned, it is worth observing that the injection event triggers the rail instantaneous pressure drop (Figs. 2.7 and 2.8). For a given ET, the injection duration corresponds for all of the considered cases. Still, the average pressure during injection turns out to be higher for the higher speeds where the average injection pressure gets closer to the average rail one due to the angular widening of the injection window. Such trend can easily be observed for the two cases sharing the same ET in Figs. 2.7 and 2.8, namely case 14 and 24. Consistently, the percentage mismatch reaches its maximum for the lower speed case (case 1) with a value of 1.28% to drop down to 0.22% for the higher speed case (case 40).

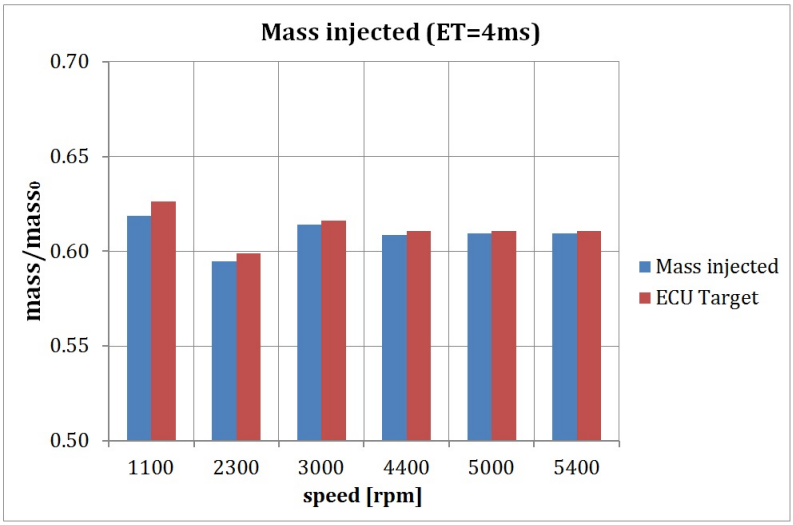

(a)

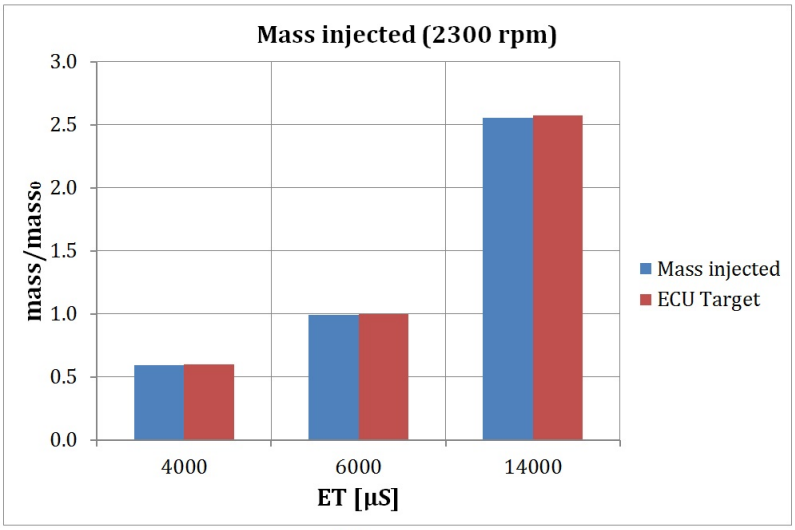

(b)

Fig. 2.11 Comparison between the target mass as calculated by the ECU and the measured injected one at constant ET (a) and at constant speed (b).

2.7 Sensitivity analysis

The numerical and experimental results assessed for a relevant influence of the dynamic behaviour of the system in terms of pressure waves on the injected mass and hence on the engine performance. Therefore, innovative solutions and control strategies need to be investigated into in order to achieve a more effective control of the cylinder air-to-fuel ratio. The response of the injection rail has proved to be strictly related to the engine operating conditions, i.e. speed and load, as well as to the geometry adopted [84]. Thus, a sensitivity analysis has been carried out with respect to two of the system main geometric parameters, such as the rail volume and the hose length. The simulation cases have been distinctly performed for the two parameters so as to properly separate the effects induced by each of the latter.

The rail volume is one the injection system main design parameters. Still, some specific constraints should be encountered when choosing its proper value. As a matter of fact, the rail length is committed to the injectors sites distance on the engine intake apparatus. Moreover, its cross section diameter is strictly correlated to the limits deriving from the engine positioning in the vehicle bonnet. Finally, it is worth recalling that the rail holds a potentially explosive gas volume at a relatively high pressure. Thus, the rail volume should be held down for safety reasons. Slight variations in the rail volume have been produced by correspondingly modifying the rail diameter. Similarly, the length of the fuel hose is subdued to constraints deriving from the positioning layout as well as from safety issues. The charts in Figs. 2.12 and 2.13 present the simulation results for the sensitivity analysis carried out on the two aforementioned parameters. More specifically, Fig. 2.12 introduces the effect of a change in the rail diameter (Fig. 2.12a) as well as of the hose length (Fig. 2.12b) on the instantaneous rail pressure for case 10. The black solid line refers to the output of the model for the standard configuration whereas the coloured traces address to the sensitivity analysis results. The corresponding injected masses are depicted in Fig. 2.13.

As one would expect, an increase in the rail diameter and hence in the rail volume produces a consequent dampening in the wave amplitude. The peak-to-peak value reduces from 0.65 bar for the smallest rail volume down to 0.25 bar for the larger diameter. Moreover, despite the constant frequency of the main excitation deriving from the injection sequence, the pressure wave period slightly increase as higher rail diameters are adopted. The reduction of the pressure oscillation amplitude and frequency both lead to an average injection pressure closer to the rail average pressure. The percentage error in the injected

masses hence decrease as the rail volume is increased (Fig. 2.13a). Still, an increase in the rail volume is not advisable due to safety issues.

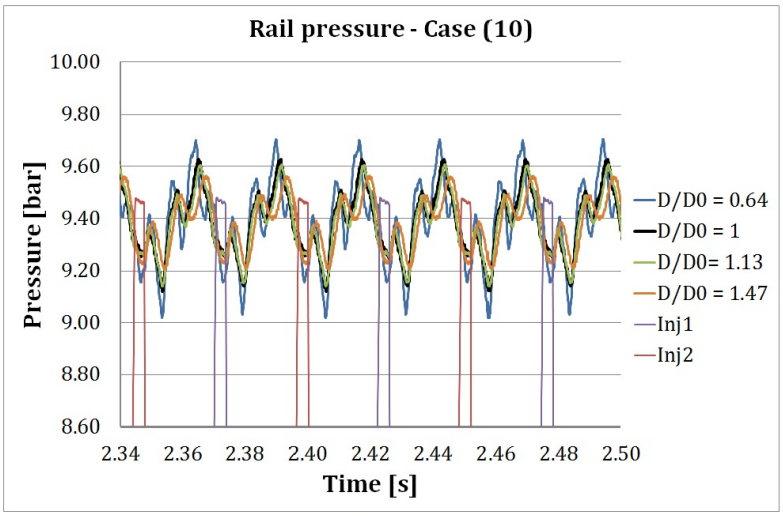

(a)

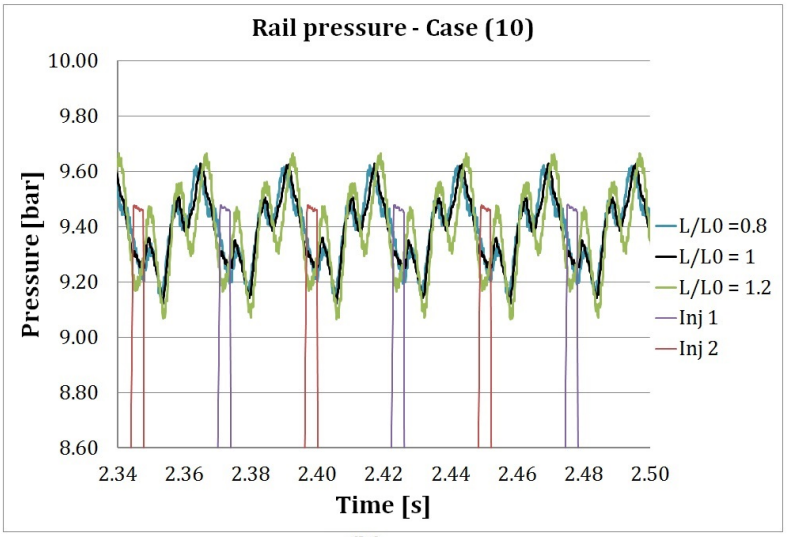

(b)

Fig. 2.12 Simulated rail pressure as a function of the rail diameter (a) and of the fuel hose (b). The injection events are also depicted in the figure for the two injectors (red and purple lines).

Similar results are obtained if a reduction in the hose length is attained (Figs. 2.12b and 2.13b). Greater lengths lead to an increase in the wave period, which in turn produces a lower injection average pressure (black line). Conversely, a shorter hose allows for smaller pressure variations and for minor fuel mass mismatch (Fig. 2.13b). Such results set a trend for the injection system control and design strategy and assess for the need of a compact fuel delivery line.

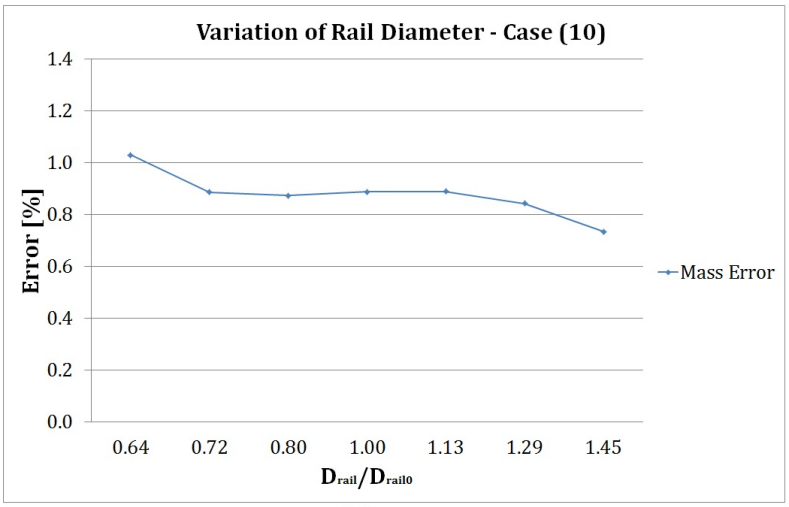

(a)

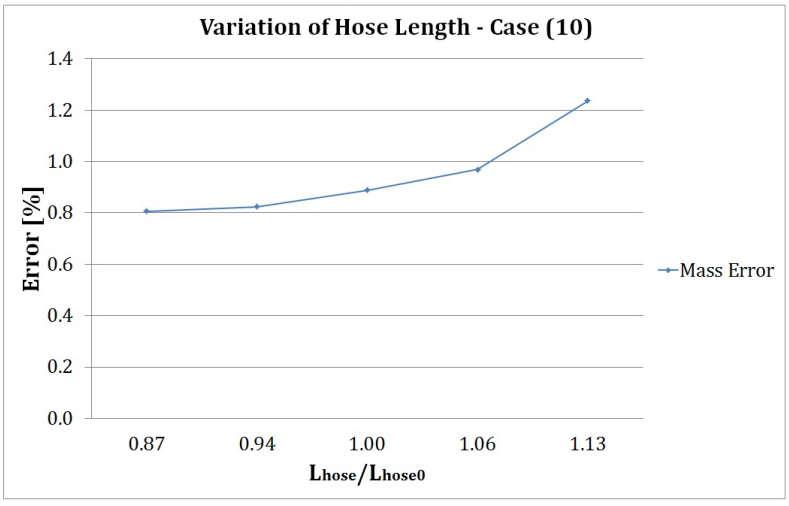

(b)

Fig. 2.13 Percentage error in the injected mass as a function of the rail diameter (a) and of the fuel hose (b).

2.8 Summary

The model calibration phase highlighted the intimate bond between the excitation driven by the injection events and that produced by the pressure regulator functioning. The two excitations determined the instantaneous pressure time history in the injection rail and assessed for the wave amplitude and frequency. The generally lower pressure within the injection window with respect to the rail average pressure level leads to an overestimation of the injected fuel mass. The amounts of injected fuel turned out to be smaller with respect to the target masses as set by the ECU. Such a difference reflects in the air-to-fuel ratio and is mostly likely to affect the cylinder-to-cylinder variability and the engine performance in terms of power output and emissions.

The simulations also allowed investigating into the effects of the energizing time at a given speed as well as of the speed at a constant energizing time on the mass mismatch. The results assessed for a modest effect of the energizing time as opposed to the stronger influence exerted by the engine speed. An increase of the latter led to a reduced mismatch.

Finally, the model underwent a sensitivity analysis for the two main geometrical parameters, namely the rail volume and the fuel hose length. Similar results were obtained for an increase of the rail diameter as well as for a reduction of the hose length. Still, the former would contradict the on-board storage requirements in terms of safety issues. The latter in turn meets the aforementioned constraints and hence appears to be feasible.

Chapter 3

Development of a predictive model of pressure regulator for CNG MPI system

* *Part of the work described in this chapter has been previously published in:"Baratta, M., Kheshtinejad, H., Laurenzano, D., Misul, D., Brunetti, S. (2015). Modelling aspects of a CNG injection system to predict its behavior under steady state conditions and throughout driving cycle simulations. Journal of natural gas science and engineering, 24, 52-63. "*

3.1 Introduction

In chapter 2 a thorough and detailed fluid-dynamic simulation of a two-cylinder CNG injection system was carried out. The results highlighted a strong connection between the perturbation caused by the injection events and the pressure waves produced by the regulator functioning and assessed or a fall-out on the injected mass. The lower instantaneous pressure within the injection window lead to an overestimation of the injected fuel mass, i.e. the amount of injected fuel turned out to be smaller with respect to the ECU target. Still, a thorough characterization of the injection system would not abide a poor description of the pressure control valve. As a matter of fact, proportional pressure reducing valves are an important element in modern fluid-power and specific attention is to be paid to the pressure control topic [102–106]. Digital pressure reducing valve systems proved to improve the response linearity, to reduce the valve hysteresis as well as to reduce the pressure dependence on the volume flow.

The present chapter hence focuses on the thorough fluid-dynamic modeling and characterization of a two-cylinder CNG injection system as well as on the effects of the system dynamic behavior on the engine performance throughout a driving cycle. Minor differences in the injected mass deriving from the pressure oscillations within the rail might in fact reflect into non-homogeneity between the cylinders air-to-fuel ratios and are mostly likely to affect both the cylinder-to-cylinder variability and the engine performance in terms of power output and emissions. Specific attention has also been paid to the modeling and characterization of the pressure reducer, given its key role in defining the system dynamics. The 0D-1D model has been validated by means of the experimental data collected at the test bench and hence exploited to predict the system behavior under transient operations. A detailed description of the experimental set up as well as of the model is provided in the body of this chapter.

3.2 Injection system and experimental set-up

A short description of the architecture of the natural gas feeding system for automotive applications is detailed in section 2.2.The compressed natural gas is delivered to the engine by means of a pressure regulator which reduces the gas pressure down to 9 bar. The valve is equipped with a filter to purge the impurity in the gas stream and plays a key role in the injection system functioning. The regulator should in fact guarantee a constant pressure to the rail independently of the supplied flow rate by simultaneously reducing the pressure oscillations to a minimum. The low pressure gas is hence delivered to the rail and to the injectors by means of a steel pipe and a hose. The injector phasing and timing is controlled by the engine ECU so as to meet the need for a stoichiometric mixture. More specifically, the injection timings mapped in the ECU are adjusted according to the average rail pressure and temperature in order to compensate for the injected fuel mass [64]. Still, the use of averaged quantities inevitably introduces a mismatch between the ECU estimations and the actual amounts of fuel injected (see section 2.6).

The present chapter aims at further investigating into the dynamic behavior of the injection system with specific reference to the pressure regulator behavior. Attention has been paid to the pressure waves that arise in the rail during steady and transient engine operations and that would impair the injected mass control strategies. The experimental campaign has been carried out at the CRF (Centro Ricerche Fiat) and at the Metatron laboratories and the experimental set-up has been designed so as to closely reproduce the outline of the on-board feeding system of the considered two-cylinder engine (see section

2.3). The main specifications for the tested injection system and the engine it equips are reported in Table 2.1. For the purpose of this chapter complementary tests have been carried out so as to thoroughly characterize the injection system and are listed hereafter.

- **Static run:** the injector has been kept wide open for the full test duration being fed at a constant rail pressure. The experimental test was meant to verify the nozzle cross section and discharge coefficient as well as to provide the model with the data needed to properly describe the injector nozzle.
- **Single injection:** the injector has been actuated at the beginning of the test and attention has been paid to the system free response. The case has been used to derive and assess for the injection system characteristic frequencies and damping factor.
- **Steady state points:** the injectors have been driven by the ECU so as to reproduce the actual injection phasing and timing corresponding to a given engine speed and load.
- **Driving cycle:** the test is meant to consistently reproduce the road driving cycle and has been carried out on a pneumatic test bench. The driving cycle has been replicated by adjusting the injectors ETs so as to make up for the actual NEDC driving conditions. The pressure signal at the pressure regulator outlet port has hence been acquired.

The pressure signals for the first three test cases have been acquired at a frequency of 3200 Hz whereas the driving cycle readings have been measured at a frequency of 5 Hz. The tests have been carried out using air instead of CNG and the injectors discharged the pressurized fluid in the open air at a pressure ranging around 1 bar. The experimental data-set for the steady state points consists of 10 points at different loads and speeds as depicted in Table 2.2.

3.3 Pressure regulator model description

The CNG injection system has been modeled at ICEAL (Internal Combustion Engines Advanced Laboratories) of Politecnico di Torino within the AMESim environment (see section 2.4). The model has been built according to the geometry marked by the technical drawings from the injection system supplier. Each system component has hence been properly characterized by means of its specific geometric features such as length,

diameter, bend radius, etc. Joints and connections have been carefully designed so as to account for the concentrated losses induced by the sudden changes in the flow section. The distributed losses have in turn been estimated by suitably setting the pipes surface roughness.

The model is previously represented in Fig. 2.2. As one could infer from the figure, the high-pressure line is omitted and replaced by pressure and temperature boundary conditions at the regulator inlet ('Gas tank'). The model thus embeds the pressure regulator and the low pressure line, which is made up of: the heat exchanger, the steel bending pipe, the fuel hose, the gauged orifice, the rail and the injectors. These latter discharge the injected fluid in an environment featuring the atmospheric pressure and temperature. Since a thorough and detailed fluid-dynamic simulation of the injection system was required and given the impact of the injector fluid-dynamics on the system behavior, the injector has been represented by means of a pipe coupled with a gauged orifice. The former is meant to simulate the fuel path inside the injector body whereas the latter represents the injector outflow cross section. The orifice diameter has been determined by running the model under steady state conditions so that the calculated injector mass flow rate matched the experimental one for the given rail pressure [84] .

It is also worth highlighting that the engine was not represented in the model. Therefore, a driver has been adopted in order to convert the time simulation domain into a crank angle based domain, thus allowing for properly phasing the injection events with respect to the considered engine speed. The study in the pervious chapter was focused on achieving a thorough and detailed fluid-dynamic simulation of a CNG injection system. The previous simulations represented a primary step to evaluate the impact of the injector fluid-dynamics on the system behavior. A sensitivity analysis was also carried out on some of the main geometrical parameters of the injection system with respect to the rail pressure wave frequency and amplitude. The present work aims at further enhancing the understanding of such phenomena and at investigating their effect on the injected fuel masses under steady state and transient operations. To that end, a thorough fluid-dynamic characterization of the pressure regulator as well as a sound validation of its matching to the injection system has been carried out by means of the experimentally acquired data. It is worth underlining that the behavior of the injection system significantly depends on the regulator dynamics. Hence, in the present chapter, attention has primarily been devoted to the modeling of the pressure regulator and to the detection of the main parameters that would help in defining and describing its dynamic response. The low pressure line, the rail and the injectors have been assumed to be fully characterized by the previous work presented in chapter 2.

3.3.1 First release

A rough version of the pressure regulator model was presented in section 2.4 and has been slightly modified as a starting point for the present analysis (Fig. 3.1). The pressure regulator has been modeled and built up by using the lumped-parameter AMESim libraries and its parameters have been set with reference to the actual valve geometry. The main regulator parameters have been derived from a commercial single-stage mechanical regulator and slight adjustments had to be made so as to achieve a fine model tuning (see section 3.3.4). The CNG is supplied to the valve through the 'high pressure line' whereas the regulated pressure outcomes from the highlighted 'low pressure line'. The pressure from the low pressure line is also derived to the control chamber (C) through a pilot line to control the spool position. The model embeds the representation for the springs (S) as well as for the fluid passages and an equivalent mass (M) is used to account for the overall inertial effects.

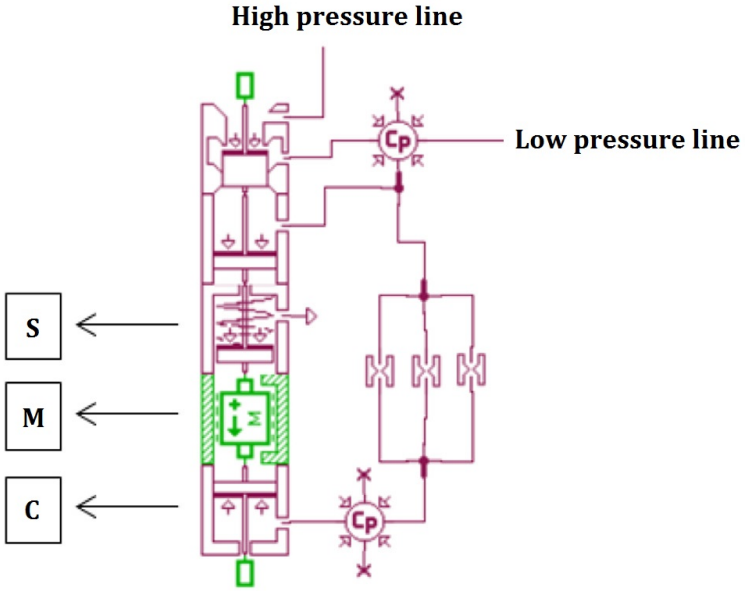

Fig. 3.1 Pressure regulator model: first release.

The spool equilibrium is set by the opening force generated by the high pressure line together with the spring as counterbalanced by the closing force determined by the pressure which is set in the control chamber from the low pressure line. For a given upstream pressure and neglecting the pressure over-ride deriving from the spring functioning, the low pressure level would hence be constant. Still, the lack of a pilot line derived from the high pressure line upstream from the regulator and acting on the spool in the closing ver-

sus is responsible for the intimate connection between the upstream and the downstream pressure levels. Thus, the natural reduction of the vessel pressure as the gas gets fed to the engine produces a consequent decrease in the pressure level set by the regulator in the low pressure line, i.e. upstream from the injectors. Such a reduced pressure level in turn reflects into an increase in the energizing time set by the ECU for a given injected fuel quantity. It is worth observing that the previously described model does not account for the friction or for the hysteresis that characterize the real valve behavior and would hence be inadequate to fully describe the dynamics of the regulator.

3.3.2 Second release

The first release misses the target of embedding the frictions that characterize the regulator functioning and that turn out to be responsible for the so called 'pressure drop' phenomenon [95]. The pressure drop effect is exemplified in Fig. 3.2.

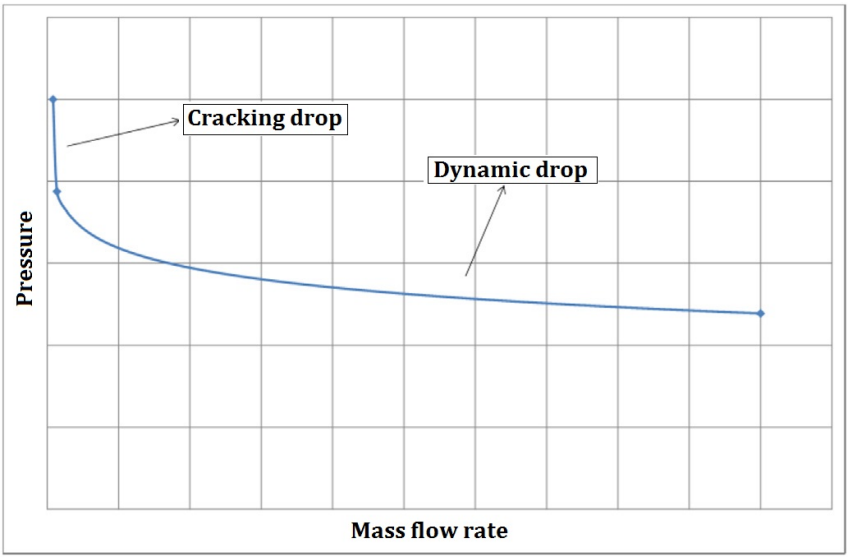

Fig. 3.2 Exemplification of the pressure drop phenomenon: pressure downstream of the regulator as a function of the mass flow rate flowing through the valve for a given pressure in the tank

The chart displays the pressure downstream from the pressure regulator as a function of the mass flow rate flowing through the valve for a given pressure level in the upstream line from the vessel. As the valve gets operated, the pressure quickly drops as a consequence of the spool and of the valve resilience as well as of the misalignments between the spool and its seat. Such a sudden and deep pressure drop is often addressed to as 'cracking drop' as it actually occurs as the valve gets cracked and is represented by the

first portion of the plot. As the mass flow rate increases, the pressure keeps decreasing with a smoother trend (dynamic drop). The latter is mainly to be ascribed to the pressure over-ride deriving from the spring stiffness as well as to the frictions that arise between the valve moving parts. In order to achieve a better fitting between the regulator architecture and the model description, additional elements were introduced in the second release (Fig. 3.3).

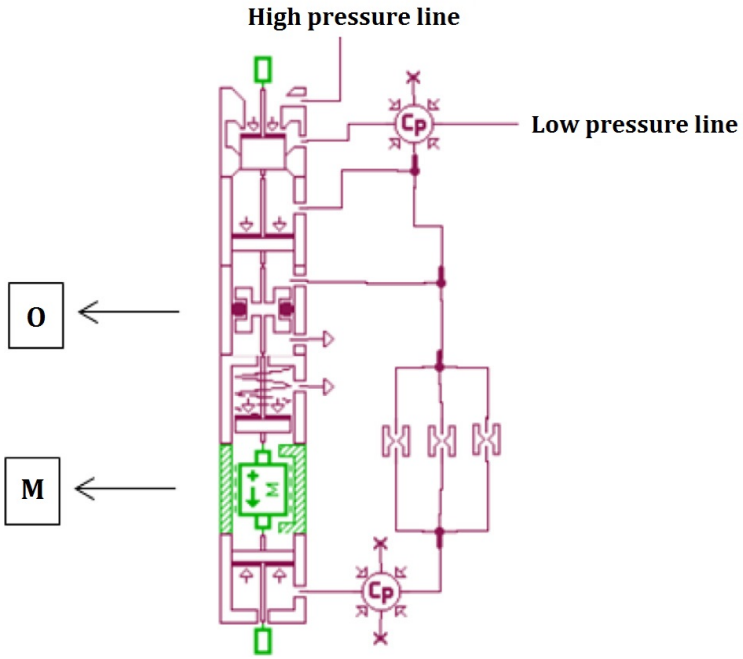

Fig. 3.3 Pressure regulator model: second release.

The original inertial element has been replaced with an equivalent mass (M) embedding both the inertial effects as well as the static and dynamic friction. The model has finally been completed by introducing an element to represent the sealing O-rings (O) and capable of reproducing the corresponding 'sealing friction'. Evidence of the enhancement produced by the second release with respect to the first one is provided by Fig. 3.4. The chart depicts the pressure level set by the regulator for a given feeding pressure as a function of the mass flow rate: the red square refer to the results produce by the first release, the green triangles address to the output of the model embedding the second release whereas the experimental data are represented by the blue diamonds. It is worth recalling that the simulation results have been obtained for both releases by matching the pressure regulator model to the previously calibrated line model. Thus, the differences that arise between the two numerical plots are definitely to be ascribed to the adopted valve model.

The chart highlights a fairly good matching between the estimations produced by the second release and the experimental measurements whereas virtually no pressure drop occurs when the first release is considered. The virtually negligible decreasing trend produced by the first release descends from the spring behavior and a better fitting can only be achieved by introducing the friction so as to account for the dynamic drop (second release). Moreover, the first release misses the target of reproducing the cracking pressure drop which characterizes the valve actuation.

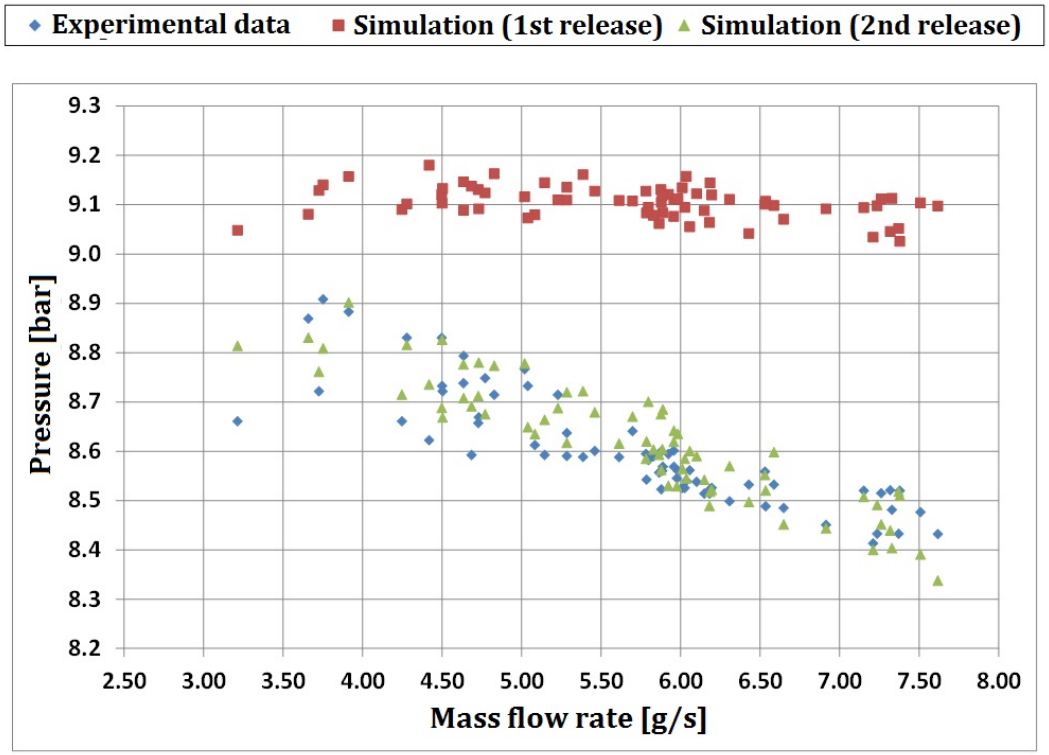

Fig. 3.4 Comparison between the first and the second release of the pressure regulator model: pressure drop.

3.3.3 Third release

A further improvement in the regulator description turned out to be necessary so as to catch the effect of the piston shim on the valve dynamic behavior. The shim is located at the end of the spool and is meant to damp down the impact of the spool against the seat during its closure. The shim holds an elastic as well as a damping behavior and mainly accounts for the imperfect sealing and for the consequent leakages working down past the valve from the high pressure to the low pressure line. These latter are in turn responsible

for the pressure build up that takes place in the line to the rail once the pressure regulator is technically closed. A sketch of the pressure regulator third release in is reported in Fig. 3.5. The sealing O-rings as well as the inertial mass are unchanged with respect to the previous release whereas a new element has been added to represent the piston shim (P).

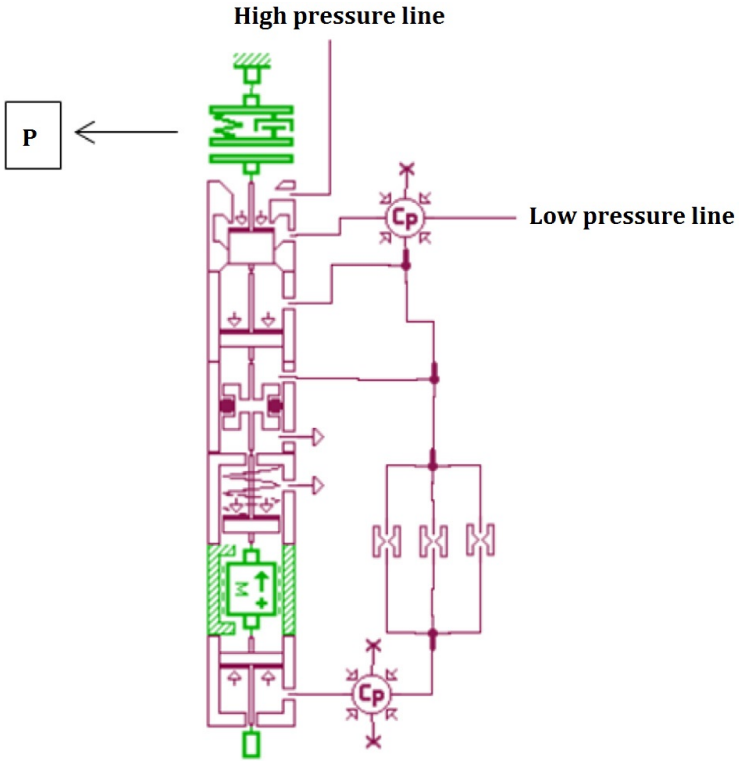

Fig. 3.5 Pressure regulator model: third release.

3.3.4 Regulator model tuning

Information about the regulator parameters setting is provided hereafter. The parameters pertaining to the three considered releases are reported in Table 3.1. As previously mentioned, some of the parameters (namely, the inertial mass, the spring stiffness and the internal surface roughness) have been obtained from the technical drawing of a commercial mechanical regulator and have been kept unchanged throughout the model calibration.

The additional regulator parameters' values have been estimated on the basis of the commercial regulator features ('baseline value'). Such values have been optimized by means of a fractional factorial DOE over the considered single shot runs as well as over the available steady state points (see sections 3.4.1 and 3.4.2) addressing the mismatch

between the simulated pressure and the experimental one. The DOE was run for the three pressure regulator releases and produced a reduced number of parameters sets which allowed for a minimizing the pressure mean error and variance. The specific set to be used for the regulator description has hence been selected on the basis of the best matching of the simulated pressure wave to the experimental one in terms of signal pattern and timing. The corresponding parameters values have been assumed to be the one to properly describe the regulator behavior and have hereafter been used to compare the outputs produced by the three proposed releases. It is worth underlining that once the parameters had been optimized for a specific release, they were hence transferred to the subsequent one. More specifically, the spring preload and the two control-chamber volumes in the second and in the third release retain the same value as for the first one. Similarly, the frictions related parameters introduced for the second release have been kept constant in the third one.

Table 3.1 Summary of the regulator parameters for the three releases.

Release number	**Parameter**	**Baseline value**	**Range**	**Best fit**
All	Mass $[g]$	25	-	-
	Spring stiffness $[N/mm]$	30	-	-
	Surface roughness $[mm]$	$5e^{-4}$	-	-
1st	Spring force at zero displacement $[N]$	680	630 ÷ 800	710
	Control Chamber Volume 1 $[cc]$	15	10 ÷ 40	30
	Control Chamber Volume 2 $[cc]$	15	10 ÷ 40	20
2nd	Dynamic friction pressure gradient $[N/bar]$	0.1	0 ÷ 100	10
	Dynamic to stiction friction coefficient [-]	1	0 ÷ 10	2
	Stick displacement threshold $[mm]$	0.2	0 ÷ 5	0.1
3rd	Maximum piston displacement for which the shim is active $[mm]$	0	0 ÷ 1	4×10^{-5}

3.4 Results and discussion

3.4.1 Single shot run

It is worth recalling that the single shot run was meant to fully characterize the system in terms of overall natural frequency and damping factor. The tests reproduce the free response of the system for a given energizing time (ET) and have been run by actuating a single injection event and by monitoring the pressure waves that arise due to the interaction of rail and of the line dynamics with the pressure regulator behavior. The experimental tests have been reproduced by running the simulations with the three aforementioned releases. and by properly tuning the pressure regulator parameters so as to achieve a satisfying matching with the experimental readings. More specifically, a DOE has been run for the main quantities (pipe roughness, friction coefficient, pressure regulator capacities, shim damping coefficient, ...) over the considered single shot runs as well as over the available steady state points (see section 3.4.2) addressing the mismatch between the simulated pressure and the experimental one. The set of parameters allowing for a reduced mean error and variance throughout the considered cases has been assumed to be the one to properly describe the release behavior and has hence hereafter been used to compare the outputs produced by the three proposed pressure regulator releases.

For the sake of conciseness, the present chapter presents the results obtained for two different operating conditions corresponding to a small ET and a larger one, respectively (Figs. 3.6 and 3.7). The energizing time pertaining to the second shot is 3.5 times the one characterizing the first run. The figure reports the comparison between the model output and the experimental pressure (blue plot) downstream from the pressure regulator (Figs. 3.6a and 3.7a) and in the rail (Figs. 3.6b and 3.7b). The light blue trace represents the injector voltage and its peak corresponds to the injection event. The three colors used for the numerical results correspond to the three proposed pressure regulator releases as specified in the legend.

The plots highlight the inconsistency of the results produced by the model embedding the first release for the pressure regulator with respect to the actual behavior of the system. The first release lacks of damping elements and fully neglects the frictions between the valve moving parts, thus resulting into a non-physical almost instantaneous recover of the pressure gap after the injection event (red plot). Still, it is worth observing that the frequency of the pressure waves is anyhow properly matched, thus assessing for a correct tuning of the equivalent mass and stiffness parameters. The elements added to the model as one moves from the first to the second release account for the friction and

for the damping behavior of the valve and lead to a decrease in the promptness by which the model makes up for the pressure drop produced by the injection event (green plot). However, the rapidity by which both the pressure downstream from the pressure regulator and that in the rail achieve the target level within the second release hints at a reduced time constant and introduces the need for further increasing the overall damping in the system characterization.

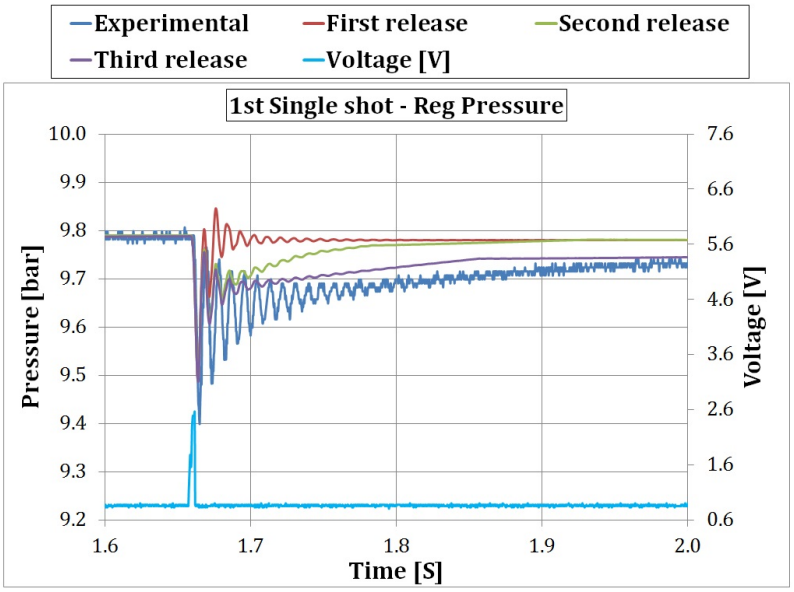

(a)

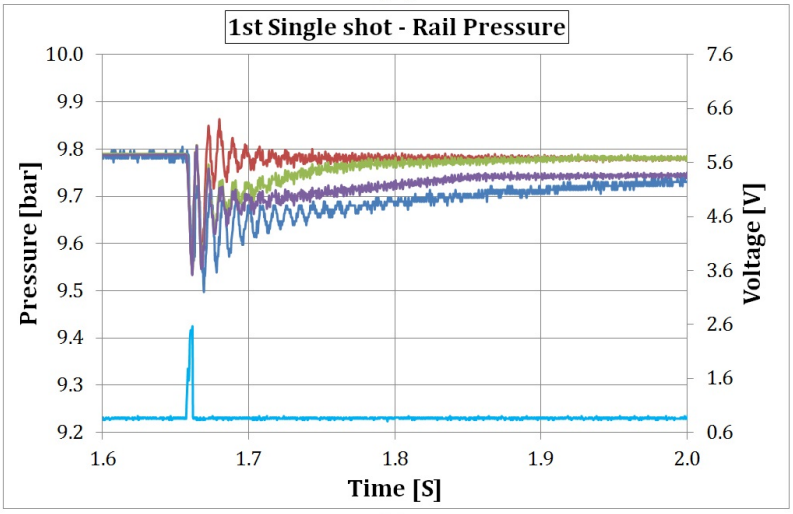

(b)

Fig. 3.6 Experimental pressure (blue line) as compared to the output produced by the three releases downstream from the pressure regulator (a) and in the rail (b) for 1st single shot run, ET=4000 ms.

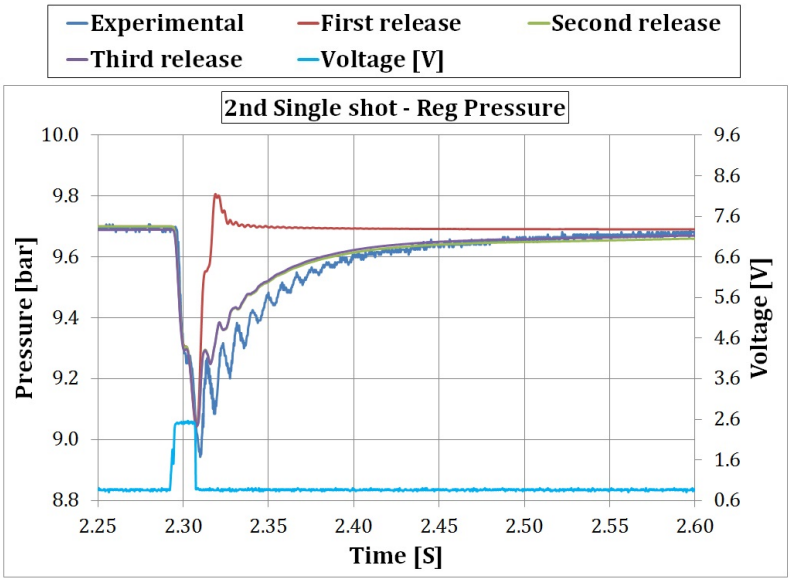

(a)

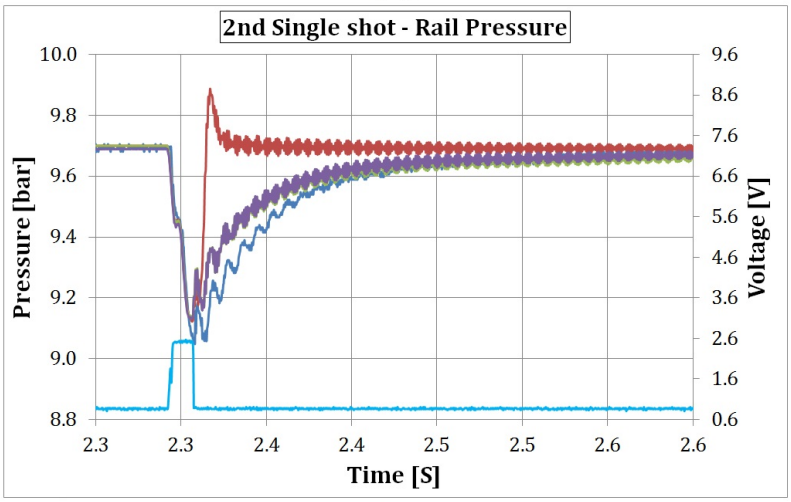

(b)

Fig. 3.7 Experimental pressure (blue line) as compared to the output produced by the three releases downstream from the pressure regulator (a) and in the rail (b) for 2nd single shot run, ET=14000 ms.

The experimental traces show a continuous slight pressure increase once the transient has expired, due to the leakages occurring from the high to the low pressure line. The model outputs produced by the third release (purple plot) appear to properly reproduce such phenomenon. As a matter of fact, the piston shim embedded in the third release is now capable of accounting for the leakages. These latter would drive fresh mass from the high pressure line to the rail line, i.e. to a confined environment, thus producing

a continuous pressure rise. The transition from the transient to the steady behavior is marked by the abrupt change in the plot steepness occurring at 1.86 s (Fig. 3.6). The regulator is fully closed and the rise in pressure is now to be ascribed to the leakages.

The different time scale which characterizes the two chart sets derives from the difference in the corresponding energizing times. More specifically, the higher ET characterizing the second single shot run (Fig. 3.7) implies a higher injected mass and is hence responsible for the increased pressure drop produced by the injection event with respect to the first single shot run (Fig. 3.6). The augmented pressure gradient across the valve in turn drives a faster response of the valve itself, thus reducing the event time scale. More specifically, as the ET enlarges, the valve displacement increases and the shim loosens its effect on the regulator performance and behavior. As a matter of fact, the shim can only exert an active influence for very low displacements during the valve opening and closure phases (see Table 3.1). Consistently, the outputs produced by the second and the third release are almost perfectly overlapping. Major differences between the two releases would only arise due to the shim behavior during long transient operations. Still, the transient produced by the high load ET is characterized by a compressed time scale and turns out not to effectively influence the shim dynamics.

3.4.2 Steady state points

The so called steady state points reproduce the functioning of the injection system at a given engine speed and load. A thorough comparison was carried out in [16] and assessed for the capability of the 0D-1D model to qualitatively reproduce the pressure waves both in the rail and downstream from the pressure regulator. Such a model embedded the first release for the pressure regulator and required a point by point calibration. It is anyhow worth observing that the research presented in [16] was targeting the effects of the energizing time as well as of the speed on the mismatch between the injected mass and the ECU estimated one and was mainly meant to identify the injection system optimal geometric parameters. Thus, the dedicated calibration was not impairing the soundness of the conclusions. Contrariwise, the present research aims at characterizing the dynamic behavior of the system with specific attention to the pressure regulator functioning and is mainly addressed to properly describing the system response throughout a driving cycle. Thus, the calibration procedure has been carried out so as to identify a single set of tuned parameters to be exploited for any given working conditions (see section 3.3.4).

Fig. 3.8 introduces a comparison between the experimental pressure in the fuel rail and the simulated signal produced by the three releases for the two extreme cases of

the test matrix, namely case 1 and 24 (see Table 2.2). The light blue and the lilac trace represent the injection events for the 2-cylinder CNG system.

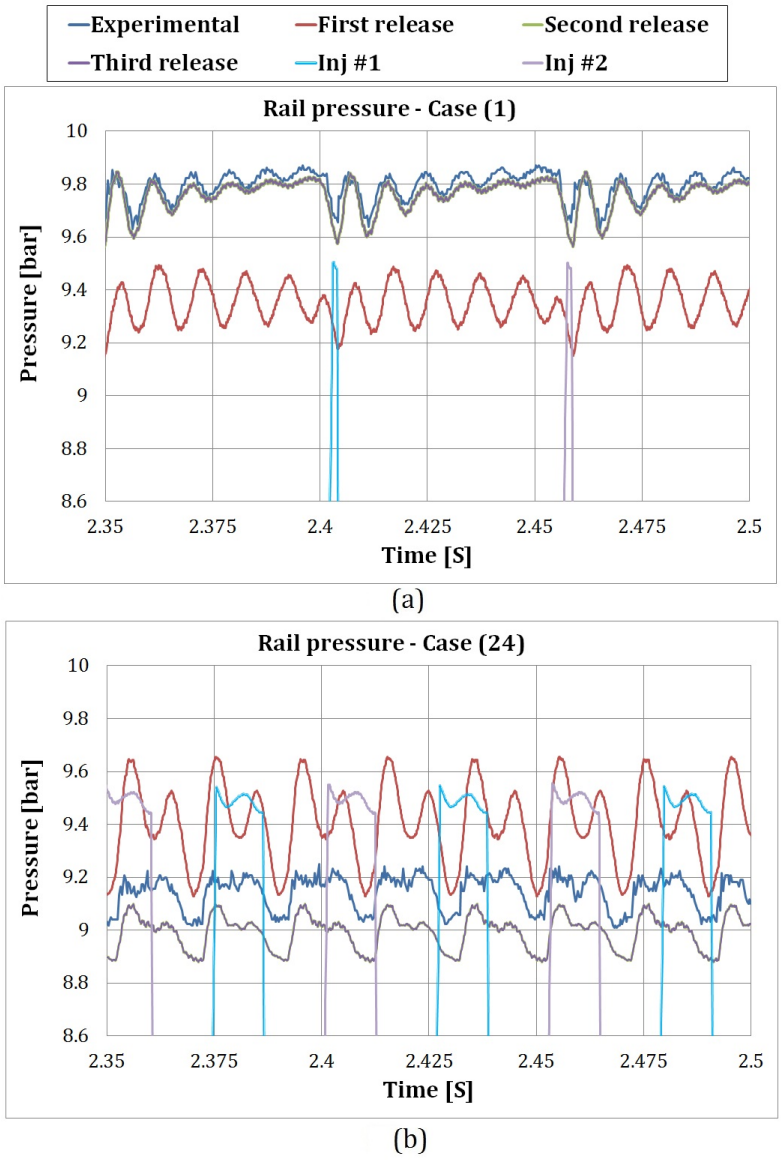

Fig. 3.8 Experimental rail pressure (blue line) as compared to the output produced by the three releases. (a) case 1 (1100 rpm, ET=4000 ms). (b) case 24 (3000 rpm, ET=14,000 ms).

Case 1 (Fig. 3.8a) corresponds to a low load and low speed engine point and is characterized by short and spaced-out injections, which in turn produce a slow dynamic response. The latter somehow reproduces the pattern of the 'single shot' behavior and assesses for the better fitting of the second and of the third release with respect to the first one. As a matter of fact, the outputs of the second and of the third release are almost

perfectly overlapping and consistently catching the rise performed by the low frequency wave (carrier) produced by the injection events. Such a correspondence is mainly to be ascribed to the damping elements introduced in the models. Contrariwise, the lack of frictions in the first release accounts for the 'resonating' behavior displayed by the red plot. Similar conclusions can be inferred for case 24 (Fig. 3.8a).

As it is specified in sections 3.3.3 and 3.3.4, the regulator third release retains all the parameters' values of the second one, whereas a new element has been added to represent the piston shim. Consequently, any differences between the two releases' behavior would be only due to the shim effect. Under steady state operations (steady state points) the piston does not press on the shim as it simply floats around a constant average displacement, which allows for meeting the average mass flow rate requirement. As a consequence, the shim does not exert any influences on the regulator behavior, thus giving consistency to the perfect matching of the results produced by the two releases. The model embedding the first release of the pressure regulator turns out to be too prompt in responding to the major excitement deriving from the injection event and overestimates the pressure peaks produced by the combination of the injection phasing to the pressure regulator functioning. Still, the faster response induced by the higher speed and load weakens the importance of the model frictions, thus allowing the first release to qualitatively match the trend in the pressure wave. It is finally worth observing that the major mismatch between the numerical and the experimental average pressure level which stems for the results produced by first release descends from the adoption of a single set of tuning parameters (Fig. 3.8a) as well as from the inability of the model to catch the so called pressure drop (Fig. 3.8b), which markedly occurs due to the increased mass flow rates involved in case 24 (see Section 3.4.2).

A general satisfactory agreement with the experimental signals has been observed within all of the considered operating points for the results produced by the second and the third pressure regulator release. Fig. 3.9 displays the comparisons between the simulation outputs and the experimental readings for an additional selection of points (as indicated in the figure captions) with respect to those previously commented. The results obtained with the first release would basically reproduce the patterns presented in Fig. 3.8 and have hence been deliberately omitted. Once more, the outputs of the two releases are almost perfectly overlapping. Despite the noise that arises on the experimental signal, a quasi-perfect matching can be inferred for all of the cases. The pressure oscillations are accurately reproduced in terms of both frequency and amplitude and the slight mismatch between the average pressure levels is to be ascribed to the adoption of a single set of tuning parameters.

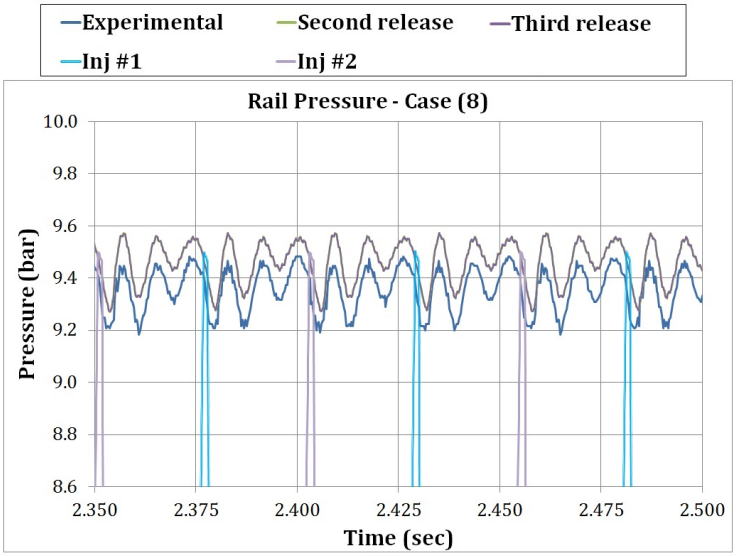

(a)

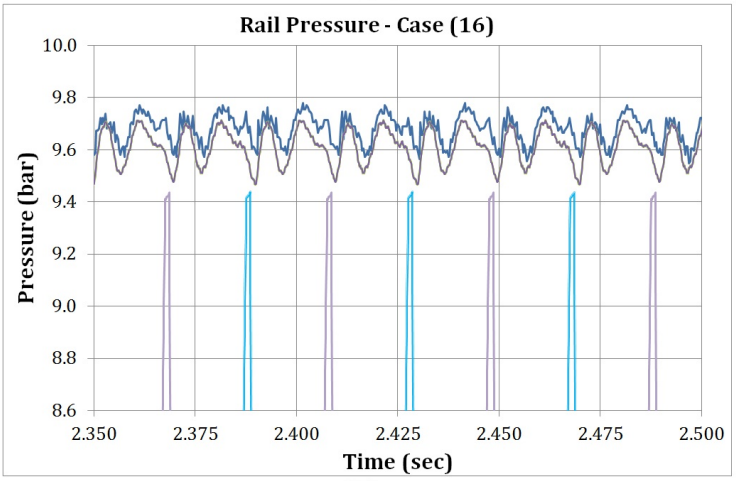

(b)

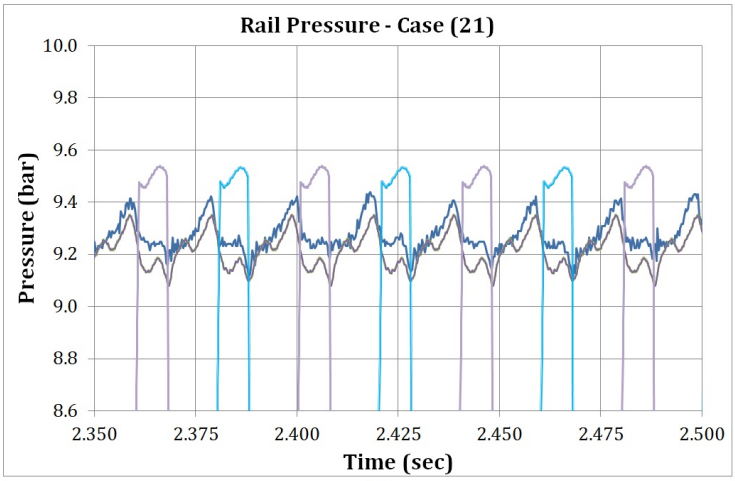

(c)

Fig. 3.9 Experimental rail pressure (blue line) as compared to the output produced by the second and the third release. (a) case 8 (2300 rpm, ET=4000 ms). (b) case 16 (3000 rpm, ET=4000 ms). (c) case 21 (3000 rpm, ET=10,000 ms

3.4.3 Driving cycle simulations (cut-off phases)

The so assessed pressure regulator models have hence been used to simulate the injection system behavior throughout an NEDC driving cycle. The charts in Fig. 3.10 report the comparison between the simulated pressure (red plot) and the experimental time history (blue plot) at the regulator controlled port, i.e. in the line to the rail. It is worth observing that the sampling rate in the driving cycle acquisitions has been chosen so as to capture the relevant phenomena for the specific analysis. As far as the injection-system behavior within the NEDC cycle is concerned, the focus is set on the low-frequency variation of the average rail pressure versus time, with specific reference to the cut-off phases and the dynamic drop effect. The duration of such phenomena can be estimated to range from 1 to 10 s and the adopted 5 Hz frequency hence turns out to be consistent with the time scale of the investigated phenomena.

The experimental readings have been collected at the test bench reproducing the actual on-board injection system set-up. Hence, the regulator feeding pressure was subject to a natural decrement as time elapsed due to the vessel emptying. Given that the balance of the valve spool is determined by the opening forces set by the feeding pressure and by the spring and by the closing force generated by the pressure in the line to the rail, the pressure at the outlet port of the regulator displays a corresponding decreasing trend in its average value (blue plots). Such a behaviour is fully reproduced by the patterns set by the three releases and clearly stems from the chart pertaining to the first one (Fig. 3.10a). The lack of dynamics which characterizes the first release allows for highlighting such a low frequency behaviour Still, the model turns out to be inadequate to simulate the pressure rises produced by the cut-off phases. The introduction of the frictions and consequently of the ability to account for the cracking as well as for the dynamic pressure drop taking place at increased speeds and/or loads, leads to a better matching between the output produced by the second release and the experimental readings and allow for detecting the occurrence of the cut-off and acceleration phases within the driving cycle (Fig. 3.10b). The pressure climb up is anyhow limited due to the instantaneous closure of the pressure regulator once the target pressure is achieved. A further enhancement is finally represented by the results pertaining to the third release (Fig. 3.10c). The piston shim embedded in the model guarantees the natural leakages which characterize the real valve functioning, thus allowing for an additional pressure increase during the cut-off phase. As a result, the magnitude and duration of the pressure peek peak produced by the produced by the engine cut-off strategy is events are almost perfectly reproduced by the model.

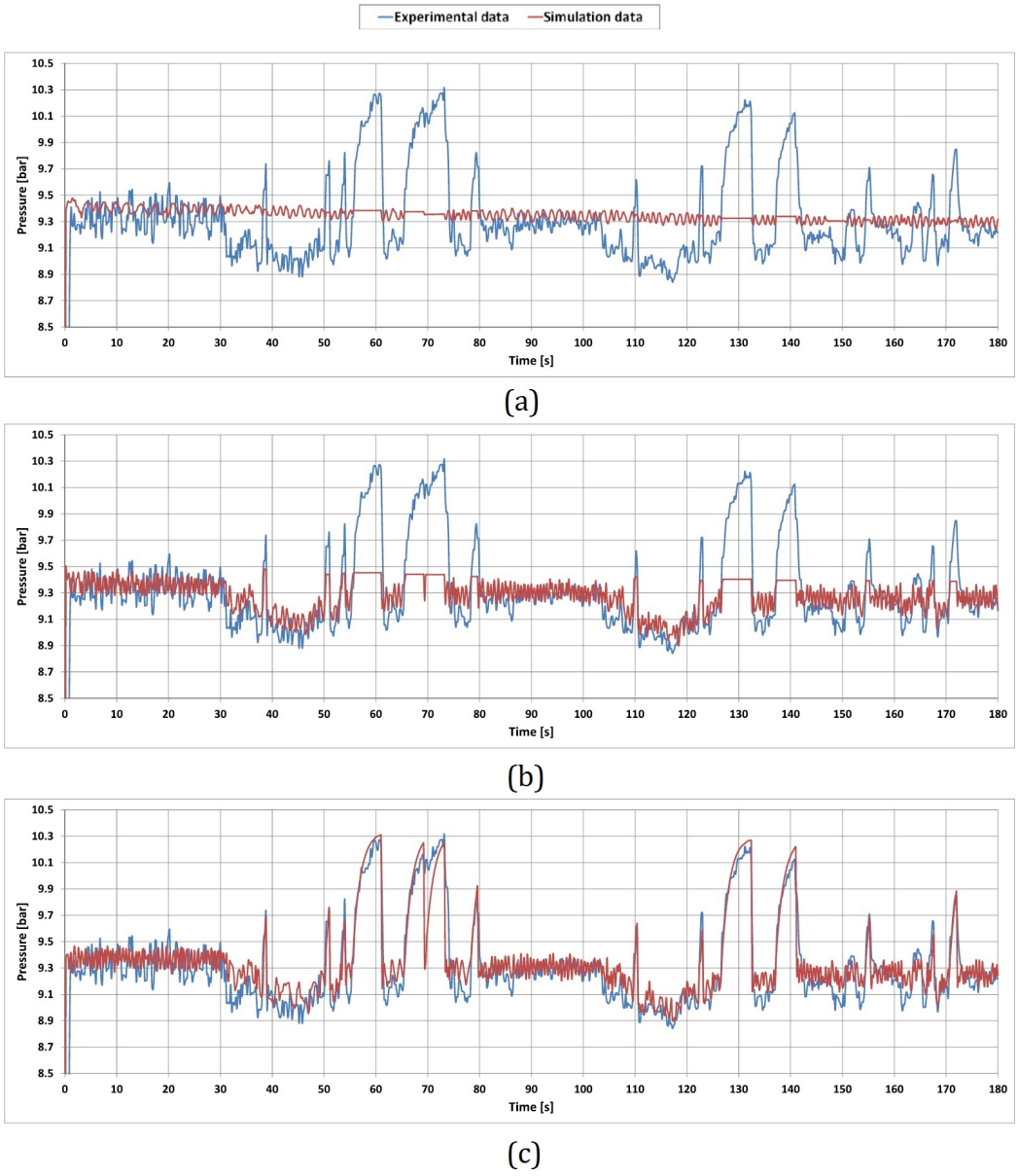

Fig. 3.10 Driving cycle simulation for the first (a), the second (b) and the third (c) release adopted for the pressure regulator description

The time scale of the figure allows for assessing for the superiority of the third release of the pressure regulator. Still, it prevents a thorough comparison of the numerical results to the experimental readings throughout faster transient operations. A better insight is hence provided by the chart in Fig. 3.11. The colours retain the same meaning as before and the time scale of Fig. 3.10c has been enlarged so as to widen a restricted portion of the driving cycle. Despite the noise that arises in the experimental plot data, represented

with symbols, the picture displays an almost perfect matching of the numerical output to the experimental readings, thus reinforcing the reliability of the numerical model.

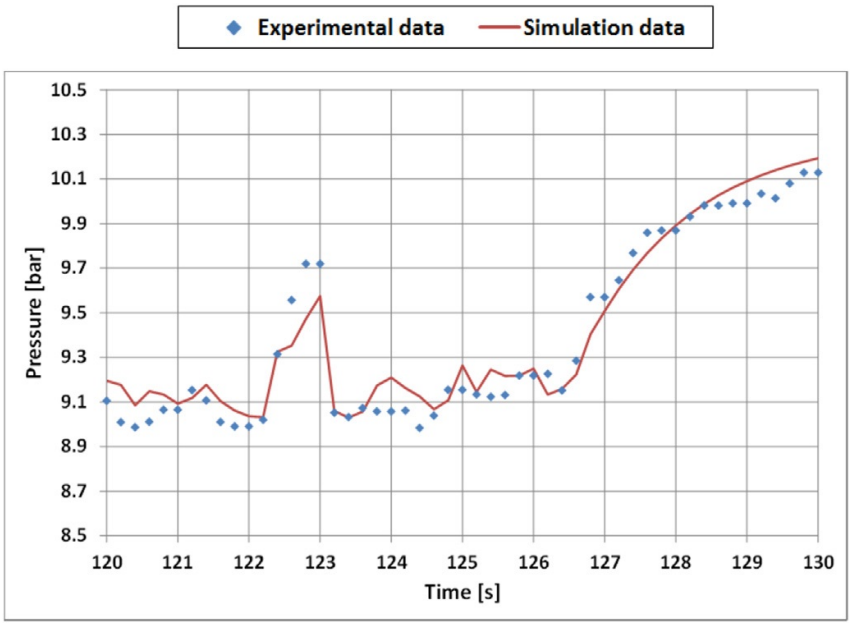

Fig. 3.11 Highlight on the driving cycle simulation for the third release adopted for the pressure regulator description.

3.4.4 Transient simulations

The results produced by the steady state points (section 3.4.2) together with the outputs of the driving cycle simulations (section 3.4.3) prove the third release to be the one suitable to properly reproduce the dynamic response of the system. A better understanding of the system behavior throughout the driving cycle would anyhow be provided by a deeper investigation into the injection system dynamics during fast transient operations. Simulations have hence been carried out by using the model embedding the third regulator release in order to reproduce a change in either the engine speed or load and are presented in Figs. 3.12 and 3.13, respectively. The charts in the two figures report the simulated rail pressure (red line) as a function of the time step. The injection events are once more represented by the light blue and the purple traces and additional information are provided by the average pressure within the injection window (light bluered squares) and by the injected fuel mass (solid circles) as referred to the right axis. The charts also depict the strategy for the speed or load transition (black plot).

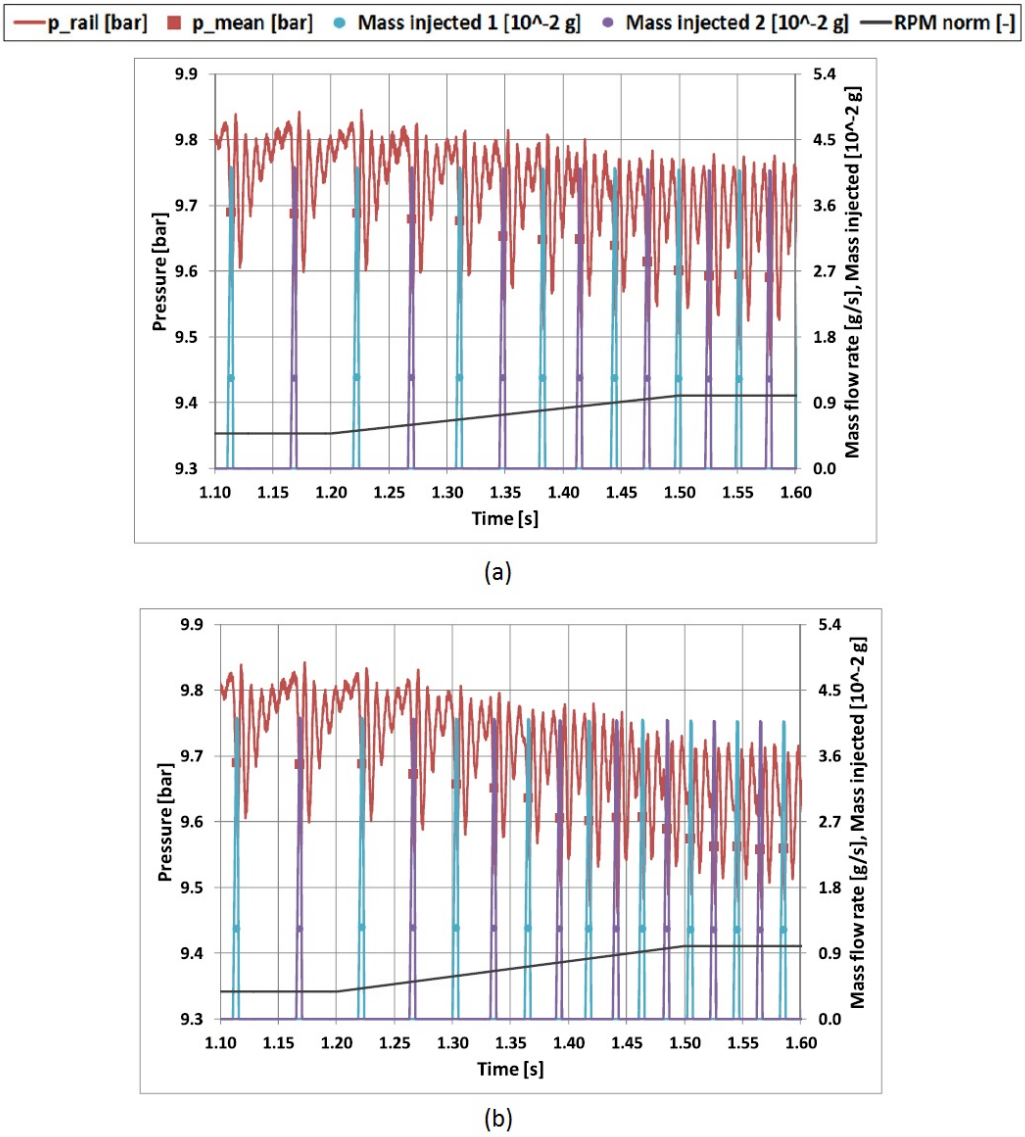

Fig. 3.12 Speed transient simulations (ET=4000 ms). (a) speed ramp from 1100 to 2300 rpm. (b) speed ramp from 1100 to 3000 rpm.

As far as the speed transient simulations are concerned (Fig. 3.12), the model has been run throughout cases 1, 8 and 16 and the engine acceleration has been replicated by using a ramp whose duration is 0.3 s. More specifically, Fig. 3.12a refers to a ramp from case 8 to case 16, whereas Fig. 3.12b shows the results of a transient maneuver from case 1 to case 16. The black trace representing the normalized speed is simply meant to highlight the starting and end point of the transition from the initial to the final speed. It is worth recalling that the model embeds a driver to convert the time simulation domain into a

crank angle based domain, thus allowing for properly phasing the injection events with respect to the considered engine speed.

The speed transition is smooth and prolonged if compared to the system time constant. Thus, the injection system quickly adjusts its response to the change in the engine speed and swiftly replicates the dynamics of the target case. The trace of the model once the transient has expired is a perfect replica of the corresponding steady state behavior presented in Fig. 3.9. The pressure drop is once more reproduced by the model and accounts for the increased average mass flow rate connected to the speed rise. Complying with the constant ET, the augmented engine speed leads to a correspondingly increased injected fuel mass within a given time interval and hence results into a gain in the average mass flow rate. The average pressure hence constantly and expectedly decreases from the lower to the higher speeds (from left to right in the figures), with the exception of the standstill which occurs from 1.40s to 1.48s in Fig. 3.12b. Such an apparent dissonance is to be ascribed to a random occurrence that lines up the injection window together with the peak in the pressure wave. Such an effect is not clearly to be seen in the figure and has been deduced from the numerical outputs. Still, the fall-out on the injected fuel mass (solid circle) is virtually negligible due to the reduced implemented ET. Should longer injection timings be actuated, the occurrence of the injection event with respect to the rail instantaneous pressure could result into a stronger mismatch between the actually injected fuel mass and the ECU target.

The aforementioned discrepancy in the injected fuel mass together with the pressure drop induced by the engine acceleration is likely to produce non-homogeneity in the air-to-fuel ratio, thus locally impairing the effectiveness of the after-treatment system. Such a fall-out assesses for the need of dedicated and proactive control strategies capable of preventing anomalies in the mixture formation. Moreover, it is worth observing that an additional difference between the injected mass and the ECU target would anyhow be induced by the distance of the average pressure level within the injection window from the average rail pressure which drives the ECU logics [16]. As a matter of fact, the results of Figs. 3.8 and 3.9 highlight pressure differences ranging around the 1% whereas higher discrepancies up to the 2.5% would emerge for some of the other cases belonging to the data-set in Table 2.2. Such a pressure mismatch would produce a mass underestimation to be summed up to the deviation of the injected fuel mass from the ECU target produced by the system transient response.

As far as the load transient simulations are concerned (Fig. 3.13), the model has been run throughout cases 16, 21 and 24 and the ET has been instantaneously adjusted so as to reproduce the sudden transition in the engine load, as indicated in the figure legend.

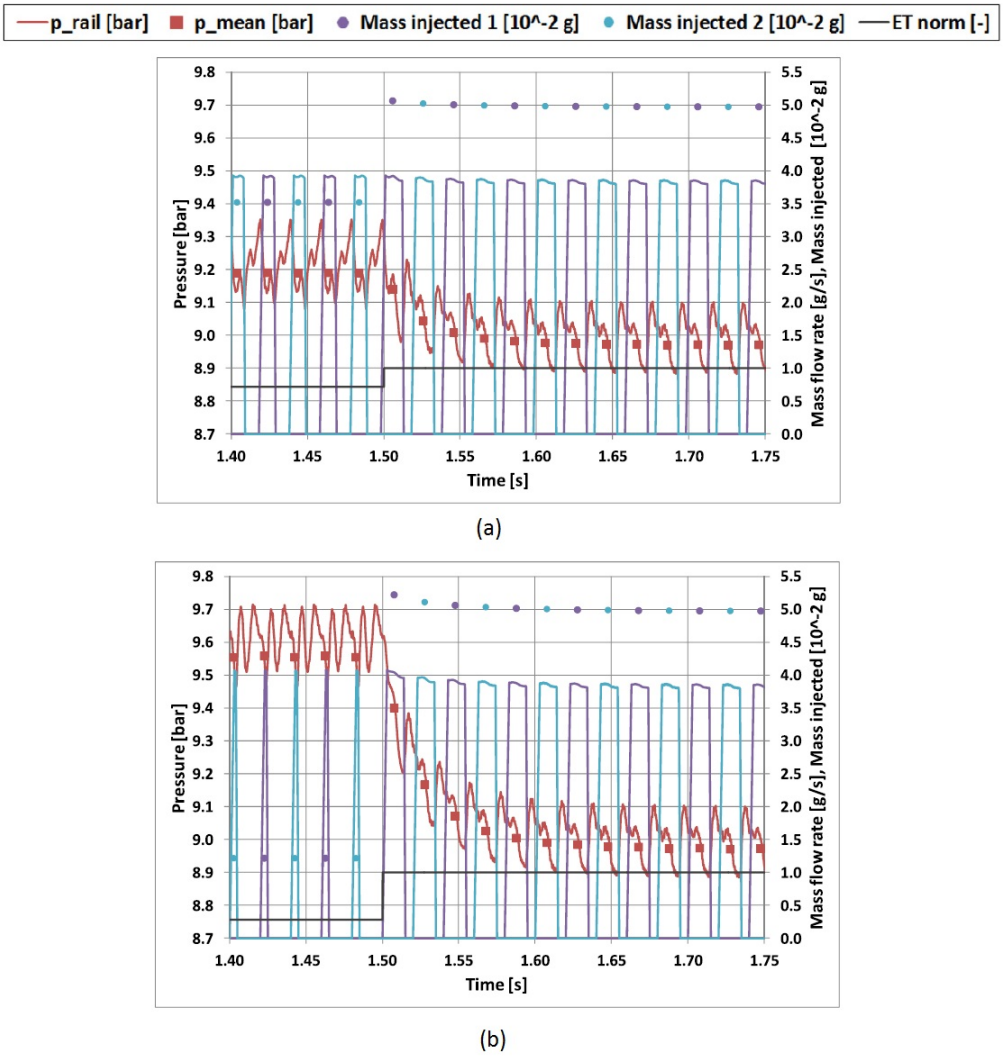

Fig. 3.13 Load transient simulations (N= 3000 rpm). (a) step from ET=10000 to 14,000 ms. (b) step from ET= 4000 to 14,000 ms.

The charts in Fig. 3.13 clearly exemplify the pressure drop phenomenon and its dependence on the fuel mass flow rate. A higher drop occurs as the change in the ET grows bigger (Fig. 3.13b). The load change is here represented by a step function. Despite the rapidity of the transition, the response of the injection system rapidly reaches the steady state point behavior. Still, as the system adjusts to the required load, the actually injected fuel mass sensibly drifts from the target one due to the gradual and progressive

pressure decrease. Such an effect is enlarged by the higher average rail pressure gap that the system covers up within the transient from case 16 to case 24 (Fig. 3.13b). As a matter of fact, the mass mismatch grows from the 1-2% of Fig. 3.13a to the 3-4% of Fig. 3.13b. Once more, innovative and low throughput control strategies would be needed to prevent operating anomalies.

3.5 Conclusions

This chapter deeply investigated into the modeling of the pressure reducing valve equipping a CNG injection system. The results proved that a thorough description of the system dynamics is only to be achieved provided that the reducer is properly described and embedded in the system model. More specifically, this chapter presented the comparison between the experimental rail pressure and the model output for three different releases of the pressure regulator and thoroughly discussed their accuracy limits. The results assessed for a rough capability of the three releases to match the system natural frequency thanks to a proper tuning of the equivalent valve mass and stiffness. The base version showed to be fairly straightforward to be calibrated as the main parameters were simply derived from the regulator technical drawings and nominal features with minor adjustments. Such a version anyhow turned out to be inadequate to properly reproduce the system dumping damping due to the lack of frictions in the model. A better description of the system behavior was achieved introducing the rubbing frictions produced by the O-rings (second release) as well as the spool dumping damping shim (third release). The frictions allowed for consistently matching the experimental readings carried out under steady state conditions and assessed for the model capability to properly reproduce the injection system behavior. Still, the second release failed to replicate the response of the system during the cut-off phase of the vehicle driving cycle. The almost perfect matching between the experimental pressure time-history and the results produced by the model embedding the third release stressed the importance of a refined and sound description of the pressure regulator in order to catch the main characteristic of the system response.

In summary, a few useful methodological indications about the modeling procedure of a pressure reducer can be drawn from the present study. The correct setting of the inertial and stiffness parameters allows for reproducing the pressure wave frequency. A satisfactory accuracy and reliability of the model results can anyhow be obtained only by properly setting the friction-related parameters. Still, a higher number of coefficients have to be optimized, thus setting the need for a considerable amount of experimental

data for the engine running at different speeds and loads. Moreover, the adoption of a specific optimization technique is mandatory in order to give consistency to the model calibration. A further enhancement in the model accuracy can be obtained by properly reproducing the reducer leakages and the additional damping effects, which occur during the valve opening and closure phases. This model refinement is mandatory so as to allow for obtaining accurate results whenever the regulator undergoes fast opening/closing duty cycles such as those which would occur within the vehicle driving cycles. It is anyhow worth observing that additional experimental data under transient conditions are required for the calibration of these modeling features.

The model was hence used to predict the actual dynamic response throughout fast transient operations. The speed transient highlighted the weight of the pressure drop phenomenon on the mismatch between the injected fuel mass and the ECU target. As a matter of fact, the average instantaneous mass flow rate increases for a given ET as the speed rises, thus producing a lower average rail pressure and resulting into an overestimation of the injected mass. Similar results were depicted by the load transient simulations. Once more, as the system adjusts to the required load, the actually injected fuel mass sensibly drifts from the target one due to the gradual and progressive pressure decrease produced by the 'pressure drop'. Mass differences ranging from 1 to 4% were found for the considered cases. Such results assess for the need of dedicated and refined control strategies capable of properly preventing the mass mismatch, thus avoiding anomalies in the mixture formation that might elsewise negatively affect the after treatment system as well as the engine performance and drivability. Finally, it is worth observing that the reliability of the results solely stands on the soundness of the 0D-1D model. A proper and consistent description of any component is hence mandatory and specific attention is to be devoted to the pressure regulator modelling.

Chapter 4

Investigation into the Potentials of a Dedicated MP Injection System for a production NG SP Heavy-Duty Engine

* *Part of the work described in this chapter has been previously published in:Kheshtinejad, H.; Baratta, M.; Laurenzano,D.; Maino, C.; Misul, D. "Investigation into the Potentials of a Dedicated Multi-Point Injection System for a production NG Single-Point Heavy-Duty Engine. In: SAE INTERNATIONAL JOURNAL OF ENGINES." - ISSN 1946-3936 (In Press)*

4.1 Introduction

The present work investigates into the potentials of a dedicated MP injection system for a heavy-duty CNG engine originally designed to exploit a refined version of an SP one. The research has taken advantage of a wide and exhaustive experimental data set for the engine running with both systems, thus allowing for a thorough comparison of the steady state and transient performance of the engine equipped with the base SP injection apparatus and with the prototypal MP one. The effects of the different injection systems on the mixture formation have been deeply investigated into analysing the cycle-to-cycle as well as the cylinder-to-cylinder variation. Moreover, the response of the MP system to changes in the injection phasing, i.e. end of injection (EOI), for a given energizing time (ET) has been accounted for.

4.2 Experimental Set-up

4.2.1 Test engine

As previously stated, the present work represents an innovation for the management of heavy duty NG engines. A thorough investigation has been carried out into the actual behaviour of the SP system equipping a production engine as well as into the response of the engine to a purposely developed MP injection system. More specifically, different engine operating parameters have been considered for the analysis and a dedicated strategy has also been implemented on a numerical basis for the MP configuration.

The engine tested for the present research is a turbocharged heavy duty 7.8 litre Yuchai YC6G engine propelled with CNG. The main characteristics of the engine are listed in Table 4.1. Derived from an original diesel engine, it was modified with a specifically built-in fuel system as well as intake and exhaust systems which specifically line up with the characteristics of a production CNG engine. In the present study, the engine has been equipped alternatively with two different types of fuel injection systems: a Single-Point (SP) and Multi-Point (MP) one.

Table 4.1 Characteristics of the studied engine

S.no	Specifications	Value
1	Type	Vertical, In-line, 2-valve, turbocharged, CNG engine
2	No. of cylinders	6
3	Bore x Stroke (mm)	112 x 132
4	Compression ratio	11
5	Displacement (L)	7.8
6	Rated Power (kW)	191
7	Rated Speed (rpm)	1400
8	Injection system type	SPI/MPI

The advanced SP injection system was developed by ECI (E-controls Injection), a technology platform which enables a wide range of power solutions for buses and coaches. Fig. 4.1 depicts the layout of the SP injection system together with its four injectors. The CNG, fed by the fuel rail, is injected by injectors into a rubber pipe that connects to a

mixer and is hence mixed with the air in the intake duct. The mixer retains a toroid shape and features 24 holes in its inner surface and is located in between the throttle valve and the intake manifold.

The MP injection system is more advanced than the SP one and has been purposely developed by Metatronix for this specific case study. The fuel rail feeds six CNG injectors, these latter supplying the gas to the intake manifold close to the intake valves (port fuel injection).

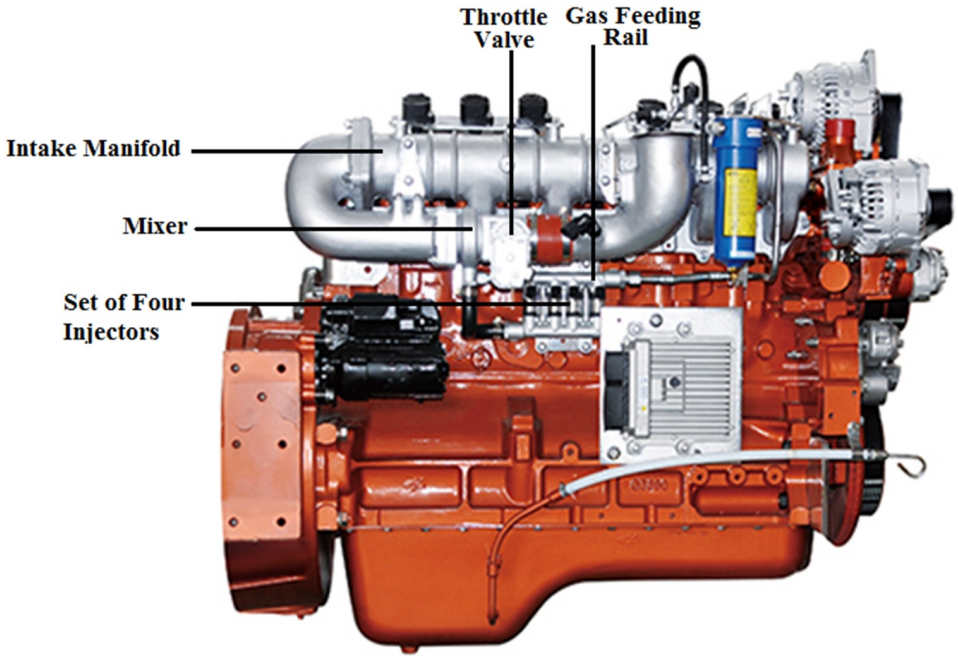

Fig. 4.1 YUCHAI YC6G Engine with SPI system.

4.2.2 Test bench and data acquisition

The experimental tests have been carried out at the Metatronix laboratories and the engine set-up used for the present research is presented in Fig. 4.2. A short description of the measuring instrumentation layout is detailed in what follows. The natural gas is stored in CNG tank at a pressure ranging around 200 bar and is delivered to the engine by means of a pressure regulator device which reduces the CNG pressure down to 5 bar. The low pressure gas hence reaches both the MPI rail and SPI rail by means of devoted rubber pipes. Four Nikki gas injectors (29B001-832 Yuchai gas YC6K13N) have been adopted for the SPI mode whereas six dedicated KEIHIN injectors (73cc YELLOW Single Injector) have been deployed for the MP mode. The injectors sequentially injected the natural gas into

intake manifold and into intake runners respectively. The electronic control unit (ECU) masters the injection duration and timing in order to guarantee the correct quantity of fuel. A pressure and a temperature sensor are mounted on the delivery pipe upstream from the rail to collect the ECU input required for the air-fuel ratio closed-loop control both for the SPI and MPI system.

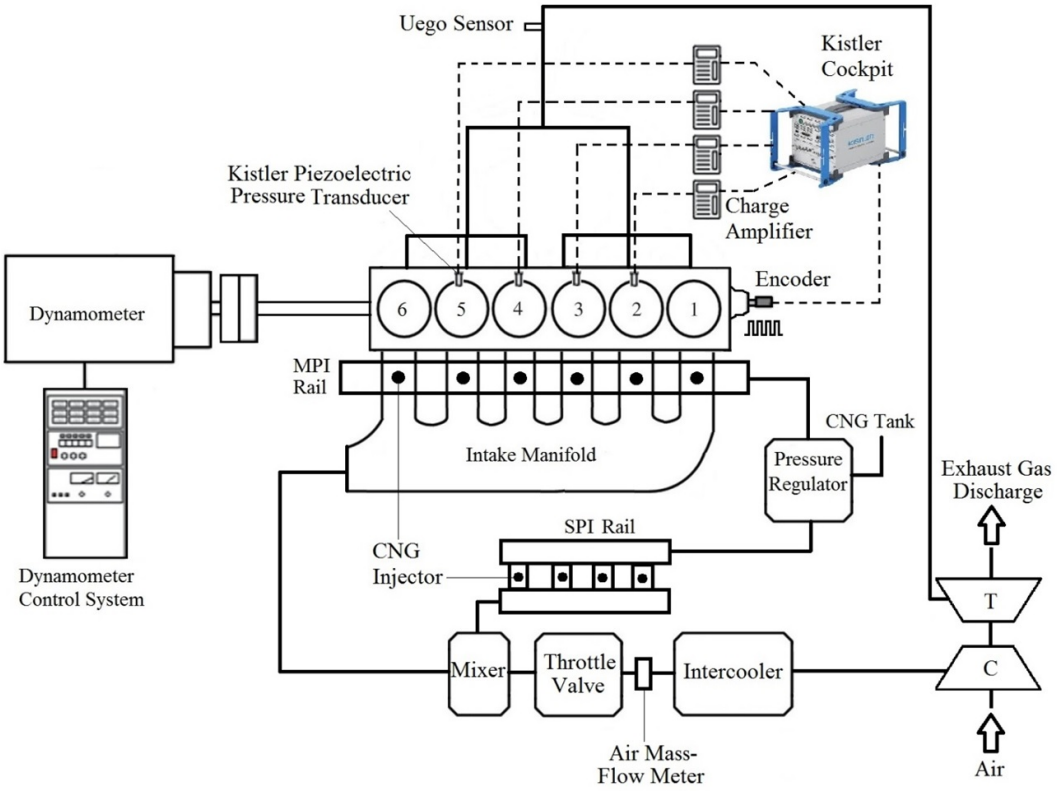

Fig. 4.2 Engine measuring set-up YUCHAI YC6G.

During the dynamometer tests the following cycle-averaged quantities have been acquired: engine speed, torque, temperatures at the exhaust ports as well as temperature and pressure at the compressor inlet and outlet, at the inter-cooler (IC) outlet, in the intake manifold, in the intake ducts and at the turbine admission. The test bench is equipped with an intake air mass flow meter, with an air-fuel ratio UEGO sensor at the turbine inlet and with six UEGO sensors (one for each cylinder) located in the six exhaust runners. The in-cylinder pressure time history of cylinder from #2 to #5 have been acquired by means of four water-cooled KISTLER piezoelectric transducers with a resolution of 0.2° CA over the entire tests duration, thus allowing for an extensive cycle-to-cycle and cylinder-to-cylinder variation analysis.

4.2.3 Experimental data set

The experimental tests have been performed on the designated engine so as to thoroughly characterize the SP and MP injection systems behaviour. The steady state tests have been carried out on 32 engine-operating points for given speeds and loads (Fig. 4.3) with the engine equipped with both systems alternatively. The experiments were mainly aimed at investigating into the influence of the MP injection phasing on the quality of mixture formation with respect to the SP system. Table 2 outlines four different injections phasing both at full loads (100% load) and partial loads (50% load). The results produced by such phasing are presented in the MPI sensitivity to injection phase variation section.

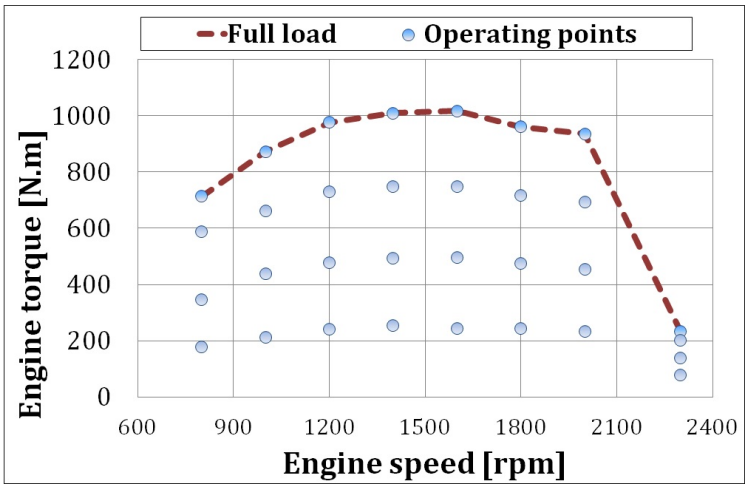

Fig. 4.3 Engine steady state operating points.

4.3 Experimental Results and discussion

4.3.1 Steady-state points

The present work aims at deeply investigating into the different behavior of a heavy-duty engine equipped with a traditional SP system or with an innovative MP one. To that end, a thorough comparison has been initially carried out between the SP and the MP mode using the experimental readings of the steady engine map (Fig. 4.3) in terms of torque, peak firing pressure (PFP), brake specific fuel consumption (bsfc) as well as turbine inlet temperature. Such a parallel is depicted by the charts in Fig. 4.3 for full load (WOT) and part load (50% load) operations, the red dots referring to the SP configuration and the blue squares addressing to the MP mode. It is worth mentioning that the MP system

features a sequentially phased injection over the six cylinders with an injection window expiring 60 deg before the compression BDC. Contrariwise, the SP system displays an optimized multiple injection with 6 shots evenly spaced over the 720 deg covering the engine cycle. The spark advance (SA) was set to a given value for both systems. Despite similar values in the full load bsfc (Fig. 4.4c) for most of the investigated points, major differences arise for the higher speeds. Similarly, a decrease in the bsfc is observed for the MP mode at part load operations both at low and at high engine speeds. Correspondingly, higher turbine inlet temperatures are observed for the SP functioning (Fig. 4.4d), thus confirming the results of [22]. Given the almost identical boost level approached with the two configurations and considering the higher pressures measured at the turbine inlet for the MPI system, Fig. 4.4d hints at a higher efficiency of the combustion process in the MPI system, hence giving consistency to the discrepancies highlighted for the bsfc in Fig. 4.4c. A better insight into the different response of the engine to the diverse injection mode is provided by the charts in Fig. 4.5 as the relative air-to-fuel ratio is plotted for the six cylinders in the SP (red circles) and MP (blue squares) configurations.

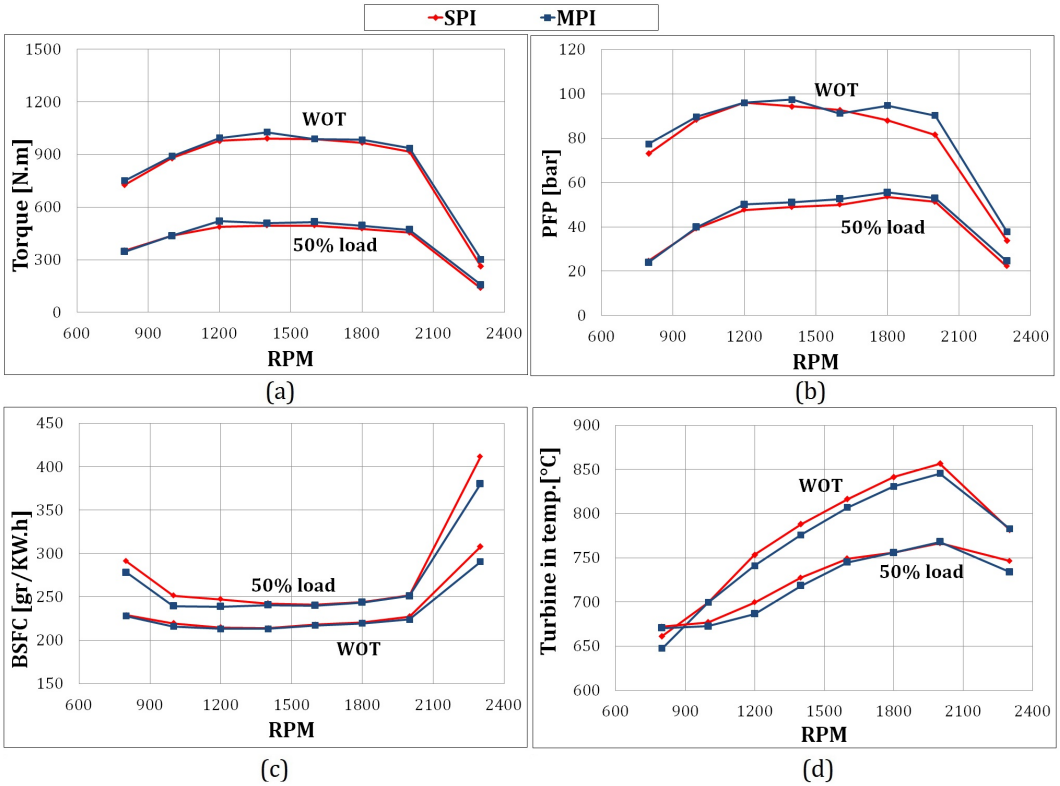

Fig. 4.4 Comparison of SPI and MPI engines performance; (a) Brake torque, (b) peak firing pressure, (c) brake specific fuel consumption, (d) turbine inlet temperature.

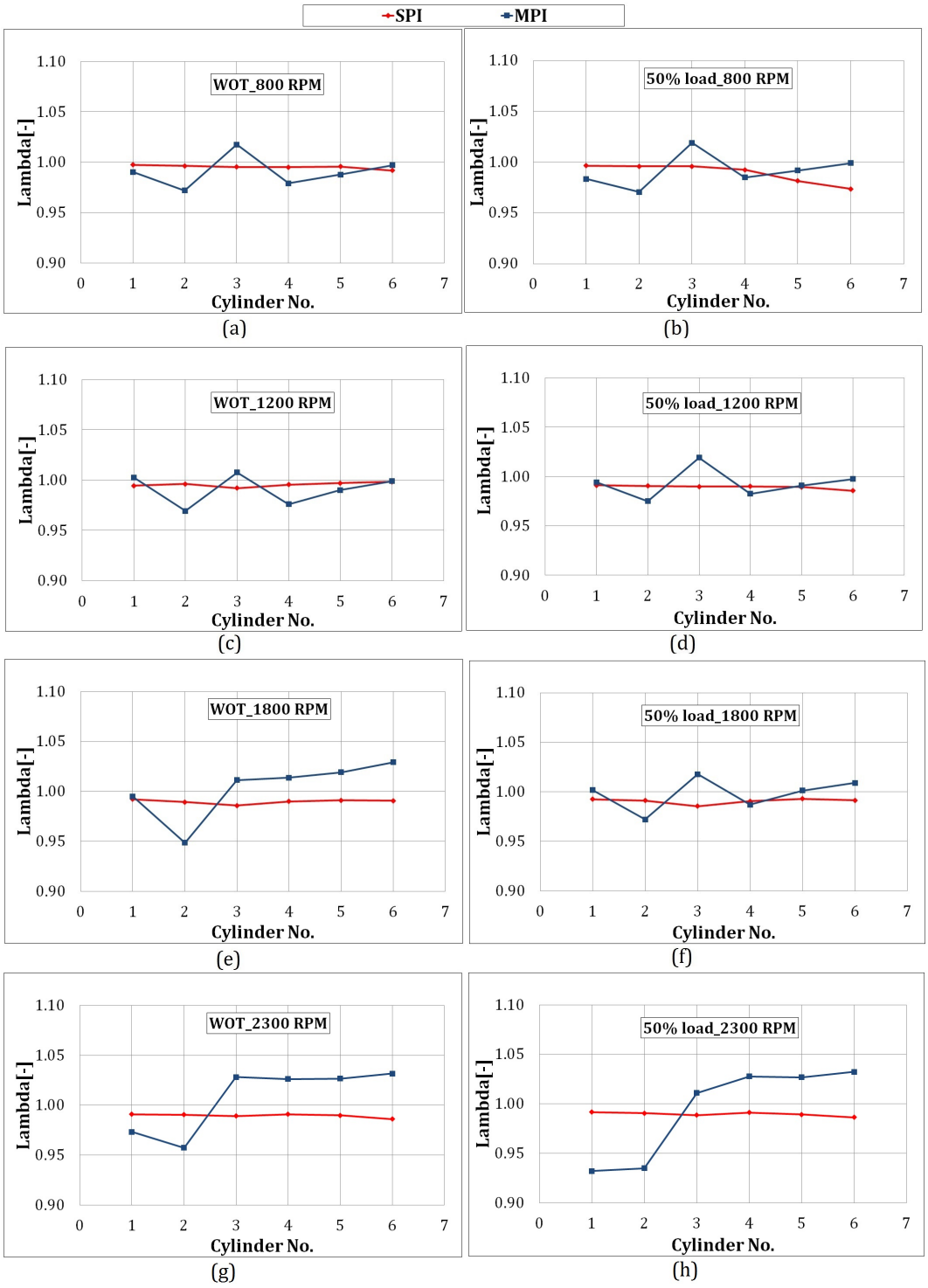

Fig. 4.5 Cylinder to cylinder lambda variations for SPI and MPI at: (a) WOT 1800RPM; (b) 50% load 1800RPM; (c) WOT 1200RPM; (d) 50% load 1200RPM; (e) WOT 800RPM; (f) 50% load 800RPM.

The multi point system is mostly likely to be affected by the intake ducts dynamics as well as by the diversified injectors' behavior and derating, thus assessing for the non-homogeneity of the relative air-to-fuel ratio for the six cylinders with respect to the one induced by the SP functioning. As far as the intake system dynamics is concerned, the MP outcomes on the mixture quality allow for inferring the effects of pressure waves and flow pulsation on the cylinders volumetric efficiency. As a matter of fact, at lower speeds, cylinder #3 induces a larger amount of air with respect to cylinders #2 and #4, thus resulting into a leaner mixture and richer ones, respectively. Such a discrepancy in the air-to-fuel ratio reflects in the mixture laminar speed and hence into the performed engine cycle, appraising the higher PFPs featured by cylinder #2 with respect to those produced by cylinder #3. As an example, the PFP measured in the former cylinder for WOT operations at 1200 rpm sums up to 95 bar, largely exceeding the 86.8 bar brought about by the latter cylinder. The pattern in the distribution of the air amongst the cylinders reproduces itself at lower speeds for WOT operations whereas (Fig. 4.5a, c) it modulates into a different trend for higher speeds (Fig. 4.5e, g). The geometry of the intake runner would now enhance the intake process for cylinders from #3 to #6, raising the unbalance in the air-to-fuel ratio to a major extent. Such an effect is damped down by the throttle at part load operations (Fig. 4.5f) and becomes evident for even higher speeds (Fig. 4.5h).

Overlapping performance were also achieved during transient operations as depicted by the charts in Fig. 4.6 for a load transient (Fig. 4.6a) as well as for a speed transient (Fig. 4.6b) for the two considered injection systems.

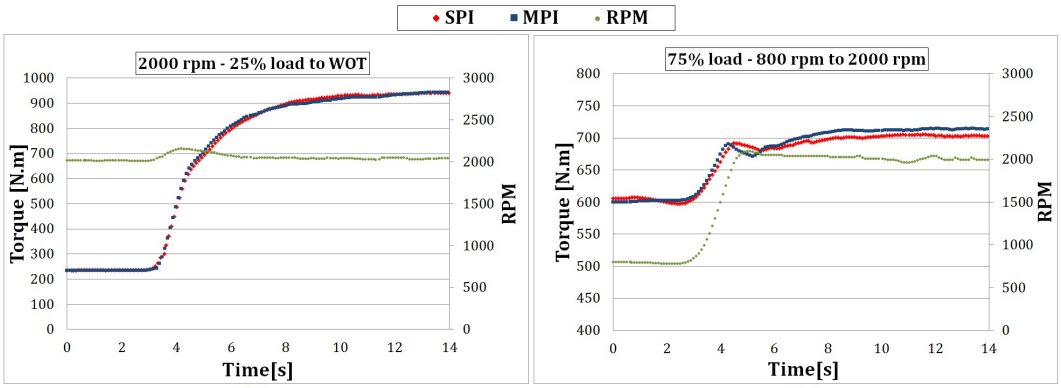

(a) (b)

Fig. 4.6 Transient operations: (a) Load transient; (b) Speed transient.

4.3.2 Cycle-to-cycle analysis

The previous investigation has been completed by performing a thorough cycle-to-cycle analysis of the engine performance, both for the SP as well as for the MP injection system. It is worth recalling that four pressure transducers alone were available for the measurement of the in-cylinder pressure time histories, namely referred to cylinder from #2 to #5. Fig. 4.7 depicts the Coefficient of Variation (COV) of the indicated mean effective pressure (Figs. 4.7a,b) as well as of the peak firing pressure (Figs. 4.7c,d) for WOT operations at the indicated engine speeds, the red bars corresponding to the SP outputs and the blue ones representing the MP engine behavior. The dashed horizontal lines assess for the average value in the corresponding COVs. Similar results are presented in Fig. 4.8 at part loads for the same speeds as for the previous figure.

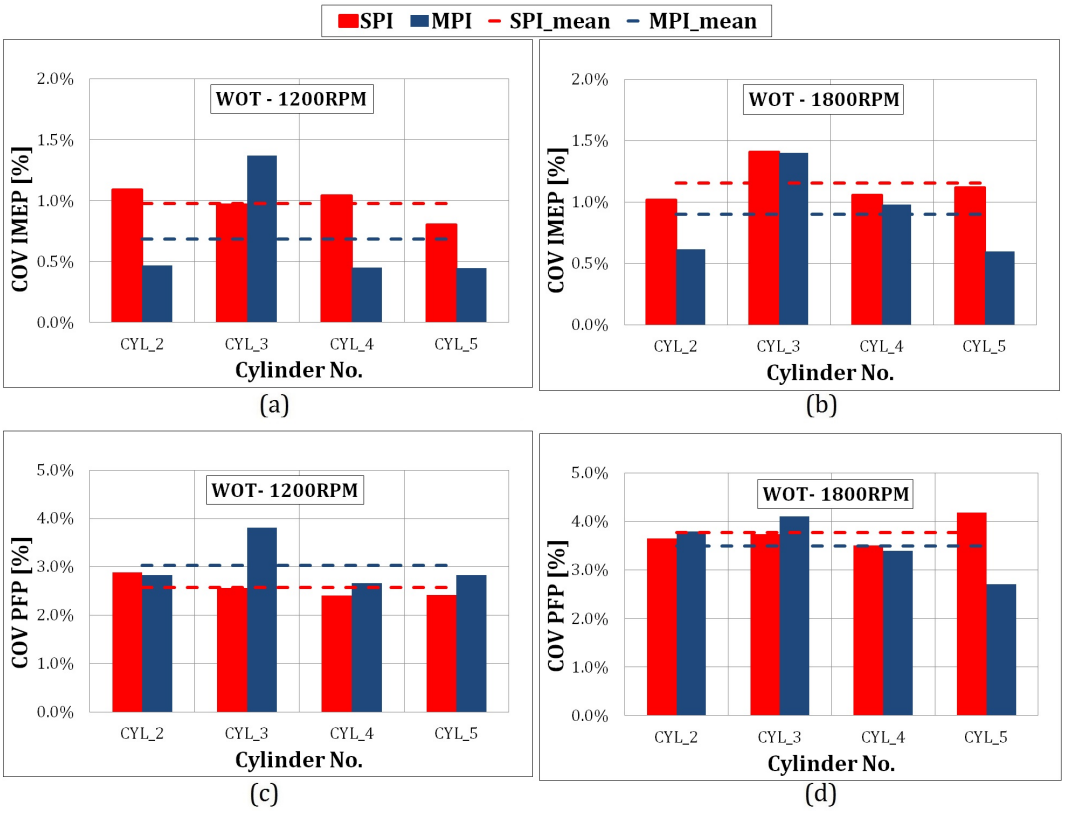

Fig. 4.7 SPI vs. MPI COV for IMEP: (a) 800 rpm, (b) 1200 rpm and (c) 1800 rpm and PFP: (d) 800 rpm, (e) 1200 rpm and (f) 1800 rpm at WOT.

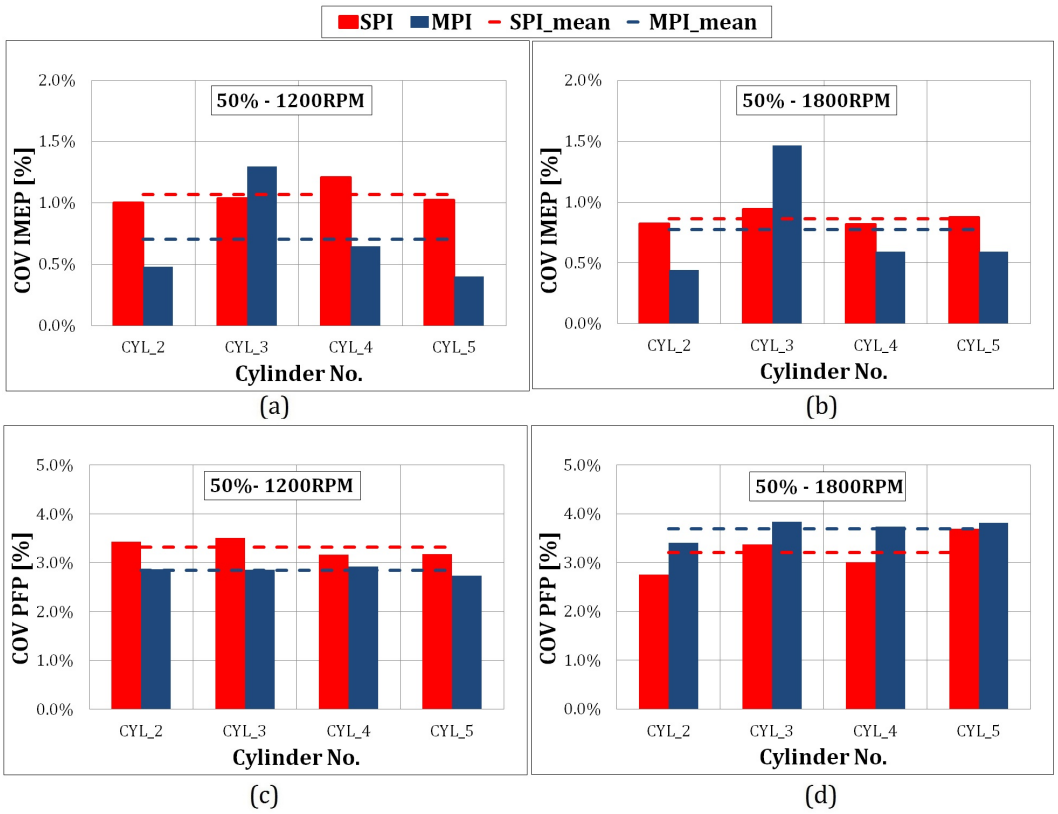

Fig. 4.8 SPI vs. MPI COV for IMEP: (a) 1200 rpm and (b) 1800 rpm and PFP: (c) 1200 rpm and (d) 1800 rpm at 50% load.

It is worth observing that, regardless of the considered operating point, the imep COV deploys below the 1.5% for both injection systems, thus remarking the satisfying matching of the injection systems architecture to the engine layout and assessing for an optimal choice of the ECU parameters. Notwithstanding, differences can be observed in the SP and MP systems outcomes. Despite a reduced cylinder-to-cylinder dispersion and variability, the SP system is responsible for a generally higher average value of the imep COV. This connects to the results presented in Fig. 4.5 for the relative air-to-fuel ratio distribution. Considering the 1200 rpm operating point and focusing the attention on the WOT operations, cylinders #2, 4 and 5 highlight slightly richer mixtures which in turn correspond to the lower COVs in Fig. 4.7a. The larger cycle-to-cycle variability displayed by cylinder #3 in turn matches the higher lambda value sketched out by Fig. 4.5c.

Furthermore, the reduced mixture quality non-homogeneity amongst the cylinders and the closer matching between the SP and the MP system rendered by Fig. 4.5f for partial load operations lines up with the approaching average values of Fig. 4.8b. The

generally lessened imep COV produced by the MP engine hint at enhanced combustion efficiencies, possibly linked to increased mixture homogeneity. This latter is most likely produced by injecting the fuel throughout the intake phase, thus fully exploiting the motion of the induced air as well as the in-cylinder macro- and micro-turbulence yielded by the tumble destruction.

Finally yet importantly, it is worth recalling that the considered engine was designed to be operated together with the analyzed SP injection system whereas the MP one has been mounted on the engine with no specific modifications to the engine layout. Thus, further improvements are to be expected for a dedicated design and architecture. This is once more fully consistent with the findings of [22], suggesting for a dedicated engine arrangement as well as for an optimized intake manifold geometry to properly take advantage of the pressure waves.

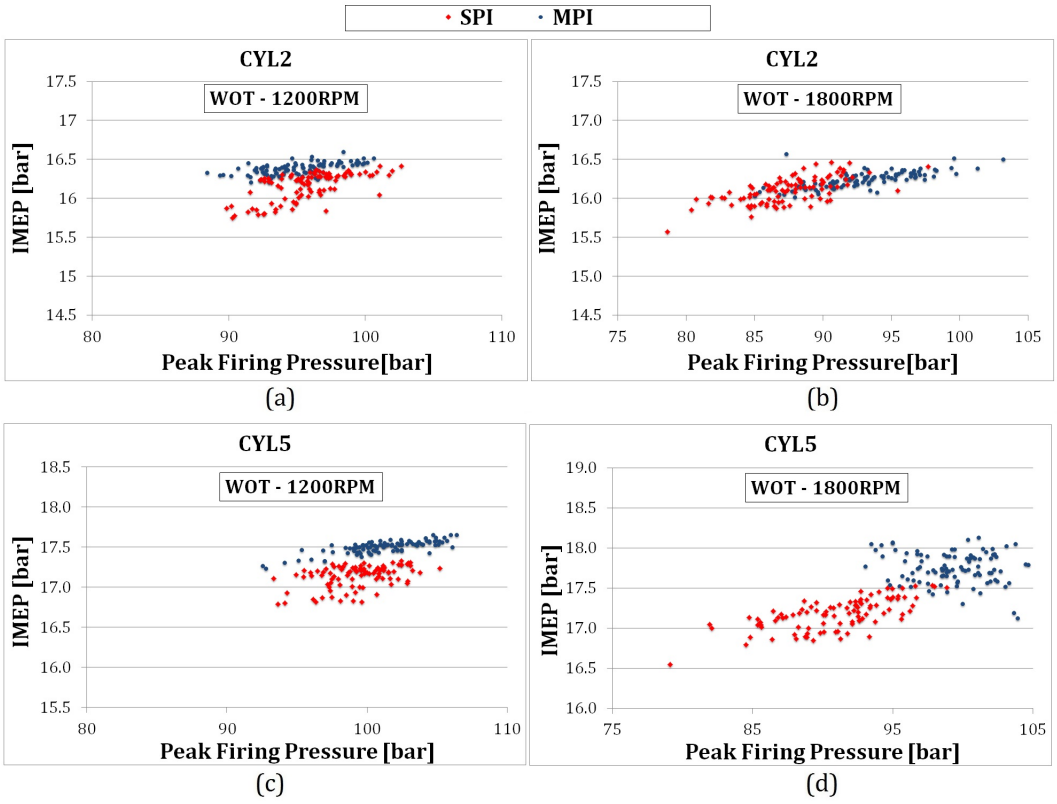

Fig. 4.9 SPI vs. MPI cyclic variation for IMEP vs. PFP at cylinder 2: (a) 1200 rpm and (b) 1800 rpm and at cylinder 5: (c) 1200 rpm and (d) 1800 rpm at WOT.

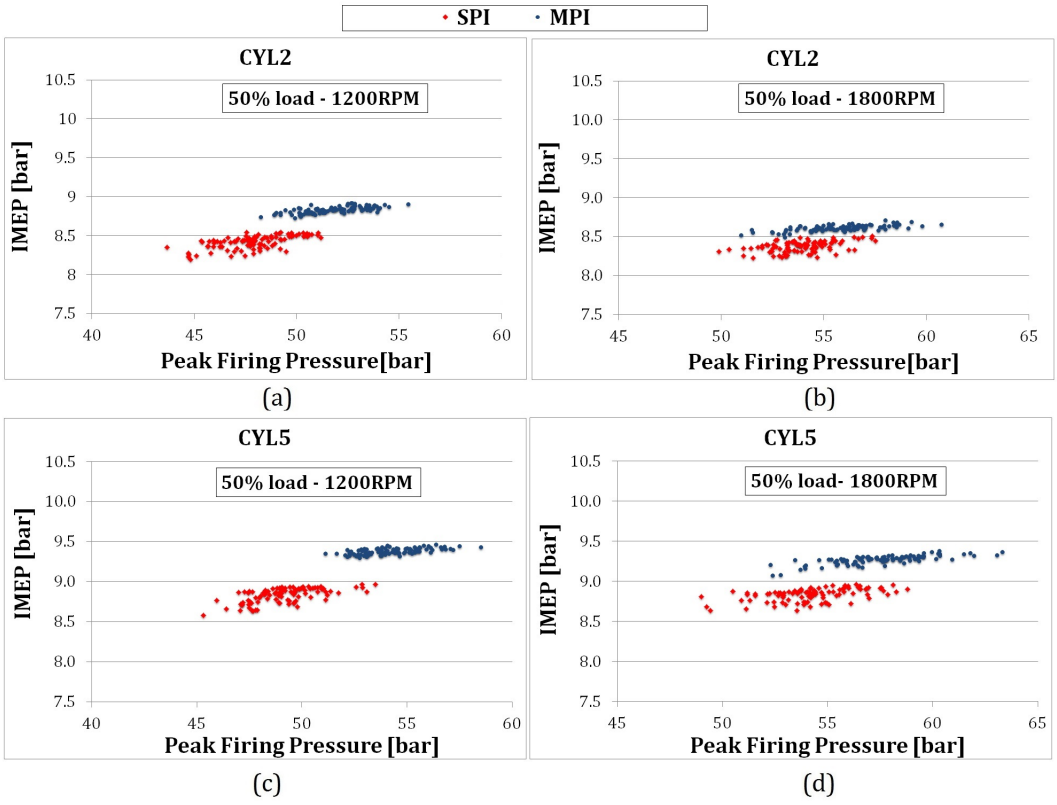

Fig. 4.10 SPI vs. MPI cyclic variation for IMEP vs. PFP at cylinder 2: (a) 800 rpm, (b) 1200 rpm and (c) 1800 rpm and at cylinder 5: (d) 800 rpm, (e) 1200 rpm and (f) 1800 rpm at 50% load.

The charts in Figs. 4.9 and 4.10 allow for a better glance at the engine cycle-to-cycle variability. The imep COV is represented as function of the PFP one for the same operating conditions as for Figs. 4.7 and 4.8. For the sake of conciseness, attention is drawn to two specific cylinders, namely cylinders #2 and #5. The cloud of points represented by the charts embeds the information carried by the bars of the previous figures. The outlines of the clouds at 1200 rpm for the WOT engine points assess for a generally lower cycle-to-cycle variability both for the SP and for the MP system. Contrariwise, considering WOT operations for cylinder #5 at 1800 rpm, the gathering of the MP dots to a limited range of PFP perfectly matches the diminished bars featured by the MP system with respect to the SP one both for the imep as well as for the PFP COVs. Moreover, the similar behavior of the two considered cylinders for part load operations at both speeds (Fig. 4.8) fully corresponds to the almost overlapping charts in Figs. 4.10 from (a) to (b).

4.3.3 MPI sensitivity to injection phasing

The present section deals with the sensitivity analysis of the MPI engine behavior to the injection phasing for WOT and part load operations corresponding to the 50% of the full load ones. Four different injection angles for each of the aforementioned load have been applied and tested (see Table 4.2). The energizing time (ET) and the spark advance have not been changed whereas the phasing has been varied by rigidly moving the end of injection with respect to the compression BDC. It is worth highlighting that the base calibration corresponds to the injection event extinguishing itself 60 deg before the BDC.

Table 4.2 Experimental cases: injection duration and EOI phasing

Speed [rpm]	**Injection duration [deg]**		**EOI advance with respect to BDC [°CA]**			
	WOT	**50% laod**				
800	111.9	65.3	0°	30°	60°	120°
1000	165.6	92.1	0°	30°	60°	120°
1200	216.6	117.1	0°	30°	60°	120°
1400	268.5	142.5	0°	30°	60°	120°
1600	326.2	168.9	0°	30°	60°	120°
1800	369.6	185.4	0°	30°	60°	120°
2000	408.2	206.0	0°	30°	60°	120°
2300	158.8	128.2	0°	30°	60°	120°

For the sake of brevity, Figs. 4.11 and 4.12 report the imep and PFP COVs for the four instrumented cylinders for two given engine speeds, namely 1200 and 1800 rpm. The different colors correspond to the various phasing as indicated in the legend (the blue bars match the base calibration). Regardless of the considered speed and load, a retarded injection leads to increased imep COVs for all of the cylinders, thus assessing for a poor exploitation of the dynamics effects during the intake phase. In fact, mixing requires time to fully deploy and an untimed injection might hence produce a mediocre quality of the mixture formation which in turn would cause increase COVs values. Such a behavior is even more evident at the lower speed and for part load operations. This is mostly to be ascribed to the scaled down turbulence connected to the reduced speed as well as to the damped flow motion produced by the throttle. The aforementioned results are in line with the findings of [49, 52]. Moreover, a reverse trend is observed for highly advanced injection events (MPI_120 – yellow bars) due to the injection occurring mostly out (1200rpm) or fully out (1800 rpm) of the intake window (see Table 4.2).

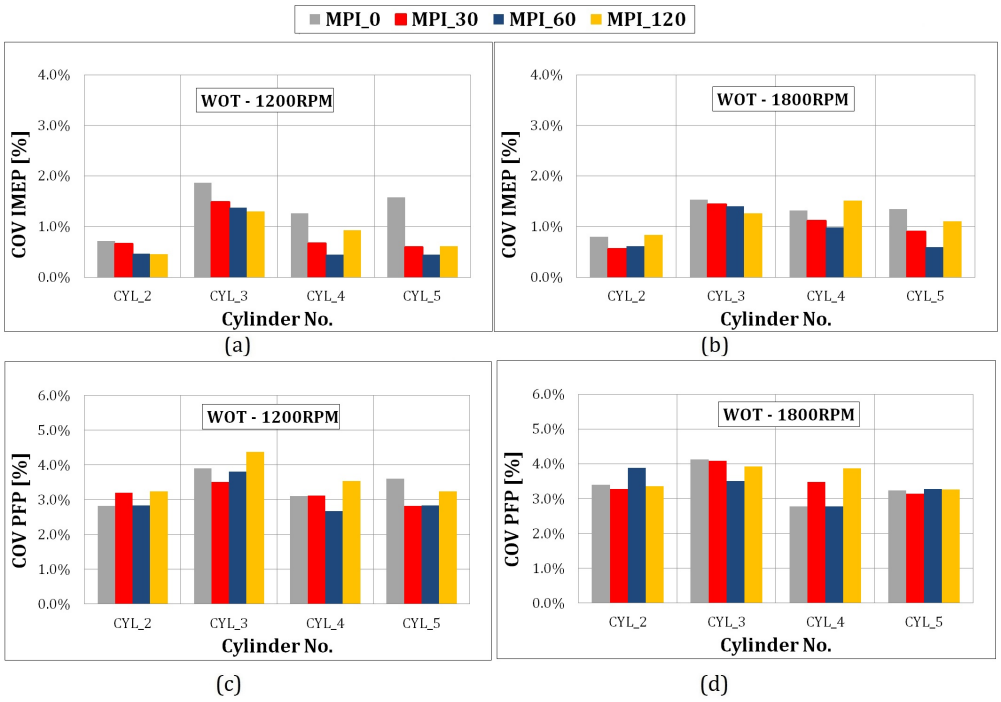

Fig. 4.11 MPI sensitivity to phase variation COV for IMEP: (a) 1200 rpm (b) 1800 rpm and PFP: (c) 1200 rpm (d) 1800 rpm at WOT load.

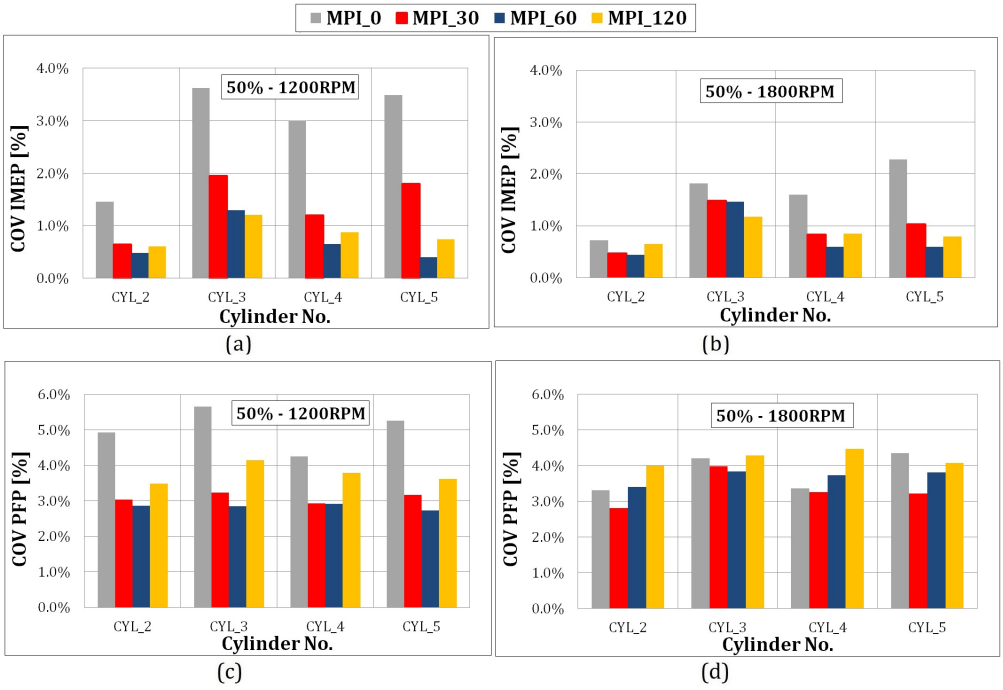

Fig. 4.12 MPI sensitivity to phase variation COV for IMEP: (a) 1200 rpm (b) 1800 rpm and PFP: (c) 1200 rpm (d) 1800 rpm at 50% load.

4.4 Numerical model

The CNG engine has been modelled at ICEAL (Internal Combustion Engines Advanced Laboratories) of Politecnico di Torino using GT-POWER v7.4, a 0/1D simulation tool licensed by Gamma Technologies. The model has been built based on the specific geometry characteristics of each engine component provided by the technical drawings from the engine producer as well as referring to the specific test bench layout. The calibration of the engine 1D model has been carefully carried out in order to achieve accurate results. The calibration procedure includes the tuning of the specific model coefficients, such as heat transfer coefficients, wall friction coefficients and valves discharge flow coefficients, and aims at matching the numerical results to the experimental readings obtained for the steady-state operating points. These tuned coefficients are hence used as semi-empirical input data in the model in order to make the model capable of predicting the engine fluid-dynamics and behaviour for different operating conditions.

The combustion model considered for the simulations is the GT non-predictive combustion one which calculates the burn rate from the measured cylinder pressure. The ensemble average of 100 experimental in-cylinder pressure traces obtained for each of the 32 steady-state operating points was the main reference data set used to build up the corresponding combustion rates by means of 'Two-Zone Combustion Methodology'. The heat transfer coefficients have been carefully calibrated so as to achieve an almost perfect matching to the experimental pressure time-history and were hence exploited to set up the look-up tables for the engine model implementation. Moreover, the turbocharger has been thoroughly characterized: the waste gate dimeter (WD) has been in turn identified by targeting the measured pressure at turbine inlet and the turbine efficiency multiplier (EM) have been determined addressing to the measured boost level.

The tuned values of the turbine waste gate diameters and efficiency multipliers have been exploited to frame the corresponding look-up tables and have hence been included in the turbocharged engine model to generate the internal maps defining the performance of the turbocharger over wide range of operating conditions. As far as the injection system is concerned, two different model configurations have been developed to characterize the SP and MP injection systems. The models have been properly calibrated in order to match the simulation outputs to the experimental data obtained from the experimental tests.

4.4.1 Single-point and multi-point injection system models

The GT-POWER model map for the SP injection system is reported in Fig. 4.13. The system is made up of:

- four CNG injectors;
- a steel delivery pipe;
- a plastic robber bending pipe;
- the mixer.

The mixer itself consists of an orifice and two flow splits. It is worth underlining that the fuel rail has not been explicitly considered in the model. In fact, a defined model for the sequential CNG injectors has been used to reproduce the injection event for a given air-to-fuel ratio. The injection pulse width has in turn been calculated setting the injection delivery rate and air-to- fuel ratio provided by the experimental data. The four injectors perform six injection events evenly spaced at 120° deg during the engine cycle. The orifice used in mixer model is meant to represent the effect of the 2 mm diameter 24 holes featured by the actual mixer. The diameter of the mixer orifice has been optimized by running the model under steady state conditions so that the static pressure in the steel delivery pipe would match the experimental one for a given delivery rate.

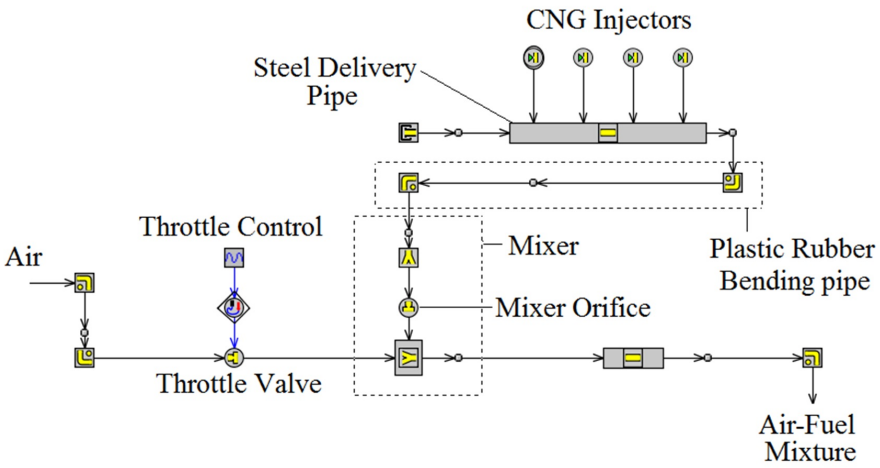

Fig. 4.13 SP Injection system, GT-POWER model map

Similarly, the MP system has been simulated by means of a properly adjusted GT-Power map (Fig. 4.14). Given the common characteristic in terms of rail pressure and mass

flow rates, identical CNG injector as for the SP injection system have been considered for MP GT-Power map. The injection phasing for the steady state operating points has been set according to the experimental readings.

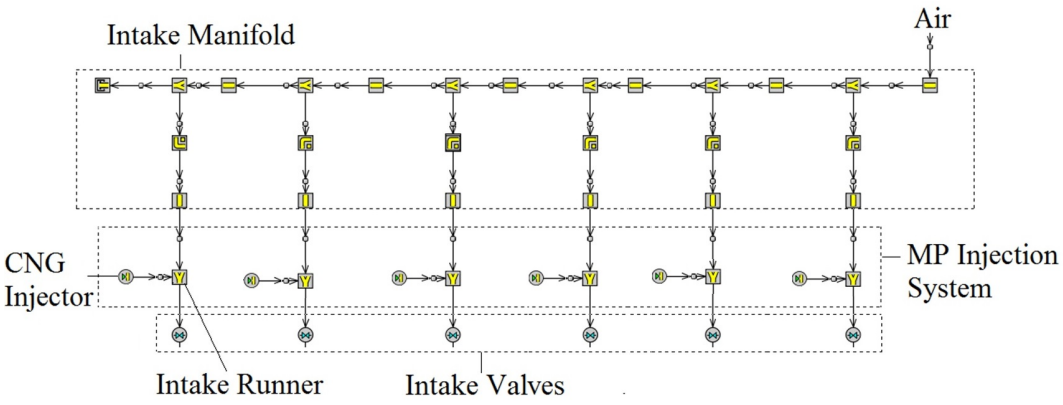

Fig. 4.14 MP Injection system, GT-POWER model map

4.4.2 Models validation

The engine models parameters have been tuned to reproduce the engine behaviour at any of the 32 steady-state test points. It is worth recalling that the experimental points were chosen to reasonably represent the whole engine operating range. Figs. 4.15 and 4.16 compare the experimental readings (light blue dots) to the model outputs (red squares) in terms of induced air mass flow rate, boost pressure, peak firing pressure and indicated mean effective pressure. For the sake of conciseness, the charts simply depict the results obtained for the WOT functioning as well as for part load operations corresponding to the 50% of the full load ones.

Fig. 4.15 specifically refers to the SP injection system outcomes whereas Fig. 4.15 refers to the MP ones. The plots highlight a quasi-perfect matching for all of the considered quantities with minor deviations arising for the air mass flow rates at WOT operations. Still, the accuracy of the tuning as well as the reliability of the numerical models is testified by the overlapping in the imep values for all of the considered points (Figs. 4.15d and 4.16d).

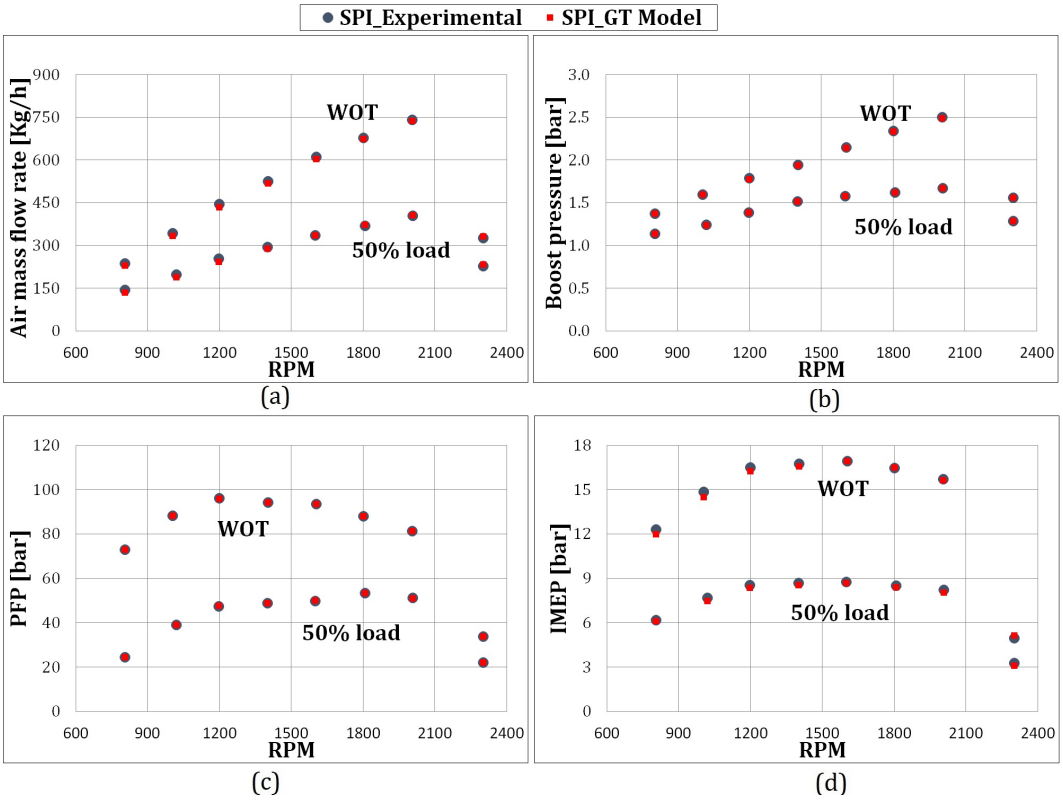

Fig. 4.15 SPI model results under steady-state operating conditions, as function of engine speed – (a) Boost pressure; (b) Air mass-flow rate; (c) Peak Firing Pressure (d) Indicated mean effective pressure.

Figs. 4.17 and 4.18 report the ensemble average in-cylinder pressure traces for two specific speeds out of the points considered for the previous figures, namely 1000 rpm and 2000 rpm. The solid line refers to the experimental pressure time-history whereas the dashed one depicts the numerical output for the SP (Fig. 4.17) as well as for the MP (Fig 4.18) engine model. Once more, a full correspondence is to be observed for the pressure time-histories and smaller differences are only observed throughout the compression phases, mainly to be ascribed to the slight differences in the induced mass flow rates rendered by Figs. 4.15a and 4.16a. The results presented in figures from 14 to 17 assess for the full reliability of the two models in representing the actual engine behavior. They have been hence used to carry out a thorough investigation into the response of the engine equipped with two different injection systems to the injection phasing as well as to the ECU strategy.

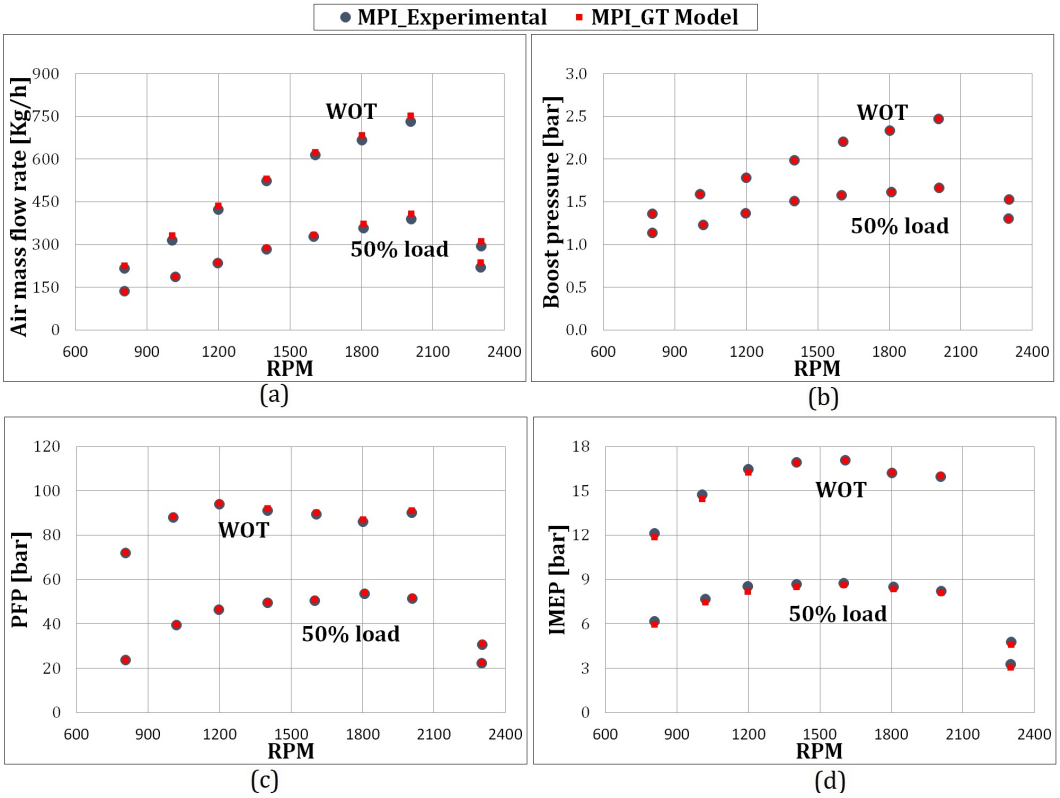

Fig. 4.16 MPI model results under steady-state operating conditions, as function of engine speed – (a) Boost pressure; (b) Air mass-flow rate; (c) Peak Firing Pressure (d) Indicated mean effective pressure.

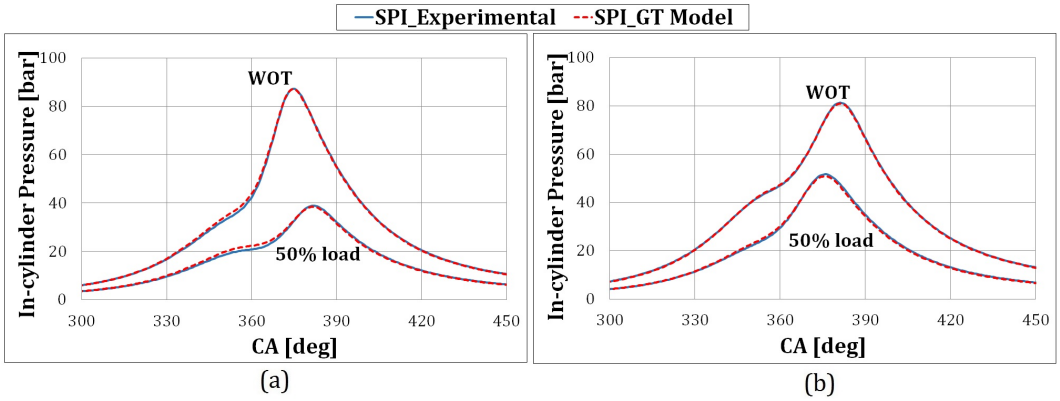

Fig. 4.17 SPI model versus experimental in-cylinder pressure (Cylinder No.2) at WOT and 50% load and at (a) 1000 RPM and (b) 2000 RPM.

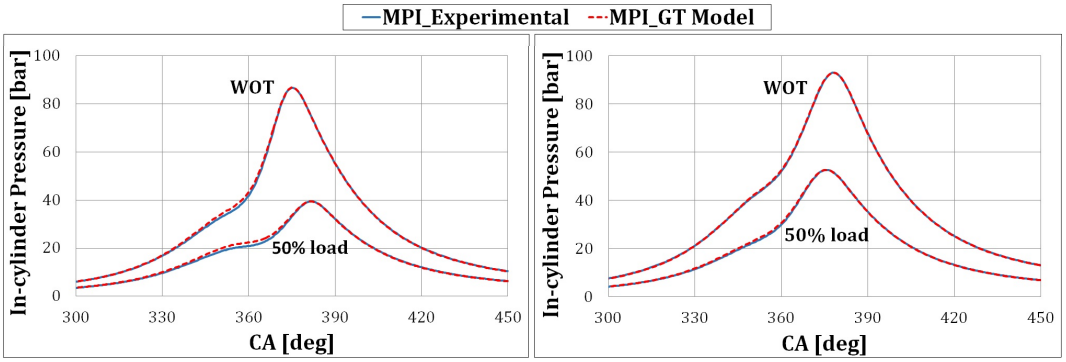

Fig. 4.18 MPI model versus experimental in-cylinder pressure (Cylinder No.2) at WOT and 50% load and at (a) 1000 RPM and (b) 2000 RPM.

4.5 SPI system: injection phasing

The previously calibrated SP injection system model has been used to predict the response of the engine to different injection phasing. The analysis was mainly aimed at appraising the optimal injection pattern in terms of number of injections and injections spacing so as to carry out a consistent comparison between the SP layout and the MP one. A number of injections varying from one to six throughout the period corresponding to one engine cycle have been considered and the results are presented in figures from 4.19 to 4.22.

Fig. 4.19 serves the purpose of allowing for explaining and giving consistency to the outcomes presented in the following figures and charts. More specifically, it reports the natural gas mass flow rate (Y scale on the right) for the different patterns of injection considered for the analysis together with the valve lift (Y scale on the left) of the six firing cylinders throughout the engine cycle for the indicated engine operating conditions. 1 (Fig. 4.19a) to 6 (Fig. 4.19d) injection events have been considered for the investigation and the engine performance have been correspondingly depicted in the following figures in terms of pressure in the intake system (MAP) (Fig. 4.20a), peak firing pressure (Fig. 4.20b), brake torque (Fig. 4.20c), turbine inlet pressure (Fig. 4.20d) as well as of relative air-to-fuel ratio for the six cylinders (Figs. 4.21 and 4.22) for different engine speeds. The overall injected mass is unchanged from 1 (the four injectors are activated at once), to 2 (two injectors are simultaneously actuated) and up to the progressively increasing numbers of injections (the four injectors are sequentially activated). It is worth highlighting that the injection events have been evenly spaced with respect to the cycle duration so that the pattern of the 6 injections would technically correspond to a fully carburetted mixture

(Fig. 4.19d). The figure outlines the procedure followed for the investigation and would merely replicate itself at speeds higher than the considered one, i.e. 800 rpm. A one figure has been reproduced for the sake of conciseness and the choice has been appointed on the speed featuring the shorter injection duration at WOT so as to better highlight the effects of the different injection patterns.

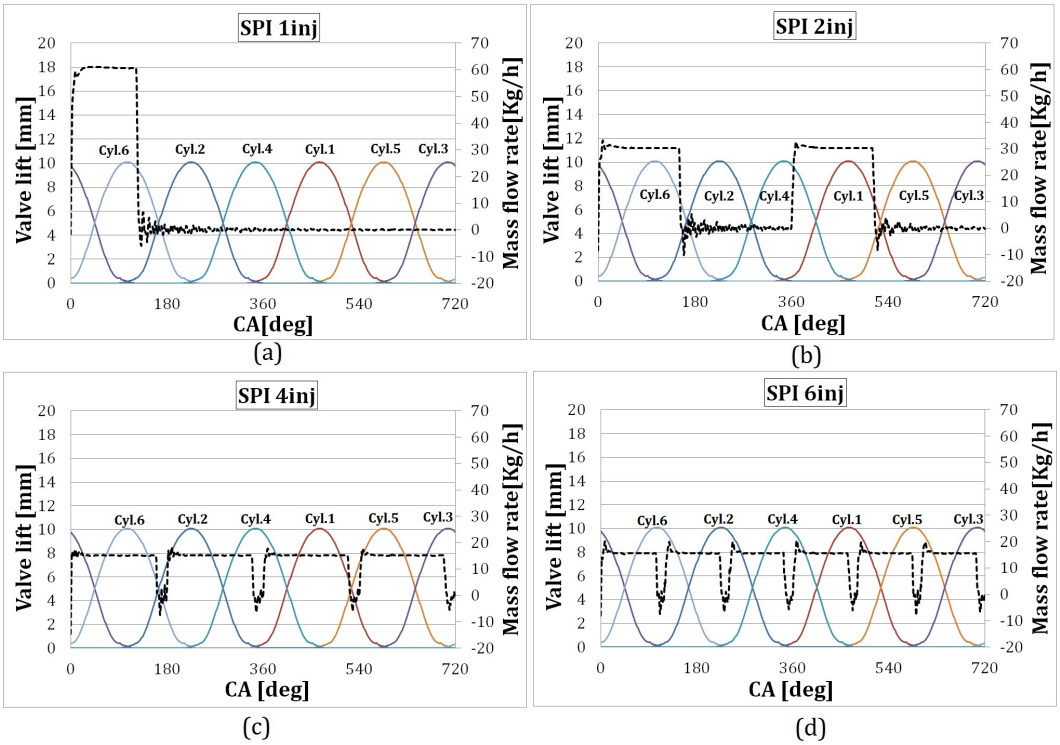

Fig. 4.19 CNG mass flow rate for 1 , 2 , 4 and 6 injection events per cycle (800 rpm – WOT).

The injection timings for the SP system are close to the ones of the MP one (see Table 4.2 for the base injection frame). It is worth considering that the diminished mass flow rates connected to the six injection events would allow for reduced rail pressure, thus reducing the mismatch between the theoretical mass set by the ECU and the actually injected one [paper ASME 2010]. One should in fact consider the advantages deriving from the adoption of an increased number of injection events as connected to the ET, i.e. injection duration, as well as to rail pressure. In fact, a reduced number of injections would necessarily imply either an augmented rail pressure for a given energizing time or an increased ET for a set rail pressure. Still, the six injection events feature a discontinuous feeding to the mixer, thus inevitably affecting the mixture quality. This is particularly true at the lower speeds, where the shorter injection durations are bound to affect the different pattern to a major extent and where the six-injection strategy would still give rise

to gaps in the fuel feeding. Higher speeds would stretch out the pattern of the six-injection solution, thus allowing for achieving an optimal homogeneity of the mixture, but would in turn impair the effectiveness of the strategies involving a reduced number of injections. In fact, given the limitations on the rail pressure and hence on the injected fuel mass, one to two injections would yield to an injection angular frame possibly exceeding that of the engine cycle.

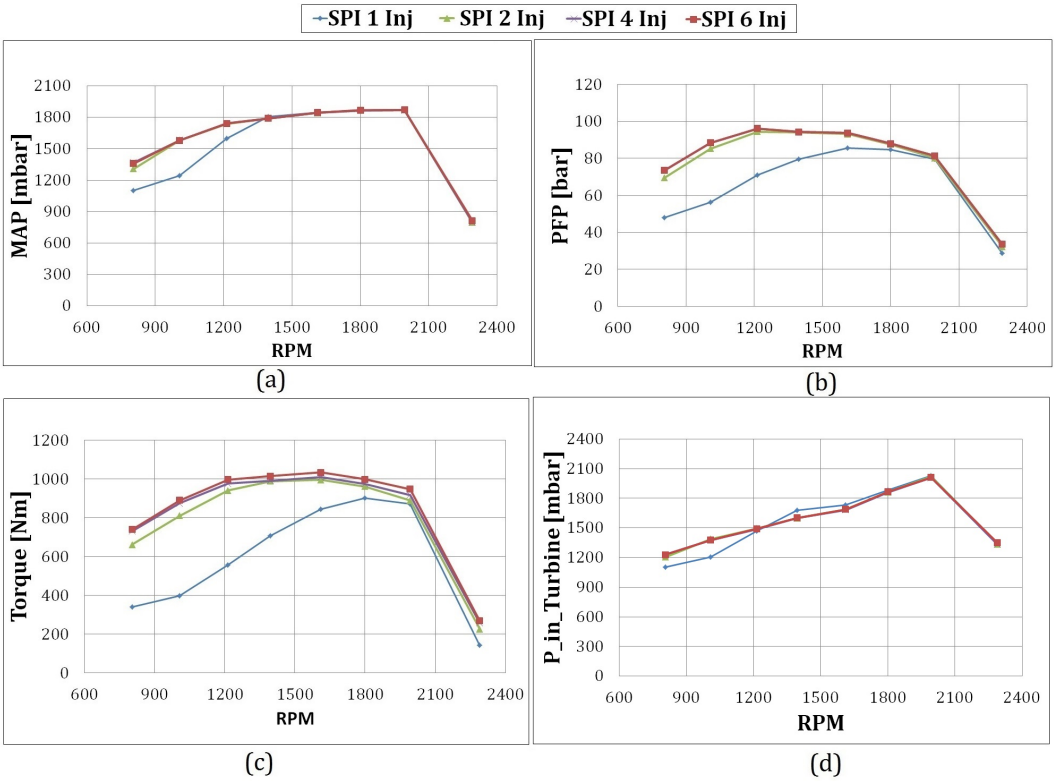

Fig. 4.20 Engine performance for the different injection patterns at WOT.

A possible solution to the aforementioned constraints is represented by the exploitation of six separate injectors performing the six injection events. In fact, the six separate injectors would allow for overlapping the injection events at the lower speeds, thus getting rid of the feeding gaps discussed in the previous paragraph and highlighted in Fig. 4.19d. Moreover, the higher mass flow rates connected to a given rail pressure would grant shorter injection durations at the higher speeds where the base duration would eventually overcome the engine cycle accomplishment. A better insight into the considered solution is represented by the numbers produced by the simulations of the 2000 rpm WOT test case. Four injections would require an injection width close to the engine cycle duration and corresponding to 612°, the latter achieved by means of a delivered fuel mass flow rate

of 15 kg/h. Contrariwise, six separate injection events would guarantee the given angular frame with a reduced mass flow rate of 10 kg/h, corresponding to an eventually lowered rail pressure value and hence to a better matching to the ECU settings. Elsewise, the given rail pressure could be exploited at the higher speeds to reduce the ET. One should hence find the proper trade-off between number of injectors and number of injection events, i.e. a trade-off between costs and benefits for the engine performance.

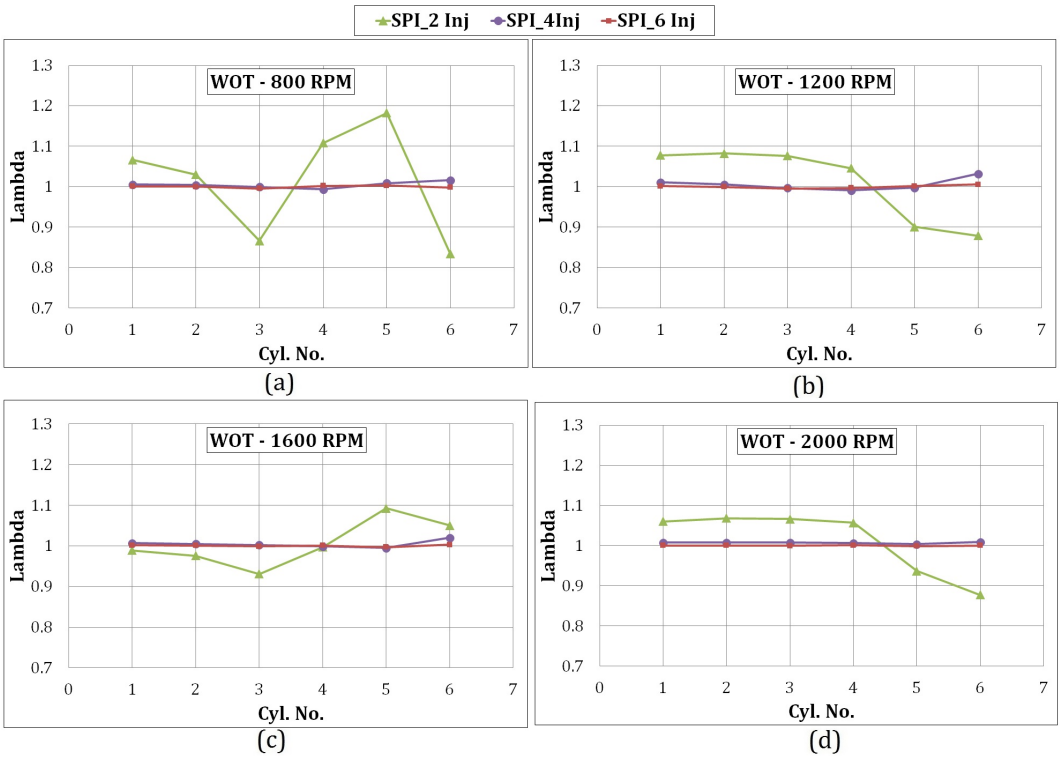

Fig. 4.21 Cylinder-to-cylinder lambda variation for the different injection strategies at WOT for the indicated speeds.

Figures 4.19-4.22 address the base settings presented in Fig. 4.19 and allowed for by the normal production SP layout, i.e. four sequentially activated injectors. The curves (symbols and colors) in Fig. 4.22 refer to the four injection strategies considered and specified in the legend to the charts. Regardless of the considered speed, the results are mostly unaffected when it comes to 4 to 6 injection events. In fact, these latter would produce an almost continuous feeding of the fuel to the cylinders, thus guaranteeing a quasi-perfect mixing which would further reflect in the homogenous relative air-to-fuel ratio distribution depicted in Fig. 4.21 (purple crosses and red dots). Conversely, major differences are observed in the engine performance for the reduced numbers of injection events (blue dots and green triangles) at lower to medium speeds. Such

a behavior is clearly to be ascribed to the spatially confined injection/injections (Figs. 4.19a, b) that would hence produce a highly discontinuous fuel feeding to the cylinders and, correspondingly, a strongly non-homogenous distribution of the air-to-fuel ratio amongst the cylinders (Figs. 4.21 and 4.22). It is worth observing that the effects of the one-injection events could not be possibly embedded in the charts of Fig. 4.21 due to scaling issues and their representation has been consequently moved to a dedicated chart in Fig. 4.22 (Fig. 4.22a). The one-injection event exerts a stronger influence on the engine performance also lasting for a wider speed interval whereas a minor impact is observed at higher speeds, mainly descending form the increasing injection duration which would now basically cover the whole engine cycle, thus erasing the upshot of the varying number of injection events. The extremely variable and poor relative air-to-fuel ratios in Fig. 4.21a would also hint at the possibility of incurring in misfire events, thus giving further consistency to the engine performance derating taking place at low speeds. Given that the production SP system already embedded the optimal sequentially phased injection pattern, no improvements are basically possible in terms of engine performance and enhancement could only be achieved by adopting specific control logics with the MP configuration.

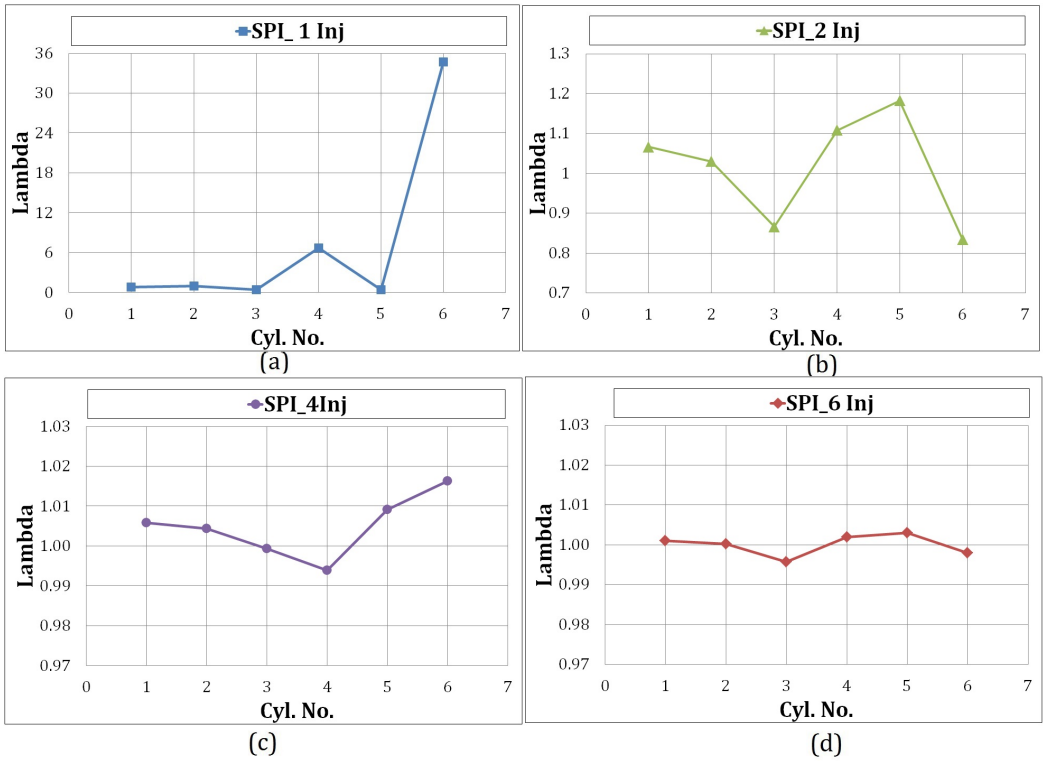

Fig. 4.22 Cylinder-to-cylinder lambda variation in the SPI system for the different injection strategies (800 rpm – WOT).

4.6 MPI system optimization by fire skipping (Cylinder deactivation)

The analysis carried out in the previous section assesses for the already optimal configuration and management strategy of the production SP system equipping the 7.8-liter engine. Hence, given the lack of room for improvement in the SP system and considering the overlapping of the performance curve for steady state and transient operations, the superiority of the MP one stems from the results produced by the simulation of the so called fire skipping or cylinder deactivation strategy. The latter can be perceived as an extreme form of engine downsizing devoted to specific operating conditions. More specifically, it is generally performed by excluding one or more of the engine cylinders by either merely cutting the injection and the ignition events for the designated cylinder/s or by eventually also exploiting the benefits of a VVA system to reduce the drawbacks of the inactive cylinder/s. Moreover, cylinder deactivation should carefully pick up the cylinder/s to be rendered ineffective accordingly to the engine firing order. The present section presents the results of the numerical model according to the fire skipping strategy for a selection of the previously considered engine working points. These latter are reported in Table 4.3 together with indications on the number of active cylinders selected for the specific ECU strategy as well as with the correspondingly attained bsfc values for 50% and 25% load operations.

Table 4.3 Fire skipping strategy benefit at part load operations

Speed [rpm]	**50% load**		**25%load**	
	No. active Cylinders	**Advantage in bsfc [%]**	**No. active Cylinders**	**Advantage in bsfc [%]**
800	5	5.1	-	-
1000	5	1.6	3	12.1
1200	5	1.3	3	9.3
1400	4	2.8	3	7.0
1600	4	2.6	3	6.1
1800	4	3.0	3	6.4
2000	4	3.3	3	7.6

The number of cylinders to be deactivated has been selected to guarantee the load and the boost pressure at the engine inlet. The waste gate position has not been modified with respect to the base cases whereas minor adjustments have been performed on the throttle position and on the SA.

Tests have also been carried out to compare the improvements on the engine performance produce by the fire skipping for different methods in achieving the desired load. More specifically, the model has been run either by acting on the waste gate position at WOT conditions or by adjusting the load by means of the throttle for a given position of the waste gate. The bsfc values produced by the two modes were presenting a quasi-perfect matching, thus isolating the benefits of the cylinder deactivation technique from the influences of the engine throttling and of the exhaust back pressure.

Fig. 4.23 reports the percentage gain in the bsfc versus the engine bmep for the fire skipping strategy together with its regression line. Consistently with the findings of [107, 108] , the gain grows bigger for reduced loads thanks to the possibility of increasing the number of deactivated cylinders, thus increasing the volumetric efficiency of the active ones and the engine thermodynamic efficiency. The latter is mostly to be ascribed to a considerable reduction in the pumping mean effective pressure. Moreover, the low pressure levels attained in the deactivated cylinders would in turn be responsible for a contraction in the rubbing friction contribution, thus enhancing the further enhancing the engine efficiency [107].

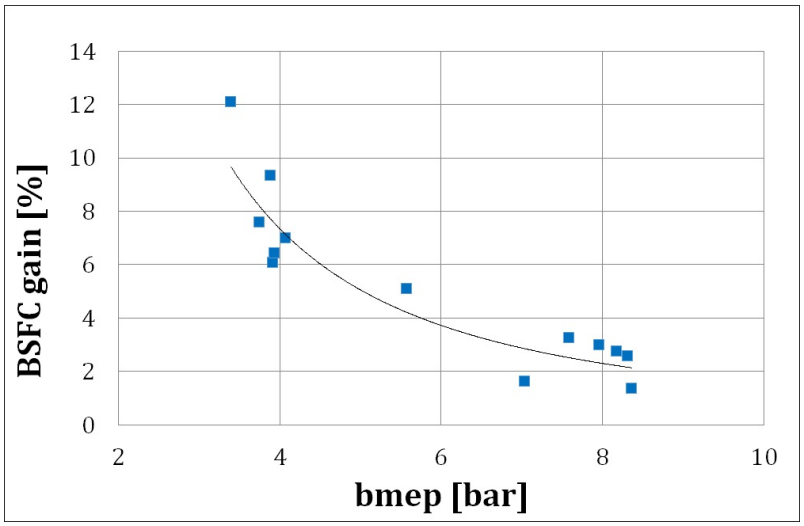

Fig. 4.23 Fuel economy gain in the fire skipping compared to throttled operations.

The charts in Fig. 4.24 depict the volumetric efficiency of cylinder #2 (a), the engine efficiency (b), the bsfc (c) as well as the temperature at the turbine inlet (d) for the base engine (red diamonds) and for the cylinder deactivation strategy (blue squares) for the loads and speeds enlisted in Table 4.3. It is worth recalling that the results have been produced by adopting the same throttle position for both sets of curves. Hence, the striking increase in the volumetric efficiency for the considered cylinder is to be ascribed to the intake system serving a reduced number of cylinders. In fact, analogous values are obtained for all of the speeds at the 25% load operations constantly involving the same number of active cylinders whereas a swerving is observed at the 50% load operation as the number of firing cylinders increase from 5 (low speeds) to 4 (high speeds). Small improvements in the engine efficiency would also be produced by the base engine control strategy adopting a WOT and attaining the desired load reduction by acting on the waste gate position. Still, the exploitation of the waste gate for the load reduction would only allow for a 60% load and the increase in engine efficiency would not reach the one produced by the fire skipping technique.

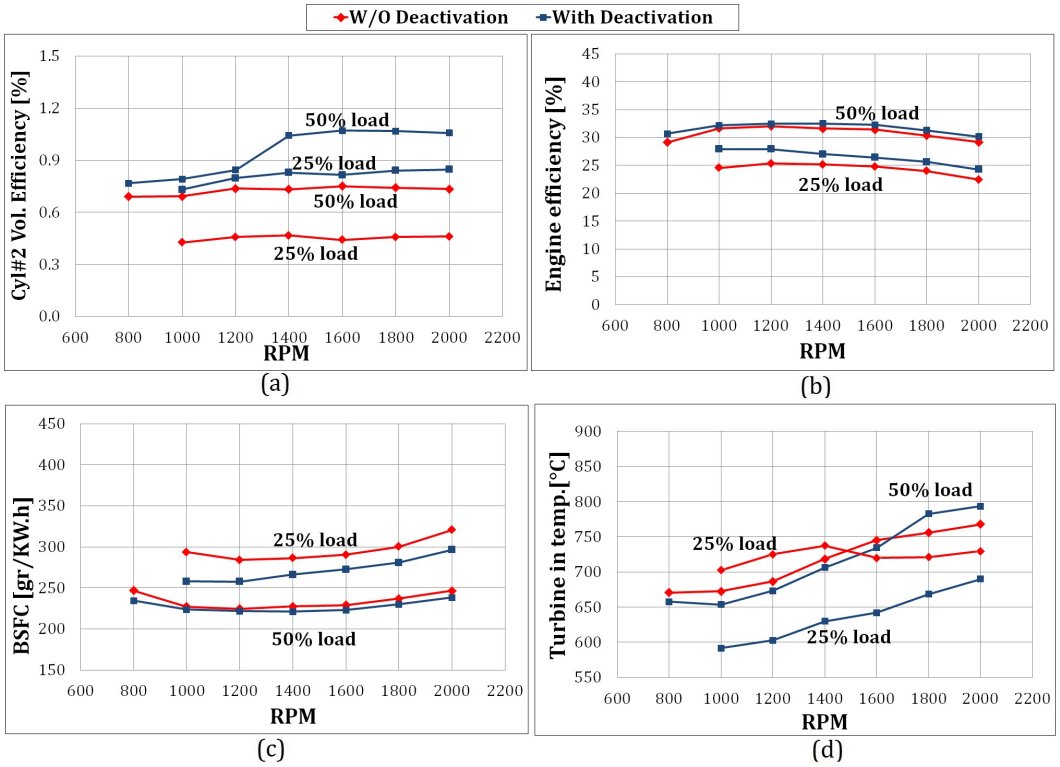

Fig. 4.24 Engine performance at part loads with and without the fire skipping strategy .

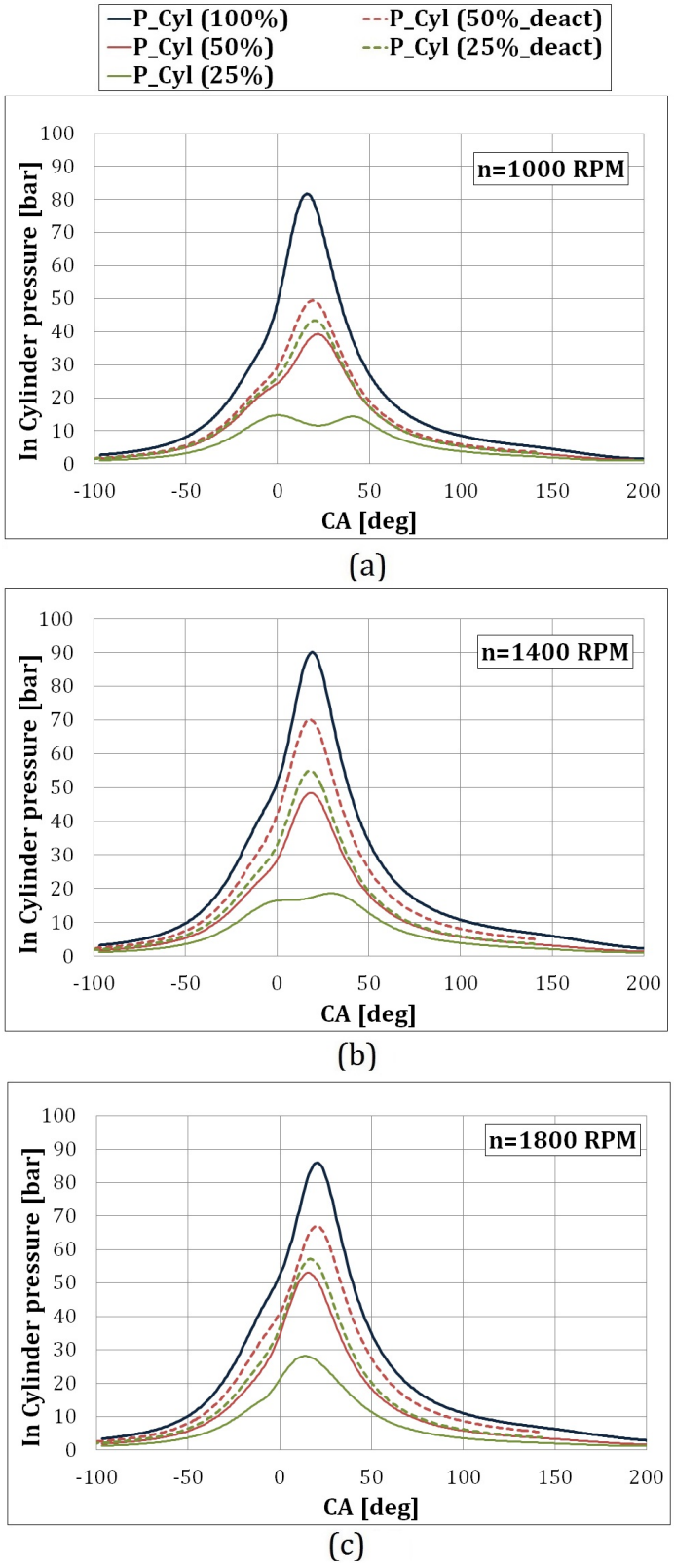

Fig. 4.25 In-Cylinder pressure traces (Cyl 2) at part loads with and without fire skipping

Finally, it is worth observing that the number of cylinder deactivated would not correspond to the load percentage reproduced by the engine working point. More specifically, the 50% load operation would not lead to halving the number of firing cylinders. In fact, the fire skipping technique normally implies lower temperatures at the turbine inlet [107, 108] thus slightly reducing the single cylinder performance with respect to base operations (see Fig. 4.25). Should the number of cylinders be reduced complying with the actually desired load, the engine settings would have to be modified to achieve higher boost level to increase the active cylinder indicated work. According to [108] the frequency by which the cylinders are deactivated in the fire-skipping mode plays a major role in affecting the engine performance. More specifically, it was proved that cylinders featuring high active-deactivate frequencies would reach peak pressures lower with respect to constantly skipped ones, mainly to be ascribed to a negative blow-by produced by the air being sucked from the crankcase. The present chapter disregarded the dynamics of the fire skipping and further improvements are to be expected if the latter was to be properly accounted for.

4.7 Conclusions

The present investigation focused on the potentials of a dedicated multi-point injection system purposely developed to be embedded on a normal production single-point NG heavy-duty engine. The experimental campaign was carried out over a wide range of operating point for the engine equipped with the two injection systems alternatively and allowed a sound comparison of the engine performance under steady state as well as transient operations. Minor differences were observed in terms of torque and power output whereas differences arouse in terms of cylinder-to-cylinder variability and air-to-fuel ratio homogeneity. More specifically, given the quasi-perfect matching in terms of engine performance produced by the two injection systems, the MP layout proved to better exploit the intake system dynamics and hinted at the need for a dedicated engine architecture and ECU management. The engine imep COV reduced by a 30% for the MP system at the lower speeds despite a higher cylinder-to-cylinder variability, possibly induced by the air-to-fuel ratio dispersion. The stronger mixture homogeneity produced by the SP system did not reflect into increased combustion efficiencies and the difference in the cyclic variation would only reduce at higher speeds. Moreover, the MP layout was tested under different injection phasing to assess for the optimal ECU setting.

Numerical models were also set up, validated and tested for both the SP and the MP system to investigate into enhanced control solutions and improved ECU logics. More specifically, the SP model was used to assess for the influence of the injection phasing on the engine performance. Major differences were only observed for reduced numbers of injection events at low speed and WOT operations. A single injection event led to a derating in the engine torque ranging around 100% whereas negligible differences with respect to the base calibration stemmed for 4-6 injection events. The numerical analysis also allowed for considering the potential of exploiting a higher number of injectors to perform the considered injection strategy, thus enabling the SP mixer to guarantee an almost constantly homogenous mixture for all of the cycles and all of the cylinders. The analysis endorsed the already optimal architecture and ECU strategy of the production SP engine and highlighted the lack of room for improvement. Hence, further enhancement in the engine management could only be achieved by means of a proper governing of the MP system. More specifically, the research investigated into the possible improvement to be attained by introducing the fire skipping strategy. The part load operations were reproduced by activating 3-5 cylinders depending on the specific operation point and differences up to the 18% in the bsfc were observed for the lowest loads and speeds, mainly to be ascribed to an increase in the cylinders volumetric efficiency. It is worth mentioning that even stronger improvement are expected - according to the findings in the literature - considering the deactivation-activation dynamics, thus suggesting for possible trends in the ECU logics. Finally, the MP system allows for exploiting advanced engine control strategies, such as the VVA solution, and for properly taking advantage of the internal EGR, this latter solution being unfeasible for a pure SP injection system.

References

[1] Climate change 2007: Synthesis report, 2.1 emissions of long-lived ghgs., 2007. [online] https://www.ipcc.ch/publications_and_data/ar4/syr/en/contents.html.

[2] The state of natural gas. *Journal of Natural Gas Science and Engineering*, 1(1–2):1 – 13, 2009.

[3] Natural gas issues and trends 1998, us epa: Gwp estimates, 1998. [online] http://www.eia.gov/pub/oil_gas/natural_gas/analysis_publications/natural_gas_1998_issues_trends/pdf/chapter2.pdf.

[4] Choongsik Bae and Jaeheun Kim. Alternative fuels for internal combustion engines. *Proceedings of the Combustion Institute*, 2016.

[5] Muhammad Imran Khan, Tabassum Yasmin, and Abdul Shakoor. Technical overview of compressed natural gas (cng) as a transportation fuel. *Renewable and Sustainable Energy Reviews*, 51:785 – 797, 2015.

[6] Sonia Yeh. An empirical analysis on the adoption of alternative fuel vehicles: The case of natural gas vehicles. *Energy Policy*, 35(11):5865 – 5875, 2007.

[7] Uwe Thien, Alexander Schaerfl, Markus Rudolf, Friedrich Quissek, Helmut Eichlseder, and Axel Bernt. Engine and new fuel management system for cng powered vehicles. 01 2007.

[8] Ngva europe report of activity 2015/2016., 2016. [online] https://www.ngva.eu/downl-oads/NGVA_Europe_Report_of_Activities_2015-2016.pdf.

[9] M.I. Jahirul, H.H. Masjuki, R. Saidur, M.A. Kalam, M.H. Jayed, and M.A. Wazed. Comparative engine performance and emission analysis of {CNG} and gasoline in a retrofitted car engine. *Applied Thermal Engineering*, 30(14–15):2219 – 2226, 2010.

[10] Poulton ML. *Alternative fuel for road vehicles*. WIT Press/ Comput ational Mechanics, 1994.

[11] PM Darade and RS Dalu. Investigation of performance and emissions of cng fuelled vcr engine. *Int J Emerg Technol Adv Eng*, 3(1):77–83, 2013.

[12] R Ebrahimi and M Mercier. Experimental study of performance of spark ignition engine with gasoline and natural gas. *International Journal of Engineering*, 24(2010):65–74, 2010.

[13] Rosli Abu Bakar Semin. A technical review of compressed natural gas as an alternative fuel for internal combustion engines. *Am. J. Eng. Appl. Sci*, 1(4):302–311, 2008.

[14] Amir Hossein Shamekh, Nima Khatibzadeh, and Abazar Shamekhi. A comprehensive comparative investigation of compressed natural gas as an alternative fuel in a bi-fuel spark ignition engine. *Iranian Journal of Chemistry and Chemical Engineering (IJCCE)*, 27(1):73–83, 2008.

[15] CK Samantaray, BB; Mohanta. Analysis of industrial flame characteristics and constancy study using image processing technique. *Journal of Mechanical Engineering and Sciences (JMES)*, 9(1):1604–1613, 2015.

[16] Kasianantham Nanthagopal, Rayapati Subbarao, Thangavelu Elango, Ponnusamy Baskar, and Kandasamy Annamalai. Hydrogen enriched compressed natural gas- a futuristic fuel for internal combustion engines. *Thermal Science*, 15(4):1145–1154, 2011.

[17] Mirko Baratta and Daniela Misul. Development of a method for the estimation of the behavior of a cng engine over the nedc cycle and its application to quantify for the effect of hydrogen addition to methane operations. *Fuel*, 140:237–249, 2015.

[18] Marco Chiodi, Alessandro Ferrari, Oliver Mack, Michael Bargende, and Donatus Wichelhaus. Improvement of a high-performance cng-engine based on an innovative virtual development process. Technical report, SAE Technical Paper, 2011.

[19] MA Kalam, SN Kazi, and MH Jayed. Power boosting of a modified natural gas engine. *International Journal of Physical Sciences*, 6(28):6548–6557, 2011.

[20] Saad Aljamali, Wan Mohd Faizal Wan Mahmood, Shahrir Abdullah, and Yusoff Ali. Comparison of performance and emission of a gasoline engine fuelled by gasoline and cng under various throttle positions. *Journal of Applied Sciences*, 14(4):386, 2014.

[21] Nils-Olof Nylund and Alex Lawson. Exhaust emissions from natural gas vehicles. *IANGV Emission Report*, pages 31–40, 2000.

[22] M Mansha, AR Saleemi, SH Javed, and Badar M Ghauri. Prediction and measurement of pollutant emissions in cng fired internal combustion engine. *Journal of Natural Gas Chemistry*, 19(5):539–547, 2010.

[23] Mohammad I Jahirul, HH Masjuki, R Saidur, MA Kalam, MH Jayed, and MA Wazed. Comparative engine performance and emission analysis of cng and gasoline in a retrofitted car engine. *Applied Thermal Engineering*, 30(14):2219–2226, 2010.

[24] Muhammad Imran Khan, Tabassum Yasmin, and Abdul Shakoor. International experience with compressed natural gas (cng) as environmental friendly fuel. *Energy Systems*, 6(4):507–531, 2015.

[25] Xiaoyan Huang, Yang Wang, Zhenyu Xing, and Ke Du. Emission factors of air pollutants from cng-gasoline bi-fuel vehicles: Part ii. co, hc and no x. *Science of The Total Environment*, 565:698–705, 2016.

[26] N John Beck, Robert L Barkhimer, William P Johnson, Hoi C Wong, and Kresimir Gebert. Evolution of heavy duty natural gas engines-stoichiometric, carbureted and spark ignited to lean burn, fuel injected and micro-pilot. Technical report, SAE Technical Paper, 1997.

[27] A Manivannan, P Tamil Porai, S Chandrasekaran, and R Ramprabhu. Lean burn natural gas spark ignition engine-an overview. Technical report, SAE Technical Paper, 2003.

[28] RRJ ter Rele and JJ Seppen. Analysis of the performance and exhaust gas emissions of four hd gaseous fuelled engines, using engine test data and computer stimulation. Technical report, SAE Technical Paper, 1990.

[29] John T Kubesh, Daniel J Podnar, and Christopher P Colucci. Lean limit and performance improvements for a heavy-duty natural gas engine. Technical report, SAE Technical Paper, 1996.

[30] Pasquale Corbo, Michele Gambino, S Iannaccone, and A Unich. Comparison between lean-burn and stoichiometric technologies for cng heavy-duty engines. Technical report, SAE Technical Paper, 1995.

[31] Patrik Einewall, Per Tunestål, and Bengt Johansson. Lean burn natural gas operation vs. stoichiometric operation with egr and a three way catalyst. *SAE Special Publications*, 2005(SP-1972):343–362, 2005.

[32] Fan Zeng and Keith L Hohn. Modeling of three-way catalytic converter performance with exhaust mixture from natural gas-fueled engines. *Applied Catalysis B: Environmental*, 182:570–579, 2016.

[33] Richard Tilagone and Stephane Venturi. Development of natural gas demonstrator based on an urban vehicle with a down-sized turbocharged engine. *Oil & gas science and technology*, 59(6):581–591, 2004.

[34] James P Chiu, James Wegrzyn, and Kenneth E Murphy. Low emissions class 8 heavy-duty on-highway natural gas and gasoline engine. Technical report, SAE Technical Paper, 2004.

[35] Lei Zhu, Zhuoyao He, Zhen Xu, Xingcai Lu, Junhua Fang, Wugao Zhang, and Zhen Huang. In-cylinder thermochemical fuel reforming (tfr) in a spark-ignition natural gas engine. *Proceedings of the Combustion Institute*, 2016.

[36] John B Heywood et al. *Internal combustion engine fundamentals*, volume 930. Mcgraw-hill New York, 1988.

[37] MA Kalam and HH Masjuki. An experimental investigation of high performance natural gas engine with direct injection. *Energy*, 36(5):3563–3571, 2011.

[38] Richard Tilagone, Stéphane Venturi, and Gaétan Monnier. Natural gas-an environmentally friendly fuel for urban vehicles: the smart demonstrator approach. Technical report, SAE Technical Paper, 2005.

[39] Fuquan Zhao, M-C Lai, and David L Harrington. Automotive spark-ignited direct-injection gasoline engines. *Progress in energy and combustion science*, 25(5):437–562, 1999.

[40] Ford ecoboost engine presentation, 2009. [online] http://www.ford.it/Tecnologie/Prestazioni/Ford-EcoBoost.

[41] Sukrut S Thipse, Shailesh B Sonawane, Ashwin FD'Souza, SD Rairikar, Kishor Kumar Kavathekar, and Neelkanth V Marathe. Injection strategies, optimization and simulation techniques on di cng technology. Technical report, SAE Technical Paper, 2015.

[42] Mingi Choi, Sanghoon Lee, and Sungwook Park. Numerical and experimental study of gaseous fuel injection for cng direct injection. *Fuel*, 140:693–700, 2015.

[43] Mingi Choi, Jingeun Song, and Sungwook Park. Modeling of the fuel injection and combustion process in a cng direct injection engine. *Fuel*, 179:168–178, 2016.

[44] Mirko Baratta, Andrea E Catania, Ezio Spessa, Lothar Herrmann, and Klaus Roessler. Multi-dimensional modeling of direct natural-gas injection and mixture formation in a stratified-charge si engine with centrally mounted injector. *SAE International Journal of Engines*, 1(2008-01-0975):607–626, 2008.

[45] Jianjun Zheng, Zuohua Huang, Jinhua Wang, Bin Wang, Dezhong Ning, and Yingjia Zhang. Effect of compression ratio on cycle-by-cycle variations in a natural gas direct injection engine. *Energy & Fuels*, 23(11):5357–5366, 2009.

[46] YF Liu, Bin Liu, Liang Liu, Ke Zeng, and ZH Huang. Combustion characteristics and particulate emission in a natural-gas direct-injection engine: effects of the injection timing and the spark timing. *Proceedings of the Institution of Mechanical Engineers, Part D: Journal of Automobile Engineering*, 224(8):1071–1080, 2010.

[47] S Shiga, S Ozone, HTC Machacon, T Karasawa, H Nakamura, T Ueda, N Jingu, Z Huang, M Tsue, and M Kono. A study of the combustion and emission characteristics of compressed-natural-gas direct-injection stratified combustion using a rapid-compression-machine. *Combustion and Flame*, 129(1):1–10, 2002.

[48] Alberto Boretti, Petros Lappas, Bingjie Zhang, and Siti Khalijah Mazlan. Cng fueling strategies for commercial vehicles engines-a literature review. Technical report, SAE Technical Paper, 2013.

[49] Mirko Baratta and Nicola Rapetto. Fluid-dynamic and numerical aspects in the simulation of direct cng injection in spark-ignition engines. *Computers & Fluids*, 103:215–233, 2014.

[50] Oleg Zastavniouk. Study of mixing phenomena in a dual fuel diesel engine air intake manifold. Master's thesis, University of Alberta, 1997.

[51] Cheolwoong Park, Sungwon Lee, Gihun Lim, Young Choi, and Changgi Kim. Effect of mixer type on cylinder-to-cylinder variation and performance in hydrogen-natural gas blend fuel engine. *International Journal of Hydrogen Energy*, 38(11):4809–4815, 2013.

[52] Shaobo Ji, Xin Lan, Yong Cheng, Xiuliang Zhao, Xinhai Li, and Fengjuan Wang. Cyclic variation of large-bore multi point injection engine fuelled by natural gas with different types of injection systems. *Applied Thermal Engineering*, 102:1241–1249, 2016.

[53] Bosch gasoline fuel-injection system k-jetronic.technical instruction manual. [online] http://vwts.ru/injector/k-jetronic/gasoline_fuel_injection_system_k-jetronic_eng.pdf.

[54] P Dickinson and AT Shenton. Dynamic calibration of fuelling in the pfi si engine. *Control Engineering Practice*, 17(1):26–38, 2009.

[55] How Heoy Geok, Taib Iskandar Mohamad, Shahrir Abdullah, Yusoff Ali, Azhari Shamsudeen, and Elvis Adril. Experimental investigation of performance and emission of a sequential port injection natural gas engine. *European Journal of Scientific Research*, 30(2):204–214, 2009.

[56] Mohd Faisal Hushim, Ahmad Jais Alimin, Hazlina Selamat, and Mohd Taufiq Muslim. Pfi retrofit-kit as green technology for small 4-stroke si engine. In *Applied Mechanics and Materials*, volume 315, pages 453–457. Trans Tech Publ, 2013.

[57] Ivan Arsie, Silvana Di Iorio, and Salvatore Vaccaro. Experimental investigation of the effects of afr, spark advance and egr on nanoparticle emissions in a pfi si engine. *Journal of Aerosol Science*, 64:1–10, 2013.

[58] Rosli Abu Bakar, K Kadirgama, KV Sharma, MM Rahman, and Semin. *Application of Natural Gas for Internal Combustion Engines*. INTECH Open Access Publisher, 2012.

[59] HB Mathur and SL Soni. Development of timed manifold injection system for compressed natural gas (cng) operation of spark ignition engine. Technical report, SAE Technical Paper, 1999.

[60] Jan Czerwinski, Pierre Comte, and Yan Zimmerli. Investigations of the gas injection system on a hd-cng-engine. Technical report, SAE Technical Paper, 2003.

[61] Tadao Yamato, Hirofumi Sekino, Tomohiro Ninomiya, and Masaru Hayashida. Stratification of in-cylinder mixture distributions by tuned port injection in a 4-valve si gas engine. Technical report, SAE Technical Paper, 2001.

[62] M Patel Nimit and AD Patel. Conversion of diesel engine to port injection cng engine using gaseous injector nozzle multi holes geometries improvement: A review. *International Journal of Automotive Engineering*, 6(3):2220–2235, 2016.

[63] Kichiro Kato, Kohei Igarashi, Michihiko Masuda, Katsuji Otsubo, Akio Yasuda, Keiso Takeda, and Toru Sato. Development of engine for natural gas vehicle. Technical report, SAE Technical Paper, 1999.

[64] Antony Middleton, Barry Neumann, and DS Khatri. Development of dedicated cng engine with multipoint gas injection system. Technical report, SAE Technical Paper, 2008.

[65] VS Midhun, S Karthikeyan, S Krishnan, SD Rairikar, KP Kavathekar, SS Thipse, NV Marathe, et al. Development of cng injection engine to meet future euro-v emission norms for lcv applications. Technical report, SAE Technical Paper, 2011.

[66] Paolo Lino, Bruno Maione, and Alessandro Rizzo. Nonlinear modelling and control of a common rail injection system for diesel engines. *Applied mathematical modelling*, 31(9):1770–1784, 2007.

[67] Harald Ortwig Dirk Hübner. Linear modeling, simulation and experimental verification of a. pressure regulator for cng injection systems. *The 4th International Conference on Cybernetics and Information Technologies, Systems and Applications: CITSA*, 6(4), 2007.

[68] Gabriella Dellino, Paolo Lino, Carlo Meloni, and Alessandro Rizzo. Multidisciplinary design optimization of a pressure controller for cng injection systems. In *2006 IEEE Conference on Computer Aided Control System Design, 2006 IEEE International Conference on Control Applications, 2006 IEEE International Symposium on Intelligent Control*, pages 2689–2694. IEEE, 2006.

[69] Paolo Lino, Bruno Maione, and Claudio Amorese. Modelling and predictive control of a new injection system for compressed natural gas engines. *Control Engineering Practice*, 16(10):1216–1230, 2008.

[70] Matteo Corno, Sergio Matteo Savaresi, Riccardo Scattolini, Emilio Comignaghi, Marco Sofia, Antonio Palma, and Eduardo Sepe. Rapid virtual prototyping and dynamics analysis of a common rail injection system for gasoline engines. *International Journal of Vehicle Systems Modelling and Testing*, 4(1-2):17–42, 2009.

[71] Marco Cammalleri, Emiliano Pipitone, Stefano Beccari, and Giuseppe Genchi. A mathematical model for the prediction of the injected mass diagram of a si engine gas injector. *Journal of Mechanical Science and Technology*, 27(11):3253–3265, 2013.

[72] Chung Y Liu, Randy Chen, and Syed F Hussain. Development of gaseous injector for propane and cng, part i. Technical report, SAE Technical Paper, 1998.

[73] Stefano Beccari, Emiliano Pipitone, Marco Cammalleri, and Giuseppe Genchi. Model-based optimization of injection strategies for si engine gas injectors. *Journal of Mechanical Science and Technology*, 28(8):3311–3323, 2014.

[74] Lino Guzzella and Christopher Onder. *Introduction to modeling and control of internal combustion engine systems*. Springer Science & Business Media, 2009.

[75] Ke Zeng, Shiliang Lv, Bing Liu, Fanhua Ma, and Zuohua Huang. Development and calibration on an electronic control system of cng engine. In *Vehicular Electronics and Safety, 2006. ICVES 2006. IEEE International Conference on*, pages 204–208. IEEE, 2006.

[76] Christian Roithmeier. *Virtuelle Applikation von Motorsteuerungsfunktionen am Beispiel der Lasterfassungsfunktion und der Fahrdynamikfunktionen*. PhD thesis, TH Karlsruhe, 2011.

[77] Paolo Lino and Guido Maione. Accurate dynamic modeling of an electronically controlled cng injection system. *IFAC-PapersOnLine*, 49(11):490–496, 2016.

[78] F Barghi and AA Safavi. An intelligent control policy for fuel injection control of si engines (case study: Cng engine). In *2011 15th IEEE International Conference on Intelligent Engineering Systems*, pages 115–119. IEEE, 2011.

[79] S Grasreiner. *Combustion modeling for virtual SI engine calibration with the help of 0D/3D methods*. PhD thesis, Technischen Universität Bergakademie Freiberg, 2012.

[80] David Dyntar, Christopher Onder, and Lino Guzzella. Modeling and control of cng engines. Technical report, SAE Technical Paper, 2002.

[81] Umberto Montanaro, Alessandro di Gaeta, and Veniero Giglio. Adaptive tracking control of a common rail injection system for gasoline engines: a discrete-time integral minimal control synthesis approach. *IEEE Transactions on Control Systems Technology*, 21(5):1940–1948, 2013.

[82] XLJ Seykens, LMT Somers, and RSG Baert. Modelling of common rail fuel injection system and influence of fluid properties on injection process. *Proceedings of VAFSEP*, pages 6–9, 2004.

[83] Mirko Baratta, Roberto Finesso, Daniela Misul, Ezio Spessa, Yifei Tong, and Cesare Peletto. Potential of the variable valve actuation (vva) strategy on a heavy duty cng engine. In *ASME 2014 12th Biennial Conference on Engineering Systems Design and Analysis*, pages V001T02A008–V001T02A008. American Society of Mechanical Engineers, 2014.

[84] Mirko Baratta, Daniela Misul, Ezio Spessa, Giuseppe Gazzilli, and Andrea Gerini. Fluid-dynamic characterization of a cng injection system. In *ASME 2012 Internal Combustion Engine Division Spring Technical Conference*, pages 829–836. American Society of Mechanical Engineers, 2012.

[85] G D'Errico, Daniela Anna Misul, A Onorati, and Ezio Spessa. Integrated fluid dynamic modeling and combustion diagnostics of a multivalve si engine under gasoline and cng operations. 2003.

[86] A-Rashid A-Aziz and Firmansyah. The effect of fuel rail pressure on the performance of a cng-direct injection engine. In *SAE Technical Paper*. SAE International, 04 2009.

[87] Andrea Emilio Catania, Daniela Misul, Ezio Spessa, and Giuseppe Martorana. Conversion of a multivalve gasoline engine to run on cng. Technical report, SAE Technical Paper, 2000.

[88] Antony Middleton, Barry Neumann, and DS Khatri. Natural gas injection system for buses and trucks-potential to achieve future performance and emission norms. Technical report, SAE Technical Paper, 2007.

[89] Stefano d'Ambrosio, Ezio Spessa, Alberto Vassallo, Massimo Ferrera, and C Peletto. Experimental investigation of fuel consumption, exhaust emissions and heat release of a small-displacement turbocharged cng engine. Technical report, SAE Technical Paper, 2006.

[90] Mike Fry, Jason King, and Carl White. A comparison of gasoline direct injection systems and discussion of development techniques. Technical report, SAE Technical Paper, 1999.

[91] Su HaiFeng, Zhang YouTong, Wang Jun, and Liu LianDa. Researches of common-rail diesel engine emission control based on cylinder pressure feedback. In *2008 IEEE Vehicle Power and Propulsion Conference*, pages 1–6. IEEE, 2008.

[92] Hitoshi Tomishima, Takeo Matsumoto, Mamoru Oki, and Kohji Nagata. The advanced diesel common rail system for achieving a good balance between ecology and economy. Technical report, SAE Technical Paper, 2008.

[93] Michael Tomforde, Torsten Jeinsch, J Blath, and H Dnow. Modelling of a fuel supply system for model-based calibration. In *Proceedings of 17th IFAC World Congress*, pages 10710–10711, 2008.

[94] Hailin Li and Ghazi A Karim. Modeling the performance of a turbo-charged spark ignition natural gas engine with cooled exhaust gas recirculation. *Journal of Engineering for Gas Turbines and Power*, 130(3):032804, 2008.

[95] Chien-Ping Pan, Min-Chung Li, and Syed F Hussain. Fuel pressure control for gaseous fuel injection systems. Technical report, SAE Technical Paper, 1998.

[96] Vivek Kumar Gupta, Zhen Zhang, and Zongxuan Sun. Modeling and control of a novel pressure regulation mechanism for common rail fuel injection systems. *Applied Mathematical Modelling*, 35(7):3473–3483, 2011.

[97] Kalevi Huhtala and Matti Vilenius. Study of a common rail fuel injection system. In *SAE Technical Paper*. SAE International, 10 2001.

[98] Andrea E Catania, Alessandro Ferrari, Michele Manno, and Ezio Spessa. Experimental investigation of dynamics effects on multiple-injection common rail system performance. *Journal of Engineering for Gas Turbines and Power*, 130(3):032806, 2008.

[99] Qiang Hu, Sean F Wu, Ming-Chia Lai, Shari Stottler, and Ragu Raghupathi. Prediction of pressure fluctuations inside an automotive fuel rail system. Technical report, SAE Technical Paper, 1999.

[100] NH Chung, BG Oh, and MH Sunwoo. Modelling and injection rate estimation of common-rail injectors for direct-injection diesel engines. *Proceedings of the Institution of Mechanical Engineers, Part D: Journal of Automobile Engineering*, 222(6):1089–1001, 2008.

[101] LMS Imagine lab. Amesim. ifp-engine users manual, volume 14. Technical report, 2014.

[102] D. Linden. Design principles for proportional pressure reducing valves in mobile applications. *Tenth Scandinavian International Conference on Fluid Power, SICFP'07, Tampere, Finland*, 2007.

[103] T Lähteenmäki, M Ijas, and E Mäkinen. Characteristics of digital hydraulic pressure reducing valve. *In: Johnston, DN & Plummer, A.(eds.). Fluid Power and Motion Control (FPMC 2010), 15-17 September 2010, University of Bath, UK*, 2010.

[104] H Esmaili, A Aryaei, S Mohammadi, M Najar, et al. Dynamic simulation of a high pressure regulator. *Journal of Computational & Applied Research in Mechanical Engineering (JCARME)*, 1(1):17–28, 2011.

[105] Fabien Favret, Mohammed Jemmali, Jean-Philippe Cornil, Francis Deneuve, and M Jean-Pierre Guiraud. Stability of distribution-network governors. *Transactions of the Institute of Measurement and Control*, 14(2):58–64, 1992.

[106] Bezian Jean-Jacques, Grenouilleau Pascal, Menu François, et al. Stability study and modelling of a pressure regulating station. *International journal of pressure vessels and piping*, 82(1):51–60, 2005.

[107] Mark Wilcutts, Joshua Switkes, Mark Shost, and Adya Tripathi. Design and benefits of dynamic skip fire strategies for cylinder deactivated engines. *SAE International Journal of Engines*, 6(2013-01-0359):278–288, 2013.

[108] R. W. Dibble M. Sierra Aznar (University of California at Berkeley). Testing compressed natural gas fuel economy with dynamic skip fire technology. *California Energy Commission*, (CEC-500-2016-050), 2014.